SYNTHETIC CATHINONE CHARACTERIZATION AND ISOMER IDENTIFICATION USING ENERGY-RESOLVED TANDEM MASS SPECTROMETRY (MS/MS)

By

Cynthia Jeanne Kaeser

A THESIS

Submitted to
Michigan State University
in partial fulfillment of the requirements
for the degree of

Forensic Science - Master of Science

2017

ABSTRACT

SYNTHETIC CATHINONE CHARACTERIZATION AND ISOMER IDENTIFICATION USING ENERGY-RESOLVED TANDEM MASS SPECTROMETRY (MS/MS)

By

Cynthia Jeanne Kaeser

The identification of emerging designer drug analogs, such as synthetic cathinones and phenethylamines, is a necessary step in the control and regulation of these illicit compounds. The standard technique for controlled substance analysis, gas chromatography-mass spectrometry, provides reproducible results useful for comparison to a library of mass spectra, but is hindered by low-resolution mass data that limit accurate molecular formulae assignments. Extensive compound fragmentation makes determination of intact molecules ambiguous. As an alternative analysis method, collision-induced dissociation mass spectrometry (CID-MS) provides accurate mass data that facilitates molecular formulae assignments. Controlled fragmentation is achieved through the use of multiple collision energies, providing molecular formulae for both the intact compound and fragments that reveal and distinguish structural features.

Using CID-MS, this work aims first to facilitate class assignment of cathinones and phenethylamines by combining commonly observed fragmentation pathways for both drug classes into a single flowchart. This scheme is built and tested using compounds that represent the diversity of potential structural features within the drug classes. Additionally, this work leverages the use of multiple collision potentials to distinguish between cathinone isomers by specifically examining fragmentation differences between isomers at each collision potential.

ACKNOWLEDGEMENTS

I would like to thank my advisor, Dr. Ruth Smith, for her guidance and support through the challenges of not only this research but life in general over the past few years. I would like to thank my doctoral advisor and committee member, Dr. A. Daniel Jones, for sharing his insight into MS fragmentation mechanisms and instrumentation, challenging my assumptions and directions as a researcher, and encouraging the risks I've taken outside of research. Thank you also to Dr. Chris Smith for being the final member of my committee and accommodating my unique situation as student residing out of state. I would also like to thank my research advisor at LLNL, Dr. Elizabeth Wheeler, for allowing me to finish this degree while working under her guidance.

I would also like to thank the past and current members of the Forensic Chemistry Group for their support. Of this group, I am especially grateful to Fanny Chu for her timely and thorough thesis revisions and to her and Kristen Reese for the lunchtime research discussions and patience through practice talks.

I must also wholeheartedly thank my family for their love and unwavering support not only in graduate school but in every pursuit I have undertaken. Thank you also to Katie, my California family, the Inquiry Team, Thuan, and more people than I can name for celebrating with me on the good days, supporting me on the bad ones, and keeping me balanced through this process. And, most importantly, thank you to my Lord and God for every blessing You have given, guiding my life even when it makes it appear wilder than I could have ever imagined, and putting me back together every time I fall apart. This has been quite the journey – now, on to the next one!

TABLE OF CONTENTS

LIST OF FIGURES

CHAPTER ONE: Introduction to Designer Drug Regulation and Identification

1.1 Introduction to designer drugs

1.1.1 Definition, prevalence, use, and abuse

Controlled substances have become a common type of evidence submitted for forensic analysis. While the Drug Enforcement Agency (DEA) reports seizure of tens of thousands of kilograms of cocaine, marijuana, and hallucinogens and more than 30,000 drug-related arrests for possession, sale, or manufacturing each year (1), statistics from the Federal Bureau of Investigation (FBI) statistics indicate that drug-related arrests are more likely to occur because of possession than for sale and manufacturing (2). The CDC also reports that deaths associated with drug abuse now exceed those due to either automobile accidents or firearm-related injuries (3). As they become an increasing public health issue, regulation and control of synthetic designer drugs has been a growing concern in recent years (3).

"Designer drugs" is a term given to compounds that are structurally similar to and mimic the effects of an otherwise restricted or prohibited compound (4). These compounds fall into several classes that include synthetic cannabinoids, cathinones, and phenethylamines, although this work will focus only on these last two classes. Compounds within each class are modeled after similar compounds of known psychological activity that are either naturally occurring or that are developed by pharmaceutical researchers for medicinal purposes. From known molecular templates, clandestine chemists make small structural modifications, such as adding or removing

functional groups, to avoid regulation while maintaining the physiological effects of the base compound.

1.1.2 Cathinone and phenethylamine structures

Synthetic cathinones are derivatives of the naturally occurring psychoactive compound cathinone ((*S*)-2-amino-1-phenylpropan-1-one). With stimulative effects similar to cocaine and amphetamines, these drugs originally gained popularity for recreational use in part because of their unregulated status (5) and, while reports of their use have been on the decline in recent years, they are still listed as "drugs of concern" in the DEA's resource guide (6). The core structure of cathinone, shown in Figure 1.1.a., is a 6-membered aromatic ring with an ethyl (2-carbon) chain that terminates with an amine group. The substitution at the alpha-carbon is a minimum of a methyl chain and a ketone group is present at the beta-carbon.

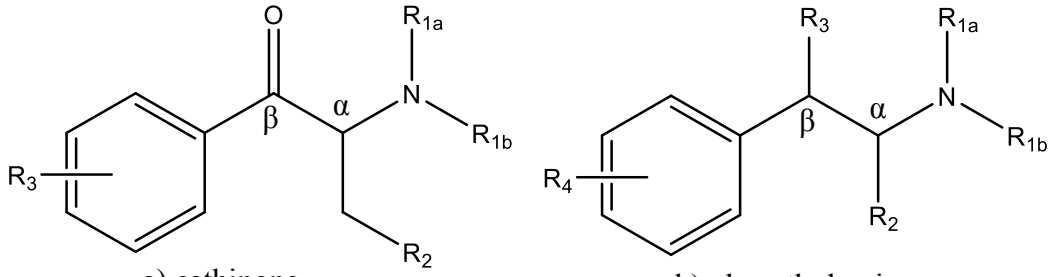

a) cathinone b) phenethylamine

Figure 1.1. Core structures of a) cathinones and b) phenethylamines.

Cathinones are closely related to another class of drugs of concern, phenethylamines. The phenethylamine core structure, shown in Figure 1.1.b., is similar but lacks the ketone group at the beta-carbon and does not have the methyl requirement at

the alpha-carbon. The "R" groups in both cathinones and phenethylamines represent possible sites of substitution. Common substituents for these locations include aliphatic (carbon and hydrogen only) chains of varying lengths, oxygen-containing groups, and halogens (*e.g.*, bromine, chlorine, or fluorine), among others (7,8). The presence of multiple substitution sites also allows for structural isomers, or compounds with identical molecular formulae but differing structural arrangements. Although the similarities in structure among designer drugs are advantageous for maintaining the physiological effects, the range of combinations of functional groups assembled around similar cores can make identification of the exact structure challenging. However, definitive identification of each compound is vital to the regulation process. As these new analogs arrive on the market, forensic scientists are tasked with their identification while lawmakers are tasked with their legislation (9).

1.1.3 Designer drug regulation

From a legislative standpoint, the Controlled Substances Act (1970) established regulation to control the production, possession, and distribution of various drugs (10). Under this Act, drugs are classified into one of five schedules based on their potential for abuse, accepted medical use, and potential for psychological and physical dependence, with Schedule I being the highest risk for abuse and Schedule V being the lowest (11). As new pharmaceutical drugs receive approval by the Food and Drug Administration (FDA), their placement as a scheduled or unscheduled drug is also determined. The scheduling process for new drugs, both legally and illegally distributed, can be a lengthy process as research in the areas of abuse and dependence must be performed and reviewed before a

classification can be made. With the rate of emergence of new analogs into the illegal drug market exceeding that of legislation, a different approach was needed.

In 1986, the Federal Analog Act was enacted to allow analogs that are structurally similar to Schedule I and II drugs to be prosecuted as though they are scheduled if the drugs are intended for human consumption. This enabled lawmakers to side-step the lengthy scheduling process and address the rapidly changing compounds on the market while keeping them readily available for labs to build the research needed for the full scheduling process. However, the two requirements of "structurally similar" and "intended for human consumption" are ambiguous and can be interpreted differently (9). With a broad range of possible chemical modifications, it is unclear at what point an analog becomes structurally dissimilar, even among experts in the field. Additionally, dealers often advertise designer drugs as "bath salts" or "plant food" in packages marked "not for human consumption" in an attempt to circumvent the latter requirement.

While both Acts provide grounds for prosecution of individuals manufacturing and distributing designer drug analogs, some analogs have still become widely available. When specific analogs become particularly prevalent and pose an imminent hazard to public safety, the compounds can be emergency scheduled as a Schedule I drug for a period of up to one year with the option to extend the scheduling by six months or longer if scheduling procedures are underway (12). For cathinones and phenethylamines, the two drug classes most commonly found in "bath salts", there are five cathinones and 27 phenethylamines categorized as Schedule I drugs as of November 2016 (13). Another 10 cathinones have been emergency scheduled, pending full scheduling.

Since federal action on illicit drug regulation is a slow process, individual states have taken action to regulate these compounds on a more local level. Since 2011, all states have placed some level of regulation on synthetic cathinones that range from banning individual compounds to more general legislature that regulates compounds that contain a specific structural feature or act on a specific chemical receptor (14). While no consistent agreement among the states exists on how to best regulate these emerging drugs, in all cases, the first step toward regulation remains the definitive identification of emerging analogs.

1.1.4 Typical forensic analysis of controlled substances

A typical forensic analysis of a sample suspected to contain controlled substances will include both presumptive and confirmatory tests. Presumptive tests, such as color tests, ultraviolet-visible spectrophotometry, or microcrystalline tests are rapid, inexpensive tests that establish whether an illicit drug may be present by indicating the presence of structural features common in controlled substances. Some presumptive techniques are specific enough to identify the class of the compound, but many lack the specificity to accomplish this. For example, the clear, colorless liquid reagent in a Liebermann's color test will become colored in the presence of alkaloids, or nitrogen-containing compounds. This test will be positive for cathinones, phenethylamines, and variety of other compounds including naturally occurring compounds (15). For complete structural identification that can define both the drug class and the actual compound present, confirmatory tests are required. Confirmatory tests include nuclear magnetic resonance (NMR), infrared (IR) spectroscopy, and mass spectrometric (MS) analyses.

The most common confirmatory technique for controlled substance analysis, gas chromatography-mass spectrometry (GC-MS), is the gold standard for identification of the substance in a submitted sample (16). GC provides separation of compounds in a mixed sample while the MS component gives information about the composition of each individual compound in the mixture. The mass spectrometer in typical GC-MS instruments uses an electron ionization (EI) source and a single quadrupole mass analyzer. During electron ionization, energy imparted to the ion results in fragmentation. When EI is coupled with high-resolution mass analysis, the mass of the intact molecular ion gives the molecular formula of the compound while the fragment ion masses give information about the structural arrangement of elements within the molecule. While the reproducible fragmentation in EI allows comparison to a library of standards for identification, it is often so extensive that no molecular ion is observed. If no library standard is available, the lack of the molecular ion can limit the identification process.

Additionally, the low mass resolution from a single quadrupole mass analyzer gives only nominal values for masses. Nominal mass data do not allow firm identification of the molecular formula for many mass values as there can be multiple formulae that have the same nominal mass but differing exact masses. Combined with a library match to the fragmentation pattern of a known substance, this resolution is sufficient for identification of the more traditional controlled substances submitted to laboratories. However, for designer drugs, the rapid appearance of new analogs often outpaces the availability of reference standards for comparison. Without a library reference, the low-resolution mass data is insufficient to definitively distinguish between the similar mass

spectra generated from structurally similar compounds. This makes the instrument configuration in GC-MS ultimately insufficient for definitive cathinone analysis.

As an alternative method of analysis, collision-induced dissociation mass spectrometry (CID-MS) has been proposed. CID-MS provides high-resolution mass data that gives confidence in the molecular formulae assignment and a variable collision potential provides some control over the extent of fragmentation observed.

1.2 Objectives of this work

Based on the limitations in standard forensic analyses and the potential use of CID-MS for identification of emerging designer drugs, the aims of this work are twofold. First, development of a characterization scheme facilitates differentiation between cathinones and phenethylamines. Scheme development is accomplished by comparing the most abundant fragments of cathinones and phenethylamines formed using CID-MS at multiple collision potentials and combining these differences into a flow chart. The scheme's foundational sample set represents the diversity of structural substitutions possible in these drug classes with further testing and refinement performed using both a test set of compounds analyzed in-house as well as a data set obtained from the literature. An overview of cathinone and phenethylamine fragmentation and the development of the characterization scheme is covered in Chapter Two.

The second aim, covered in Chapter Three, addresses the issue of isomer differentiation, specifically examining how the structural differences between isomers are revealed when cathinones are fragmented at multiple collision potentials. This is accomplished using three sets of cathinone isomers (eight compounds total) and three

collision potentials. The lowest collision potential provides information about the most energetically favorable fragmentation pathways in these compounds, while higher collision potentials yield more extensive fragmentation that reveals the structural differences between isomers.

1.3 CID-MS analysis

1.3.1 CID-MS overview

Before considering the application of CID-MS for cathinone identification, the underlying theory must first be understood. Mass spectrometry is an analytical technique that determines the ratio of the mass to the charge (*m/z*) of gas phase ions (17). The number of ions at each *m/z* are counted and displayed in a spectrum of *m/z* versus intensity. The intensity of each ion is scaled to the most abundant ion, termed the base peak. An example of a mass spectrum with the relevant terminology labeled is shown in Figure 1.2. There are a variety of methods for ion generation, analysis, and detection that can selected according to the sample type and each have their own advantages and disadvantages. In forensic analyses, mass spectrometry is often paired with a separation technique such as liquid or gas chromatography (LC or GC). Chromatography techniques separate each compound in a mixture, providing many options that can be leveraged for compound identification. While an additional confirmatory technique useful for designer drug identification, chromatographic separation of these compounds is not the focus of this work.

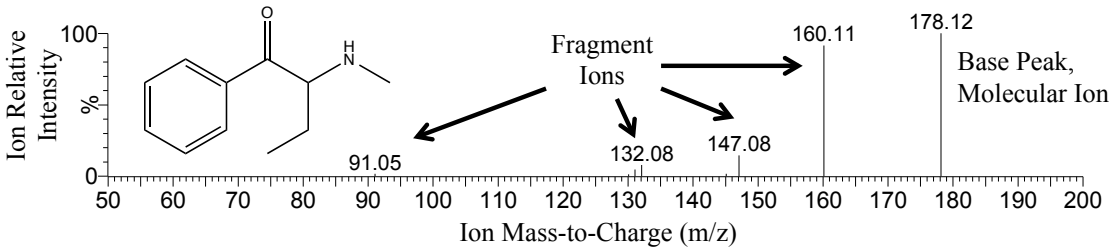

Figure 1.2. An example of a mass spectrum of buphedrone taken at a collision potential of 10 V in positive ion mode.

There are several steps involved in the process of forming and fragmenting ions that yield the final spectrum observed. In this work, all steps are performed using a Waters Xevo G2-XS mass spectrometer (Figure 1.3). Since cathinones and phenethylamines are not ionic compounds, they must first be ionized using an electrospray ionization (ESI) ion source. Ions are separated from any uncharged molecules using an ion guide before the ion of interest, called a precursor ion, is isolated using a quadrupole mass analyzer and fragmented in a collision cell. The energy imparted during the collision step dictates the extent of fragmentation of the precursor ion with increasing fragmentation occurring when using increased collision potentials. The mix of intact precursor ions and fragment ions are then pushed into a time-of-flight (TOF) mass analyzer and separated based on their *m/z* ratio. Ions of each m/z ratio are then detected using an electron multiplier.

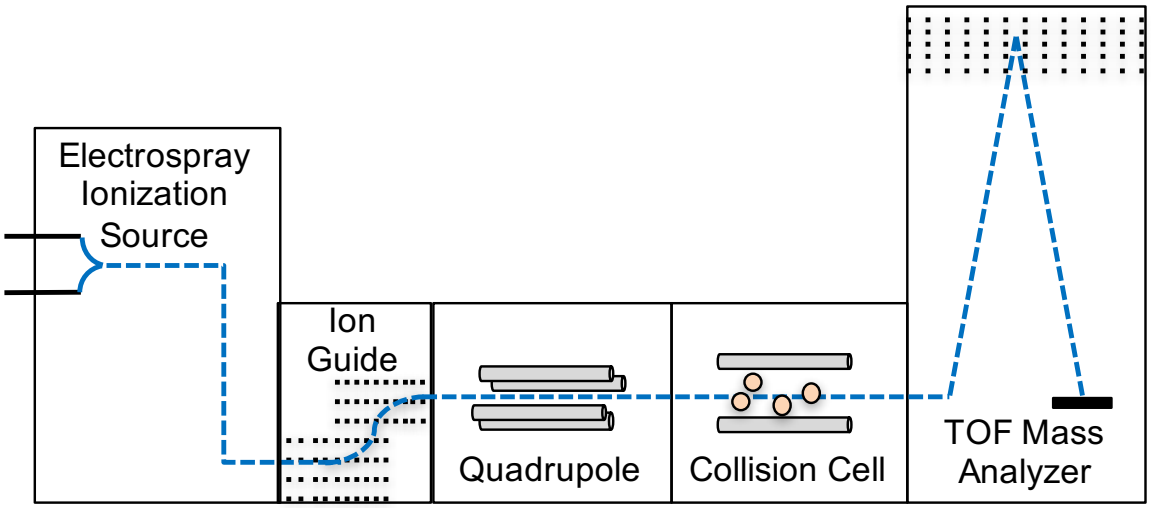

Figure 1.3. Schematic of the components in the Waters Xevo G2-XS mass spectrometer with the ion path indicated by the dashed blue line.

1.3.2 Precursor ion formation and isolation

The ESI process, summarized in Figure 1.4, includes several steps (18). First, a charged spray needle draws the ions of one polarity present in the solution (either positive or negative) to the tip of the needle. As ions of the same polarity are collected at the needle tip, their repulsion of each other forms a Taylor cone. As charge builds up in the tip, the end of the cone breaks off to form a droplet. This droplet is generally composed of both analyte molecules and charged ions from the solvent. As the solvent evaporates, the ions are forced to be physically closer to each other. The size at which the Coulombic repulsion exceeds the surface tension that holds the droplet together is termed the Rayleigh limit. At this point, a Coulombic explosion occurs, breaking the droplet into smaller droplets. This process of evaporation and explosion is repeated until all of the solvent has evaporated, leaving the analyte molecules ionized.

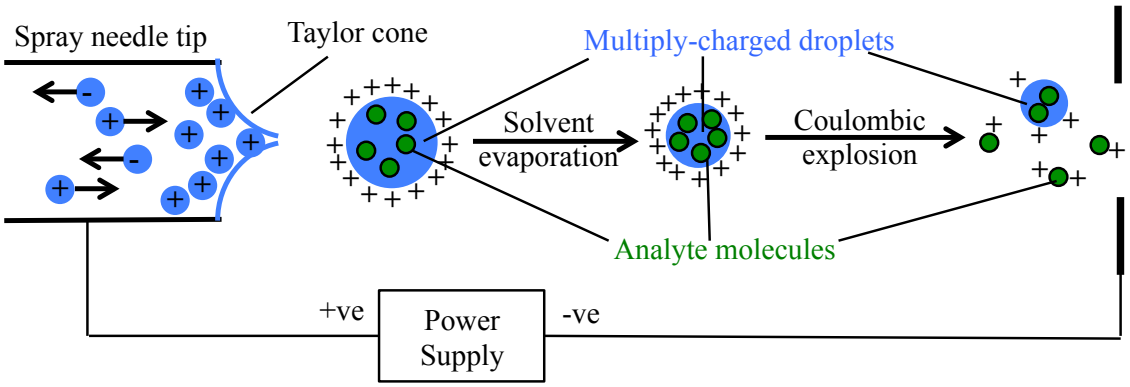

Figure 1.4. Mechanism of ion formation in electrospray ionization run in positive ion mode.

Considered a "soft" ionization method, ESI accomplishes ionization with minimal fragmentation of the analyte. This ensures that the molecular ion remains present in high abundance. However, to be sure that any fragments formed later correlate to the ion of interest alone, the precursor ion is isolated in a quadrupole mass analyzer (Figure 1.5).

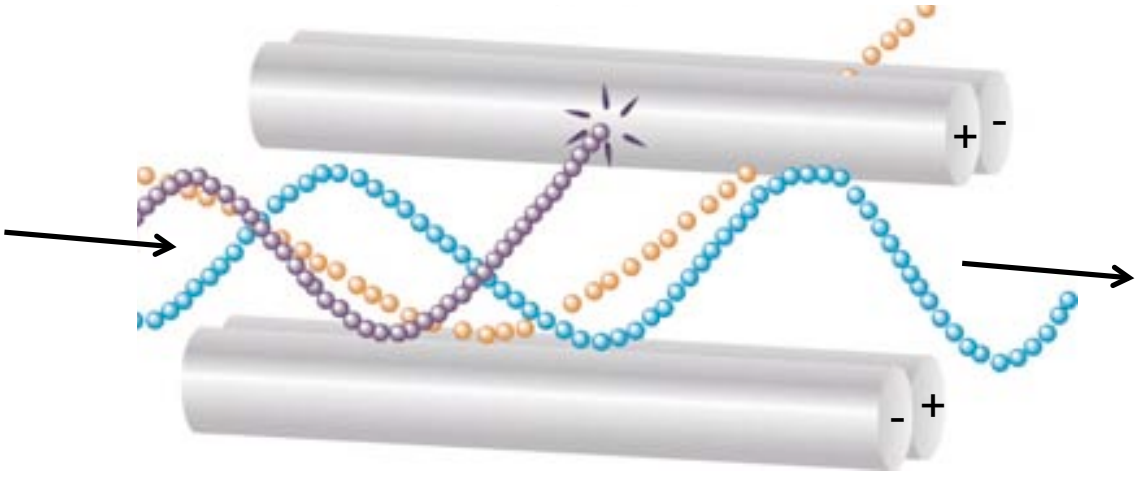

Figure 1.5. Ion isolation achieved by a quadrupole mass analyzer.

A quadrupole consists of four conducting parallel rods evenly-spaced to leave a pathway for ions through the center. The four rods are charged so that the rods diagonally opposite each other are of the same charge, either both positive or both negative (17). These rods are connected to both direct current (DC) and alternating current (AC) power sources. The AC power source produces radio frequency (RF) voltages and ultimately alternates the charge on each rod between positive and negative. Thus, while two rods are labeled as positive in Figure 1.5 at the moment of time pictured there, at another moment in time, they will be negatively charged; likewise, the negatively charged rods will become positive at the same time. This constant charge switching leads to a spiral trajectory for the ions passing through the quadrupole.

Ion selection in the quadrupole is achieved through adjusting the DC and RF potentials. An ion's trajectory through the quadrupole will only be stable if these potentials are appropriately set for the ion's *m/z* value. An ion on an unstable path will either strike one of the charged rods, as in the purple ion in Figure 1.5, or pass between the rods and be pumped away by the vacuum, as with the yellow ion. An ion with a stable path will pass through the quadrupole into the next part of the mass spectrometer. While scanning through the DC and RF potentials can allow a quadrupole to be operated as a mass analyzer, for the purposes of this study, it is operated at a single DC/RF setting to act as an ion filter so that only the precursor ion is allowed to pass through to the detector.

1.3.3 Ion fragmentation and detection

After isolation by the quadrupole, precursor ions are accelerated into the collision cell. In the collision cell, the precursor ions collide with inert argon gas molecules. Upon collision, some of the translational energy in the precursor ion is converted to internal energy (17). If the internal energy is not sufficient to break bonds, then the ion continues through the collision cell intact. However, if the internal energy is sufficiently high to breaks bonds within the precursor ion, fragmentation will occur. The precursor ions isolated in this work each have a single charge, so only one fragment formed during fragmentation will remain charged. The charged fragment is termed a product ion while the remaining uncharged fragment is called a neutral loss.

With a low collision potential, the precursor ion will have less kinetic energy entering each collision that may result in minimal fragmentation. Similarly, a higher collision potential will result in more extensive fragmentation. By using a series of collision potentials that encompasses both low and high potentials, a range of fragments are produced, revealing deep structural information about the precursor ion.

To determine the *m/z* value of the fragment ions produced, a time-of-flight (TOF) mass analyzer is used. The ions leaving the collision cell are focused by a series of lenses before entering the time of flight chamber (17). The ions are "pushed" into the chamber by a pulse of applied voltage, giving them kinetic energy in the same way as upon entering the collision cell. However, the pressure in the chamber is less than 10^{-6} mbar so these ions experience no collisions as they travel through the chamber. While the amount of the kinetic energy applied to each ion remains constant, the velocity at which the ions travel through to the chamber toward the detector is inversely proportional to the square

root of the *m/z* value of the ion. This means that ions of lower *m/z* values will travel more quickly through the chamber and reach the detector first, while those with higher *m/z* values will take longer. The time from the voltage pulse to detection ultimately correlates to the ions' *m/z* value.

A TOF mass analyzer is advantageous because it has both high mass resolution and high mass accuracy. High mass resolution means that ions of *m/z* value as similar as 0.001 Da can be distinguished from each other. Mass accuracy is defined by a low error in the mass assignment, meaning the difference between the experimentally determined value (accurate mass) and the actual value (exact mass) given in parts per million (ppm) is small (<5 ppm) (17). The calculation for this can be seen in the following equation.

$$\text{Error} = \frac{\text{Measured mass} - \text{Theoretical mass}}{\text{Theoretical mass}} \times 10^6 \qquad \text{Eqn. 1}$$

1.3.4 CID-MS as a forensic tool

CID-MS has been previously used to classify unknown compounds for both biological (19-22) and forensic applications (7, 23-27). Work by Fornal (7, 25) and Zuba (27) identified fragments that are common for cathinones. The loss of water commonly occurs when the amine group is a primary or secondary amine. Fragmentation resulting in the neutral loss of an amine group is also observed. Although less common, cleavage of the bond between the alpha- and beta-carbons has been reported (7). In this case, the charge can remain on either of the resulting fragments. For cathinones with a methylenedioxy-substitution on the aromatic ring, the loss of 48 Da (CH_4O_2) is common. Fornal (25) attributed this to a loss of the ring substitution as a methanediol group.

While the neutral losses noted above are those most commonly observed for cathinones at low collision potentials and lay a foundation for cathinone identification, there are no neutral losses that are universally present for all cathinones (7). Additionally, these neutral losses are not specific to cathinones alone, as some of these are common among other drug classes (*e.g.* amine group loss is also present in phenethylamines) (28). This complicates assignment of the drug class when relying on the presence of a limited number of fragments. For structural identification purposes, these neutral losses can reveal some features of the molecule, but with multiple substitution sites on the aromatic ring and alpha-carbon, differentiation between isomers based on these fragments alone may not be possible. Thus, additional fragmentation pathways must be considered.

1.4 Summary and specific goals

Cathinones, a class of designer drugs commonly analyzed by forensic scientists, encompasses diversity in both the composition and location of functional group substitutions within the structure. As new synthetic cathinone analogs reach the market before their standards reach the laboratory, the current technique for identification (GC with low resolution EI-MS) is ill-suited for these emerging compounds because it fails to yield molecular formulae or sufficient information to distinguish isomers. In this work, CID-MS is investigated as an alternative method for cathinone identification. With this technique, analysis can be performed over a range of collision energies, providing information about the intact molecule, as well as the common fragments at both low and high collision potentials. Additionally, the TOF mass analyzer obtains high resolution mass data which allow the molecular formula of both the precursor ion and the product

ions to be assigned with confidence. Chapter 2 presents the fragmentation of cathinones and compares the results to phenethylamines with the goal of identifying product ions that distinguish between these two classes of designer drugs. Building upon this general understanding of cathinone fragmentation, the capacity of CID-MS to differentiate isomers will be explored in Chapter 3.

CHAPTER TWO: Fragmentation of Cathinones for Drug Class Identification

2.1 Introduction to cathinone fragmentation

The structural composition of a suspected illicit drug must be defined to confirm its identity. This identification is an important step in the regulation of designer drugs. To aid this process, collision-induced dissociation mass spectrometry (CID-MS), when performed on a high-resolution mass spectrometer, provides the elemental composition of both the intact molecule as well as fragments that give additional structural information. Leveraging this, a structurally diverse set of cathinones were investigated and their CID mass spectra used to identify not only their common structural features but also those that distinguish cathinones from the structurally similar class of designer drugs, phenethylamines.

2.2 Materials and methods

2.2.1 Preparation of cathinone standards

Cathinone and phenethylamine standards were purchased from Cayman Chemical Company (Ann Arbor, MI). The selected compounds demonstrate the range of structural diversity within these classes while also including isomeric compounds. Structures of the cathinone and phenethylamine standards analyzed in this work are shown in Figures 2.1 and 2.2, respectively. Of these, buphedrone, butylone, naphyrone, ethylone, 2C-E, and 2C-B are currently Schedule I drugs. The remaining cathinones and phenethylamines are currently unregulated. Each standard was prepared at a concentration of 5 μg/mL in

methanol (HPLC grade, Fisher Scientific, Pittsburgh, PA) for subsequent CID-MS analysis.

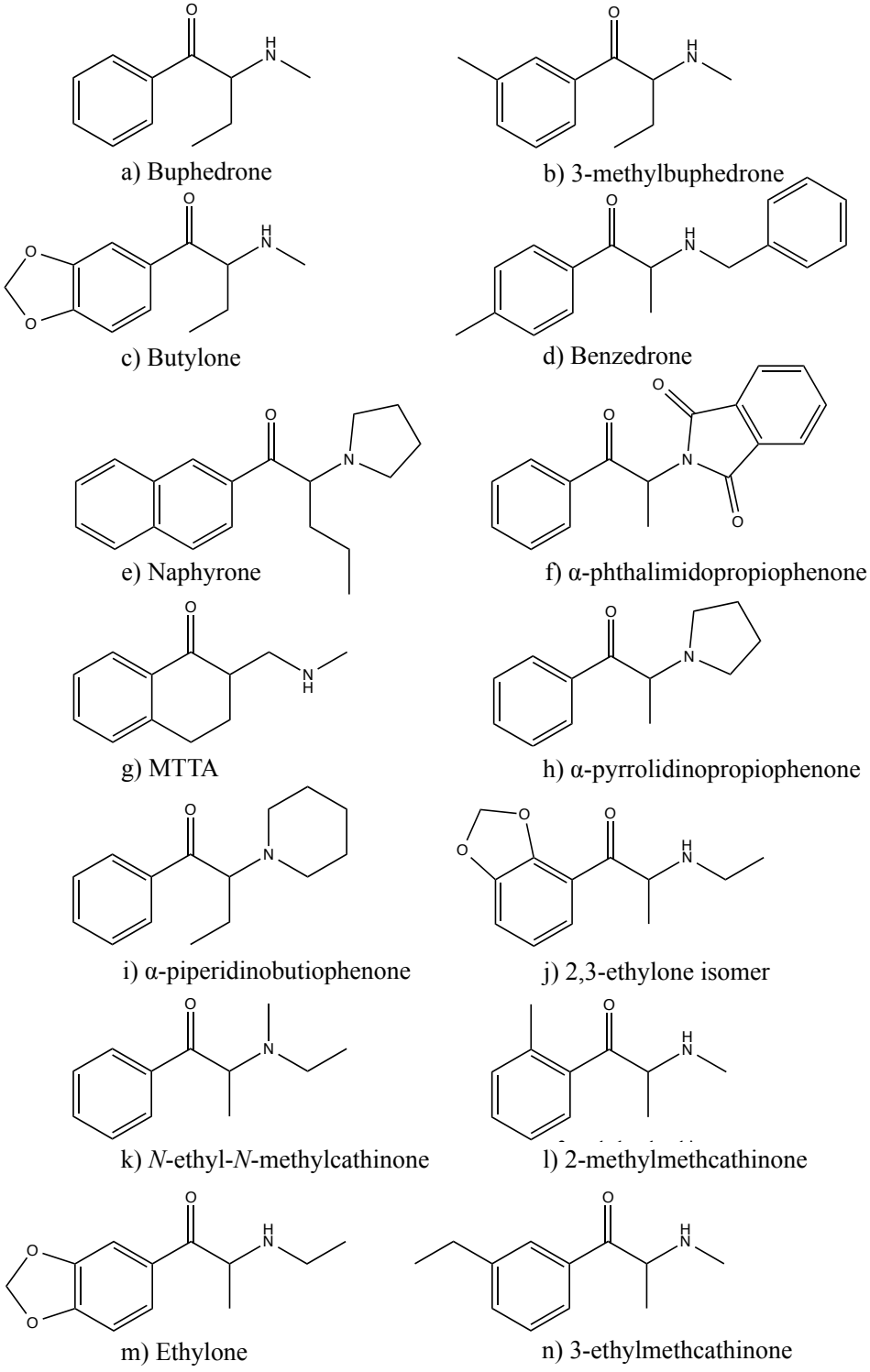

Figure 2.1. Structures of the fourteen synthetic cathinones analyzed in this study.

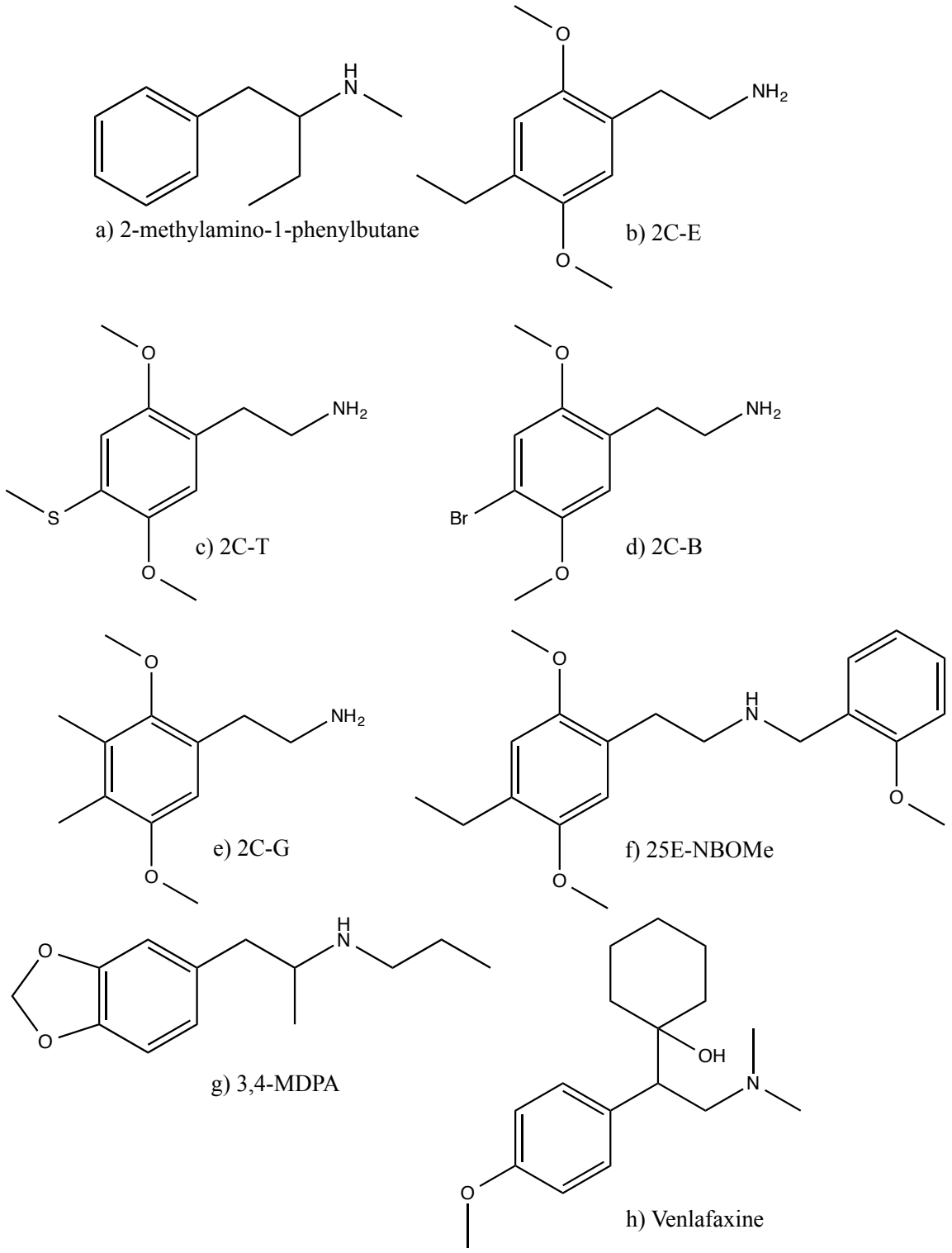

Figure 2.2. Structures of the eight synthetic phenethylamines analyzed in this study.

2.2.2 ESI-QTOF-MS analysis

All standards were analyzed using a Xevo G2-XS QToF mass spectrometer (Waters Corporation, Milford, MA). Flow injection analysis was performed using 75/25 (v/v) acetonitrile (HPLC grade, Sigma-Aldrich, St. Louis, MO) and Milli-Q® water (18.2 MΩ-cm, EMD Millipore, Billerica, MA), at a flow rate of 20 µL/min. The quadrupole-time of flight mass spectrometer was equipped with an electrospray ionization source with a capillary voltage of 3.0 kV, desolvation temperature of 250°C, and source temperature of 100°C. Nitrogen was used as the desolvation gas at a flow rate of 600 L/hr and as the cone gas at a flow rate of 50 L/hr. Mass spectra were acquired in positive-ion mode across the range of mass-to-charge ratios (*m/z*) 30-600. The collision gas was argon at 2 x 10^{-3} mbar measured at the collision cell manifold. Separate injections were used for each collision potential of 10, 20, or 40 V. Leucine enkephalin was used as a mass reference standard with data acquisition rotating between ionization of the designer drug standard and the mass reference standard. Scan times were 0.500 s for each acquisition, with inter-scan delays of 0.014 s, and mass resolution (M/ΔM) at full width half-maximum was 15000.

2.2.3 Data processing

For each designer drug standard at each collision potential, three spectra across the signal maximum were averaged and the resulting ion list was exported from Waters MassLynx software (version 4.1, Waters Corporation) into Microsoft Excel for Mac 2011 (Microsoft Corporation, Redmond, WA). The Elemental Composition tool in MassLynx was used to assign molecular formulae to all ions. The starting composition of the

standard and a mass error of 50 ppm provided the upper bounds for formulae assignment. Comparison of a fragment ion's assigned formula to the formula of the protonated molecule, $[M+H]^+$, provided the associated neutral loss.

2.3. Results and discussion

2.3.1 Mass spectral features of cathinone ring substitutions

The core structure for a cathinone can be substituted at a number of locations including the aromatic ring. There is a range of functional groups that can be used to alter the structure, each resulting in a new drug analog. To analyze how the composition of the ring substitution can be identified from a cathinone's mass spectra, three cathinones were selected for analysis. These cathinones have the same amine and alpha-carbon substitutions, but vary in the aromatic ring substitutions to include having no ring substitution (buphedrone), a methyl group (3-methylbuphedrone) and a methylenedioxy group (butylone).

2.3.1.1 Fragmentation at low collision potential

The chemical structures of buphedrone, 3-methylbuphedrone, and butylone are shown with example spectra taken at the lowest collision potential (10 V) in Figure 2.3. Because each of these compounds has a different molecular formula, the protonated molecules ($[M+H]^+$) are different in each of these spectra: *m/z* 178.12 ($[C_{11}H_{16}NO]^+$) for buphedrone, *m/z* 192.14 ($[C_{12}H_{18}NO]^+$) for 3-methylbuphedrone, and *m/z* 222.11 ($[C_{12}H_{16}NO_3]^+$) for butylone. In all three cases, $[M+H]^+$ is also the base peak.

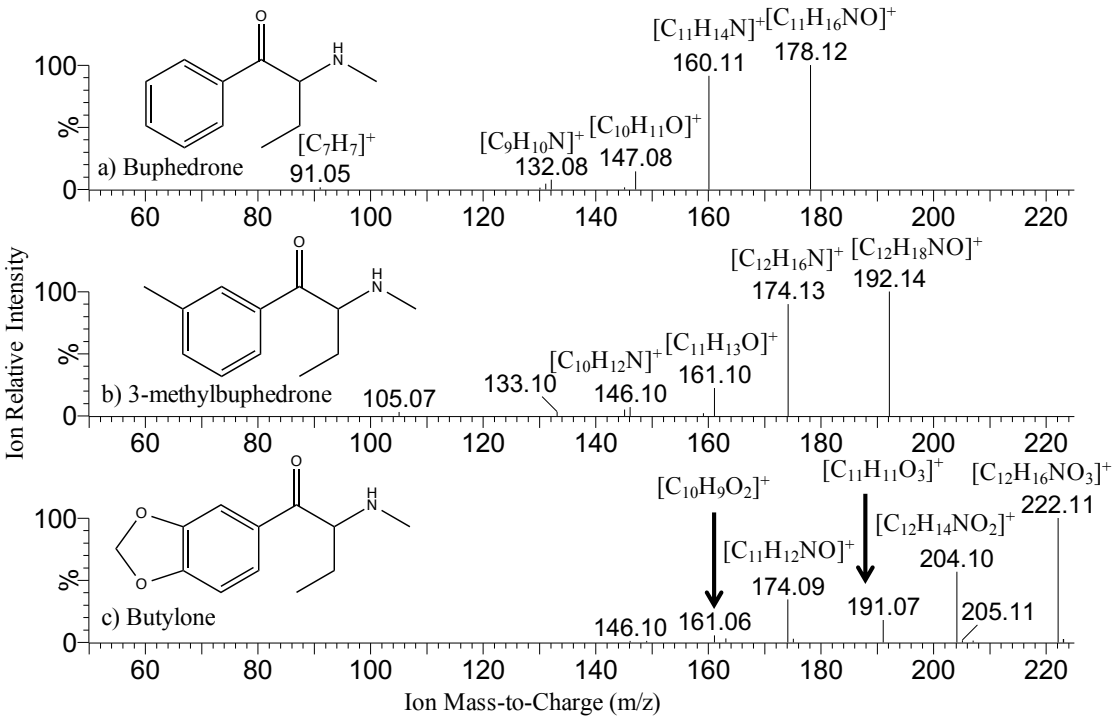

Figure 2.3. CID-MS spectra for the cathinones a) buphedrone, b) 3-methylbuphedrone and c) butylone at a collision potential of 10 V. All spectra collected in positive-ion mode.

While the fragment ion masses differ, several fragment ions observed correspond to common neutral losses. The fragment ions corresponding to the loss of water are the most abundant fragment ion in each spectrum, observed at *m/z* 160.11 for buphedrone, *m/z* 174.13 for 3-methylbuphedrone, and *m/z* 204.10 for butylone. Previous studies on cathinone fragmentation reported that the loss of water involves protonation of the ketone's oxygen and a hydrogen shift from the amine (7, 27). Thus, this loss is only observed when the amine group is a primary or secondary amine, having at least one hydrogen present (7, 27). Also observed in the spectra of these three cathinones are the fragment ions corresponding to the loss of methylamine at *m/z* 147.08 for buphedrone,

m/z 161.10 for 3-methylbuphedrone, and *m/z* 191.07 for butylone. This neutral loss of the amine group provides evidence of the methylamino group common to all three compounds.

To identify the aromatic ring substitution, other fragments must be considered. An unsubstituted aromatic ring fragmented from a larger compound is often observed as the ion $[C_7H_7]^+$ (*m/z* 91.05) (29). This is present in the 10 V CID mass spectrum of buphedrone, but is not present in CID mass spectra of the other two cathinones at this collision potential. The presence of a methyl group on the aromatic ring in 3-methylbuphedrone is indicated by the fragment $[C_8H_9]^+$ (*m/z* 105.07), which is one methylene unit (CH_2) longer than the ring fragment in buphedrone. A similar fragment with a methylenedioxy-substituted aromatic ring is not observed in butylone at 10 V. However, the fragment $[C_{10}H_{11}O]^+$ (*m/z* 147.08) in the CID mass spectrum of butylone corresponds to the loss of 48 Da. Fornal (25) has previously identified this as a loss of the methylenedioxy substitution from the aromatic ring as methanediol (CH_4O_2). However, the loss of methanediol is unlikely owing to its low stability and this neutral loss is more likely to be successive losses of formaldehyde (CH_2O) and water (H_2O). Regardless of the exact mechanism of the loss, the cumulative loss of CH_4O_2 does indicate a methylenedioxy substitution on the aromatic ring. While the fragments observed at 10 V do indicate the composition of both the amine and aromatic substitutions, fragmentation at higher energies provides confirmation of these features.

2.3.1.2 Fragmentation of aliphatic-substituted cathinones at increased collision potentials

To further interrogate the structure of buphedrone, Figure 2.4 shows the chemical structure of this compound as well as representative mass spectra collected using collision potentials of 10, 20, and 40 V. As previously mentioned, commonly observed cathinone ions including the $[M+H]^+$, fragment ions corresponding to the losses of water or the amine group, and the $[C_7H_7]^+$ aromatic ring indicator are present at 10 V. However, as the collision potential increases, more extensive fragmentation occurs owing to the greater internal energy imparted to the $[M+H]^+$. This results in an increase in the number of fragments observed, a decrease in the average mass of these fragments, and the occurrence of odd-electron species.

While not commonly generated during electrospray ionization, the formation of odd-electron ions can occur in CID-MS during fragmentation of even-electron parent ions (5) and are identified using the nominal mass and the molecular formula assignment determined by the exact mass. Odd-electron species that contain no nitrogen or an even number of nitrogen atoms will have an even number nominal mass, while even-electron species with the same nitrogen content will have odd nominal masses. For species with an odd number of nitrogen atoms, the reverse is true, with odd-electron species having an odd-number nominal mass and even-electron species having an even-number nominal mass. Of those odd-electron species identified in the cathinone spectra, one is observed in the 20 V CID mass spectrum of buphedrone as the base peak ($[C_9H_9N]^{\bullet+}$, *m/z* 131.07) (Figure 2.4.b). This fragment is part of a series of fragments that correspond to the loss of water and an ethyl group as either ethene ($[C_9H_{10}N]^+$, *m/z* 132.08), a radical species

($[C_9H_9N]^{\bullet+}$, *m/z* 131.07), or an even-electron species ($[C_9H_8N]^+$, *m/z* 130.07). Fragments from this series are observed at all collision potentials, although they are most dominant at 20 V. Given the structure of buphedrone, the ethyl group loss may result from a cleavage of the ethyl side chain at the alpha position. However, this cannot be confirmed from the data presented here.

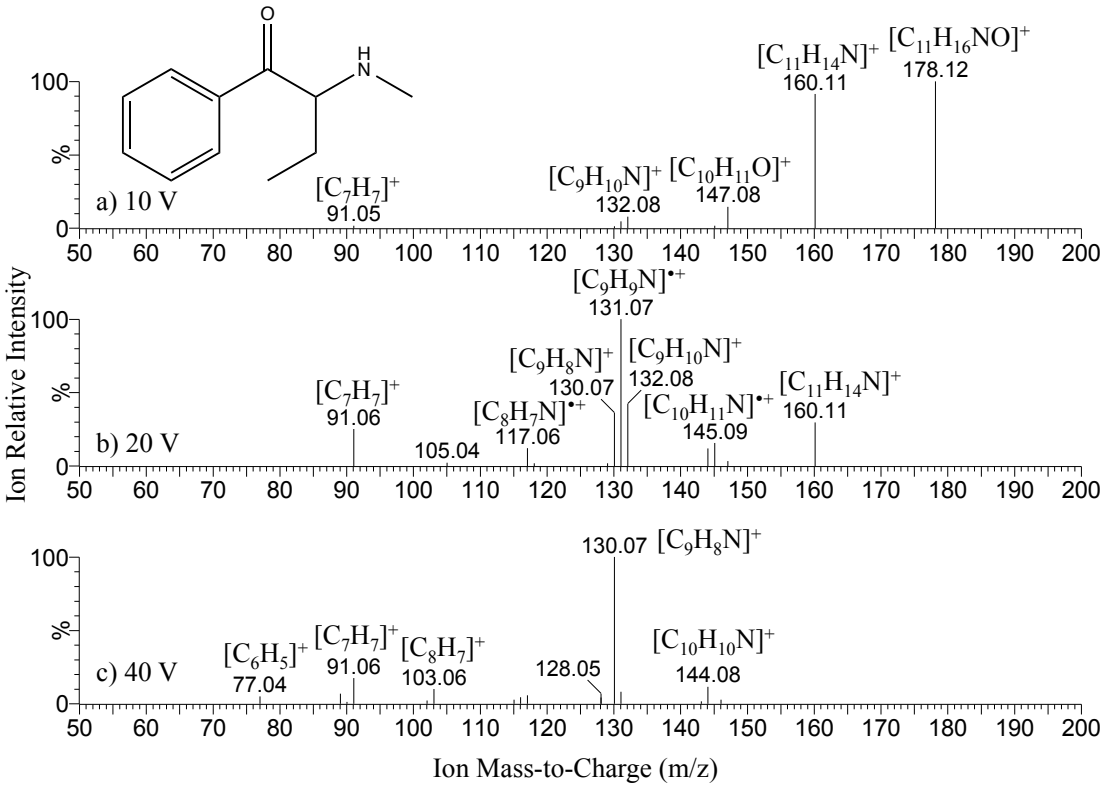

Figure 2.4. CID-MS spectra for the cathinone buphedrone at collision potentials of a) 10 V, b) 20 V, and c) 40 V. All spectra collected in positive-ion mode.

Although present at a lower abundance, a similar series of odd- and even-electron fragments results from the loss of water and a methyl group in buphedrone. These fragments occur with the methyl group lost as either a radical species ($[C_{10}H_{11}N]^{\bullet+}$, *m/z* 145.09) or methane ($[C_{10}H_{10}N]^+$, *m/z* 144.08). This methyl could be the result of cleavage

of the methyl substitution on the amine group or as a loss of part of the side chain at the alpha position. It is likely that this fragment is due to a combination of the two pathways.

While these two series of radical and even-electron losses become more prominent with increasing collision potentials, they have not been previously reported among cathinone fragmentation. For these to be considered distinguishing or characteristic fragments for cathinones, the fragments would need to be present in multiple cathinones. Continuing the trend observed, these combined loss of water and an alkyl group is also observed in 3-methylbuphedrone (Figure 2.5).

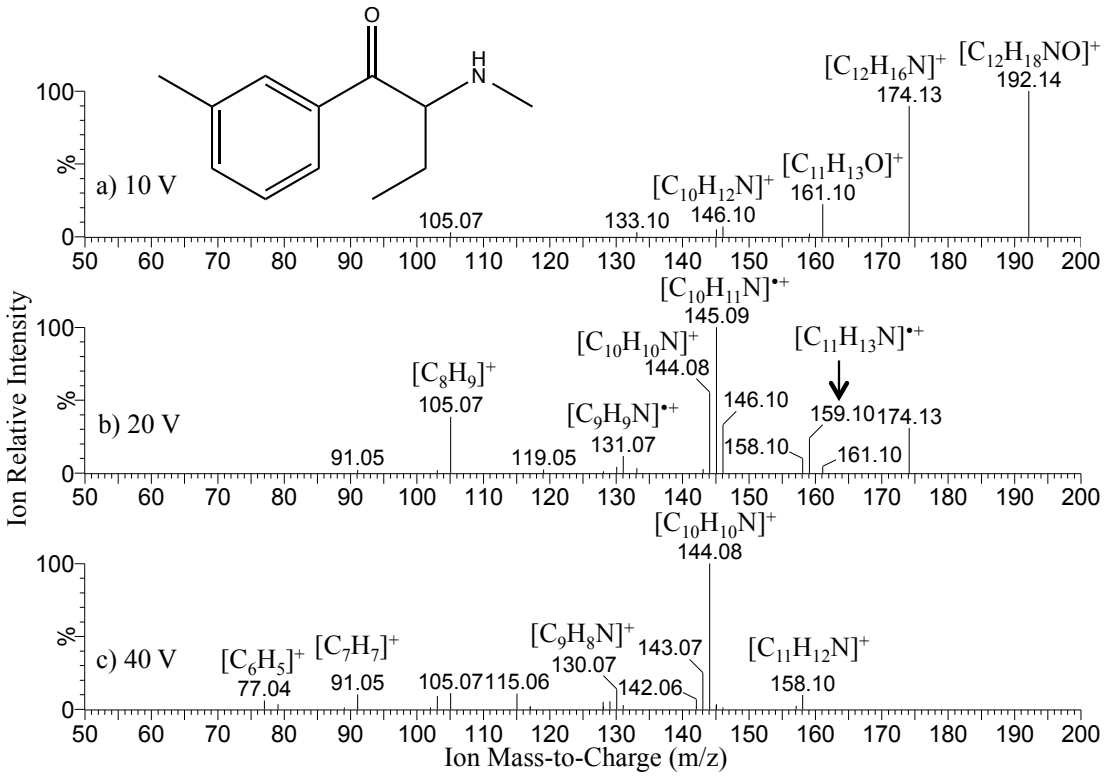

Figure 2.5. CID-MS spectra for 3-methylbuphedrone at collision potentials of a) 10 V, b) 20 V and c) 40 V. All spectra were collected in positive-ion mode.

The chemical structure of 3-methylbuphedrone, as well as representative mass spectra collected using collision potentials of 10, 20, and 40 V, are shown in Figure 2.5. With increasing collision potential, 3-methylbuphedrone yields similar fragments as buphedrone with the base peaks at 20 and 40 V corresponding to the combined loss of water and an ethyl group as either a radical ethyl group ($[C_{10}H_{11}N]^{\bullet+}$, *m/z* 145.09) or ethane ($[C_{10}H_{10}N]^{+}$, *m/z* 144.08), respectively. The loss of water and the methyl substituent as either a radical methyl group ($[C_{11}H_{13}N]^{\bullet+}$, *m/z* 159.10) or methane ($[C_{11}H_{12}N]^{+}$, *m/z* 158.10) is also observed. While these fragments correspond to the same neutral losses as observed in buphedrone, the fragments in 3-methylbuphedrone are evident at *m/z* values ~14 Da higher because of the added mass of the methyl ring substitution.

While not observed in buphedrone, the fragment ion corresponding to the combined loss of water, an ethyl group, and a methyl group is present in 3-methylbuphedrone as both the radical fragment $[C_9H_9N]^{\bullet+}$ (*m/z* 131.07) at 20 V and even-electron fragment $[C_9H_8N]^{+}$ (*m/z* 130.07) at 40 V. In 3-methylbuphedrone, the methyl group lost in these fragments could be from either the amine group or the aromatic ring. This loss does not readily occur in buphedrone, which has a similar methyl substitution on the amine, so it is more likely that the aromatic methyl group is being lost during this fragmentation.

These odd- and even-electron fragment ions are not specific to buphedrone and 3-methylbuphedrone. Analogous ions are also observed in CID mass spectra of butylone (Figure 2.6, discussed in detail in the following section) and structural isomers of these three cathinones (discussed in detail in Chapter 3). However, these are not observed in

the other cathinones investigated in this study. Spectra of all cathinones are included in Appendix A. Given that the loss of water involves the migration of a hydrogen from the amine group and this series of fragments requires the loss of water, these fragments do not occur when the amine group is a tertiary amine. Thus, the absence of these fragments in the cathinone standards with tertiary amines (naphyrone, alpha-phthalimidopropiophenone, alpha-pyrrolidinopropiophenone, and alpha-piperidinobutiophenone) is unsurprising (Figure 2.1). In MTTA, the amine group is one carbon further from the ketone than in a typical cathinone. The loss of water requires a hydrogen migration from the amine to the oxygen on the ketone, a migration that requires physical proximity. The longer carbon chain between the ketone and amine inhibits this migration so the loss of water does not readily occur. The remaining cathinone, benzedrone, has a secondary amine with a methyl-benzyl group substitution. Like other cathinones with secondary amines, benzedrone does readily lose water. However, benzedrone can fragment at either the ketone-aromatic bond or the methylbenzene-amine bond to form a methyl-substituted aromatic ring as the charged species $[C_7H_7]^+$. This ion is resonance stabilized and dominates the higher collision potentials. The combined loss of water and an aliphatic group present in other cathinones with secondary amines is not observed.

As with the other cathinone fragments reported in the literature (7, 24), the loss of water and aliphatic species as both radical and even-electron species at 20 and 40 V is not common among all cathinones. However, this neutral loss composition could be used as an indication of cathinones with aliphatic substitutions and a primary or secondary amine.

2.3.1.3 Fragmentation of methylenedioxy-substituted cathinones at increased collision potentials

As a comparison to the aliphatic-substituted cathinones buphedrone and 3-methylbuphedrone, butylone has the same amine and alpha-carbon substitutions but differs with the presence of a methylenedioxy substitution on the ring. The chemical structure for butylone as well as representative mass spectra collected using collision potentials of 10, 20, and 40 V are shown in Figure 2.6. The ion corresponding to a neutral loss of 48 Da ($H_2O + CH_2O$) at 10 V ($[C_{11}H_{12}NO]^+$, *m/z* 174.09) is observed at 10 V and has been previously noted to indicate a methylenedioxy substitution on the aromatic ring (25). However, there are additional fragments that further distinguish this methylenedioxy-substituted cathinone from those with aliphatic substitutions and can be used to identify structural features associated with methylenedioxy substitutions.

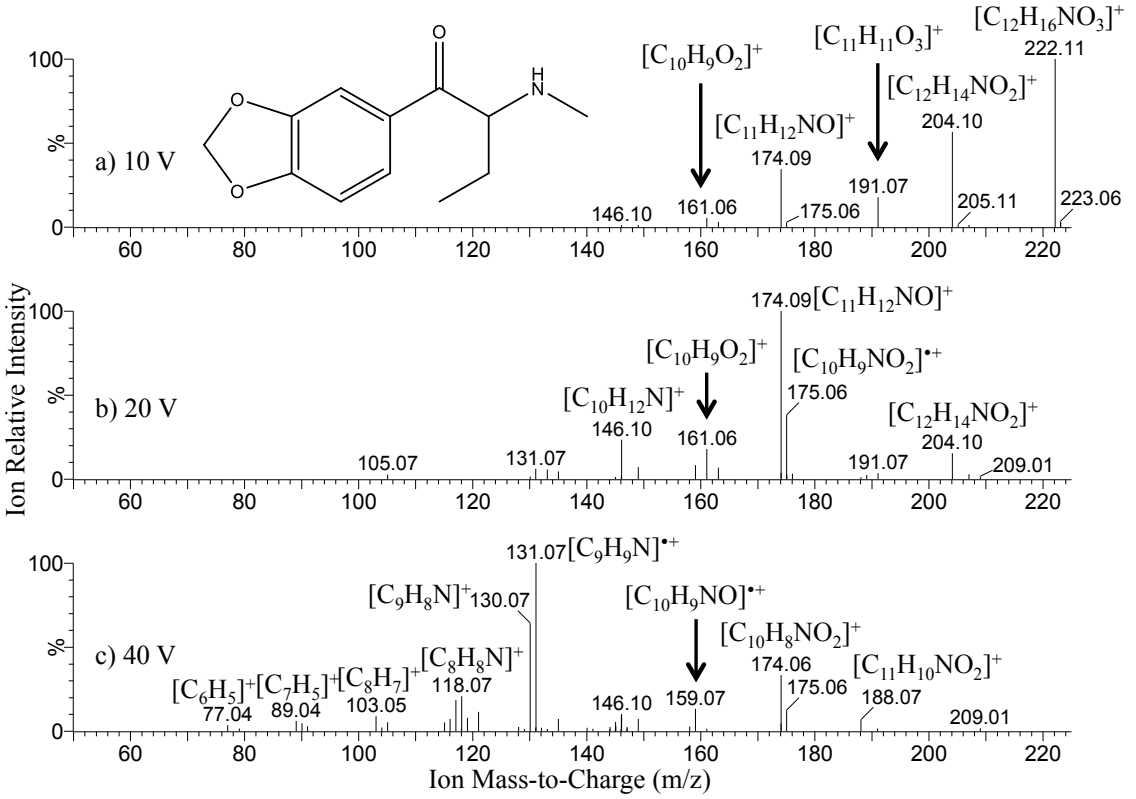

Figure 2.6. CID-MS spectra for butylone at collision potentials of a) 10 V, b) 20 V and c) 40 V. All spectra were collected in positive-ion mode.

One fragment not previously discussed is present at *m/z* 161.06 in the 10 and 20 V spectra of butylone (7, 27). This fragment corresponds to $[C_{10}H_9O_2]^+$ with an associated neutral loss of C_2H_7NO from $[M+H]^+$. Given the structure of butylone (Figure 2.6.a), there is no single bond cleavage that would result in this loss, so the loss is most likely due to a series of multiple fragmentation steps and rearrangements. One potential series of losses involves the combined loss of both the methylamine group (CH_5N) as well as the loss of formaldehyde (CH_2O) from a partial cleavage of the methylenedioxy ring. The order of this series of losses cannot be confirmed from this data, although protonation of

the methylenedioxy group is more favorable. Protonation of the methyl group on the aromatic ring in 3-methylbuphedrone is not likely, so a similar fragmentation pathway involving the neutral loss of methylamine and a methyl group from the aromatic ring was not observed in 3-methylbuphedrone. Thus, the fragmentation pathway leading to the neutral loss of C2H7NO from butylone depends on the presence of the methylenedioxy group on the aromatic ring.

As the collision potential increases and more extensive fragmentation occurs, additional differences between butylone and the aliphatic-substituted cathinones are observed. The fragments corresponding to the combined loss of water and an ethyl group, as observed in buphedrone and 3-methylbuphedrone, are also present in butylone at *m/z* 175.06 ($[C_{10}H_9NO_2]^{\bullet+}$) and *m/z* 174.06 ($[C_{10}H_8NO_2]^+$). However, these are present at lower abundances in butylone than observed in buphedrone and 3-methylbuphedrone. Notably, the base peak for butylone at 20 V corresponds to the loss of 48 Da (H_2O + CH_2O) rather than the combined water and ethyl group loss. As observed with the loss of methylamine and formaldehyde, the oxygens substituted on the aromatic ring provide sites of protonation not present in buphedrone and 3-methylbuphedrone and lead to alternate routes of fragmentation. In the case of butylone at 20 V, the fragments formed through protonation and fragmentation of the ring substitution are present at higher abundances than those produced through protonation of the ketone or amine.

Additionally, the fragments corresponding to the loss of water and a methyl group or those for the loss of water, an ethyl group, and a methyl group are not observed in butylone. This indicates that the pathway for fragmentation that leads to these water and alkyl group losses is altered by the presence of the methylenedioxy group, which

provides more favorable losses. One of these butylone-specific losses is present as the base peak at 40 V, which corresponds to the combined odd-electron loss of water, formaldehyde, carbon monoxide, and a methyl group ($[C_9H_9N]^{\bullet+}$, *m/z* 131.07). Much like in the water and alkyl losses of buphedrone and 3-methylbuphedrone, there is likely rearrangement of the molecule during fragmentation, although the resulting losses here indicate different rearrangements are occurring in butylone.

The comparison between buphedrone and 3-methylbuphedrone indicates that similar structures yield analogous fragment ions. However, the differences in the number and length of the alkyl chain substitution can still lead to fragment ions that allow distinction between the cathinones, even when the same pathway is followed. The comparison of CID mass spectra of buphedrone at the multiple collision energies with those of butylone also demonstrates that, although they share a common core structure, some substitutions can lead to different pathways. These differences in fragmentation allow structural features unique to each cathinone to be identified and can aid in the identification of new analogs.

2.3.2 Comparison of the fragmentation of cathinones and phenethylamines

The variation in fragmentation observed in cathinones that contain different functional group substitutions can present an issue when distinguishing cathinones from other designer drugs with similar core structures. This is especially true with phenethylamines, whose core structure differs only by the lack of the ketone group. Additionally, phenethylamines are often substituted with the same functional groups at analogous positions as in the cathinones. To investigate how these classes of designer

drugs can be distinguished from each other, the cathinone buphedrone is compared to the phenethylamine 2-methylamino-1-phenylbutane which has analogous functional group substitutions.

2.3.2.1 Comparison of buphedrone and 2-methylamino-1-phenylbutane

Buphedrone fragmentation has been already discussed in section 2.3.1 (Figure 2.4), but several features are of note here. First, the most abundant ions observed at 10 V correspond to $[M+H]^+$, the loss of water, and the loss of methylamine. However, the base peaks in the spectra collected at 20 and 40 V correspond to the loss of water plus the ethyl group as odd- or even-electron species. Additionally, the range of fragment ions grows increasingly complex as the collision potential increases.

The chemical structure for 2-methylamino-1-phenylbutane as well as representative mass spectra collected using collision potentials of 10, 20, and 40 V are shown in Figure 2.7. Although the difference in structure between 2-methylamino-1-phenylbutane and buphedrone is only in the presence of the beta-ketone, the fragmentation patterns of these compounds are markedly different. With no oxygen present, 2-methylamino-1-phenylbutane does not (and cannot) lose water and the extent of structural rearrangements is more limited, even at the highest collision potential. The fragments that are present in 2-methylamino-1-phenylbutane are driven by the protonated amine and indicate structural features common to both 2-methylamino-1-phenylbutane and buphedrone. For example, the fragment $[C_{10}H_{13}]^+$ (*m/z* 133.10) in 2-methylamino-1-phenylbutane corresponds to the loss of the methylamine, while $[C_7H_7]^+$ (*m/z* 91.05) and $[C_5H_5]^+$ (*m/z* 65.04) indicates the presence of an aromatic ring. These substructures are

present in both buphedrone and 2-methylamino-1-phenylbutane. However, with the ketone in buphedrone providing an alternate site of protonation, the extent of fragmentation and additional losses in buphedrone can be used to distinguish these two drugs.

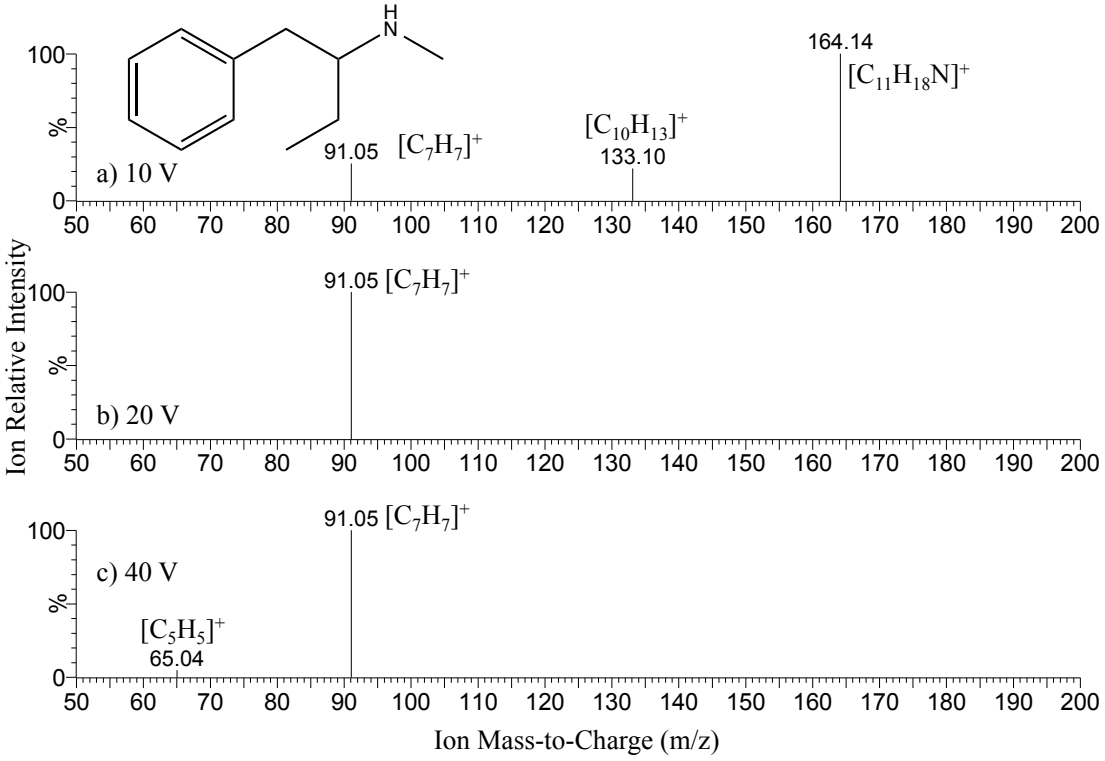

Figure 2.7. CID-MS spectra for the phenethylamine 2-methylamino-1-phenylbutane at collision potentials of a) 10 V, b) 20 V, and c) 40 V. All spectra collected in positive-ion mode.

2.3.2.2 Additional phenethylamine (2C-E) and overall comparison

While the spectra for 2-methylamino-1-phenylbutane may suggest that extremely simple fragmentation patterns are common among phenethylamines, there can be extensive fragmentation when the phenethylamine is more intricately substituted. As an

example, the chemical structure for the phenethylamine 2,5-dimethoxyethylamphetamine (2C-E) as well as representative mass spectra collected using collision potentials of 10, 20, and 40 V are shown in Figure 2.8. For 2C-E, the 10 V spectrum remains simple, with the most abundant ions corresponding to the protonated molecule ($[C_{12}H_{20}NO_2]^+$, *m/z* 210.15), loss of ammonia ($[C_{12}H_{17}O_2]^+$, *m/z* 193.12), and loss of ammonia plus a methyl radical ($[C_{11}H_{14}O_2]^{\bullet+}$, *m/z* 178.10). The loss of ammonia plus ethene ($[C_{10}H_{13}O_2]^+$, *m/z* 165.10) is also present, albeit at low relative abundance (1.1%). These fragmentation pathways are driven by protonation of the nitrogen in the amine group, a more polar site than the oxygens in the ether functional groups of the methoxy substitutions. Thus, these pathways are more common among phenethylamines than cathinones since the ketone group of the cathinones is the more favorable site of protonation.

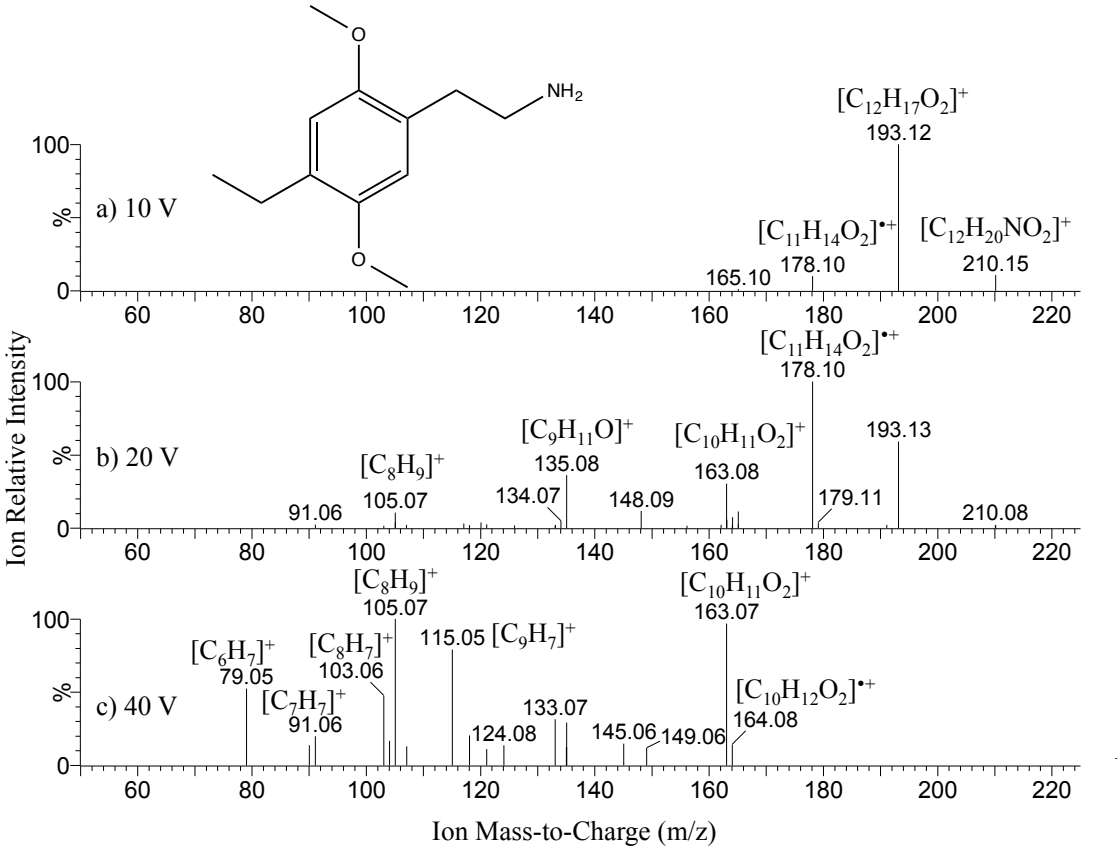

Figure 2.8. CID-MS spectra for the phenethylamine 2C-E at collision potentials of a) 10 V, b) 20 V, and c) 40 V. All spectra collected in positive-ion mode.

With increased collision potential again comes more extensive fragmentation for 2C-E. While some of these fragments are indicators of the aromatic ring (*e.g.* $[C_7H_7]^+$ at *m/z* 91.06 and $[C_6H_7]^+$ at *m/z* 79.05), most fragments for 2C-E at 20 and 40 V are the result of multiple losses and rearrangements. This observation is analogous to fragmentation observed in the cathinones discussed in section 2.3.1 However, a main difference between these compounds is that the loss of water from the ketone group is the most abundant loss observed in the cathinones at 10 V, while the loss of the amine group

dominates for the phenethylamines, according to the acidity of the site of protonation. Overall, these differences provide the basis for a classification scheme to facilitate distinction of cathinones from phenethylamines.

2.3.3 Cathinone and phenethylamine classification

2.3.3.1 Development of a classification scheme

Given that the cathinone and phenethylamine classes include a variety of possible functional groups as substitutions, a training set of nine cathinones and seven phenethylamines was selected to represent a range of possible structures (Figures 2.1.a.-i. and 2.2.a.-f., respectively). The spectra at 10 V for the phenethylamines (Figure 2.9) and cathinones (Figure 2.10.) were initially interrogated to identify the molecular formulae for ions of highest abundance. Of specific interest were the ion compositions or corresponding neutral losses that were specific to only one of the two drug classes. Once identified, these provided a foundation for the generation of a classification scheme. As seen with the phenethylamine 2C-E discussed in the previous section, the base peak for the all three 2C phenethylamines (2C-E, 2C-B, and 2C-T; Figure 2.9.a-c, respectively) corresponds to the loss of the amine group rather than the protonated molecular ion, denoted $[M+H]^+$. Thus, these compounds can be distinguished from the rest of the training set based on that characteristic.

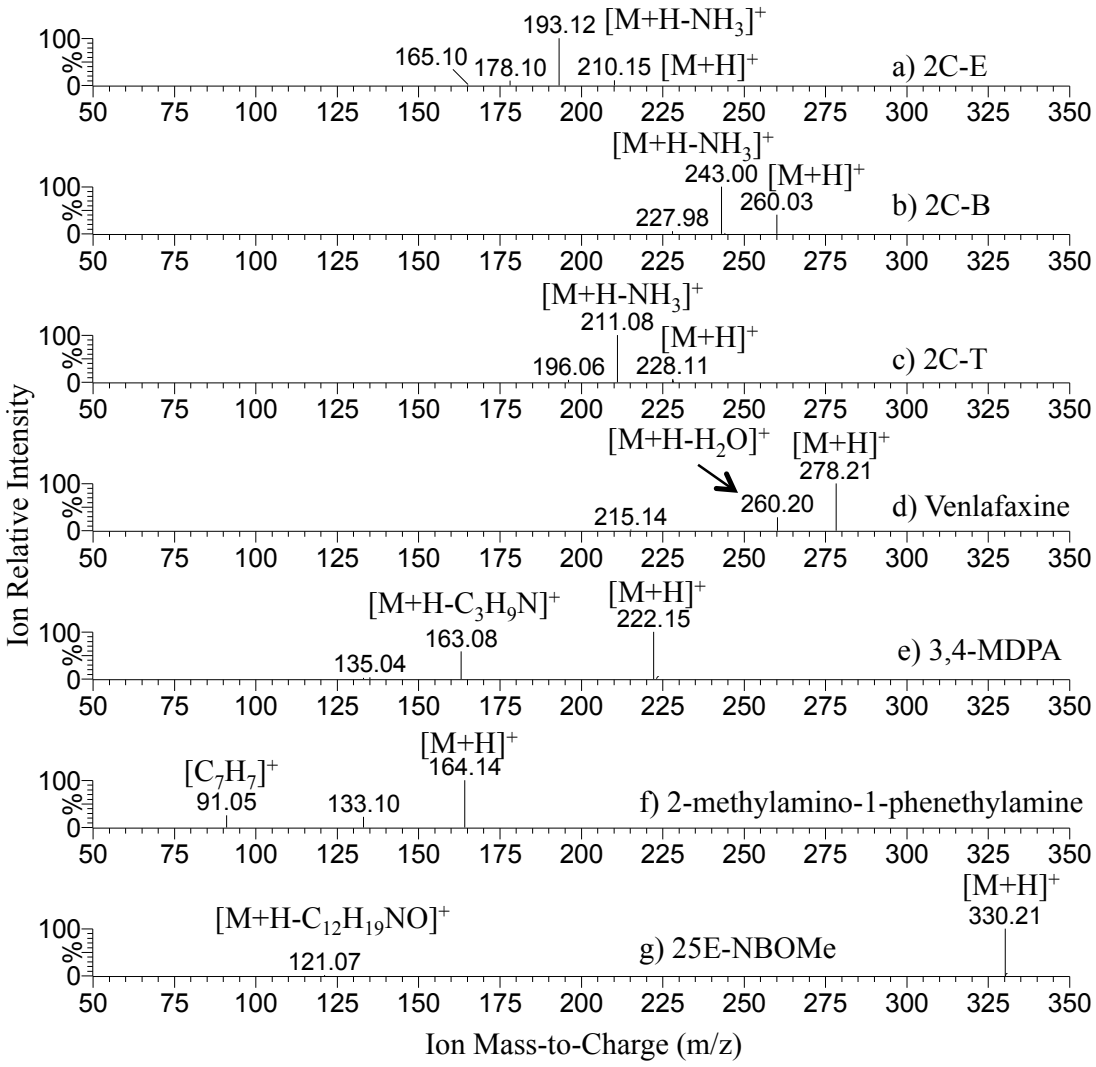

Figure 2.9. CID-MS spectra of the training set phenethylamines collected in positive mode at a collision potential of 10 V.

The remaining compounds in the training set all have $[M+H]^+$ as the base peak. Of those compounds with $[M+H]^+$ as the base peak, one phenethylamine (venlafaxine, Figure 2.9.d) and five of the cathinones (α-phthalimidopropiophenone, butylone, buphedrone, 3-methylbuphedrone, and benzedrone; Figures 2.10.a-e, respectively) have the fragment corresponding to the loss of water as the 2nd most abundant ion at 10 V. For

these cathinones and phenethylamine, their base peaks at 20 V can be used to distinguish between them (Figure 2.11.). The only phenethylamine in this grouping, venlafaxine, differs from the other phenethylamines in that it has an alcohol group that gives rise to the loss of water at 10 V, a loss that is not otherwise observed among phenethylamines in the training set. To differentiate venlafaxine from cathinones with similar base peak at 10 V, the base peak at 20 V can be used. At 20 V, venlafaxine fragments to leave the ion $[C_8H_9O]^+$ as the base peak (Figure 2.11.a), a fragment and corresponding neutral loss ($C_9H_{19}NO$) that is unique among this group of compounds to venlafaxine, differentiating it from the cathinones. The base peaks for the five cathinones at 20 V vary in composition and include fragment ions corresponding to the loss of water in α-phthalimidopropiophenone (Figure 2.11.b), the combined loss of water and formaldehyde in butylone (Figure 2.11.c), and the combined loss of water and an alkyl radical in buphedrone and 3-methylbuphedrone (Figure 2.11.d-e). The $[C_7H_7]^+$ ion, an indicator of an aromatic ring, is also the base peak for benzedrone at 20 V (Figure 2.11.f).

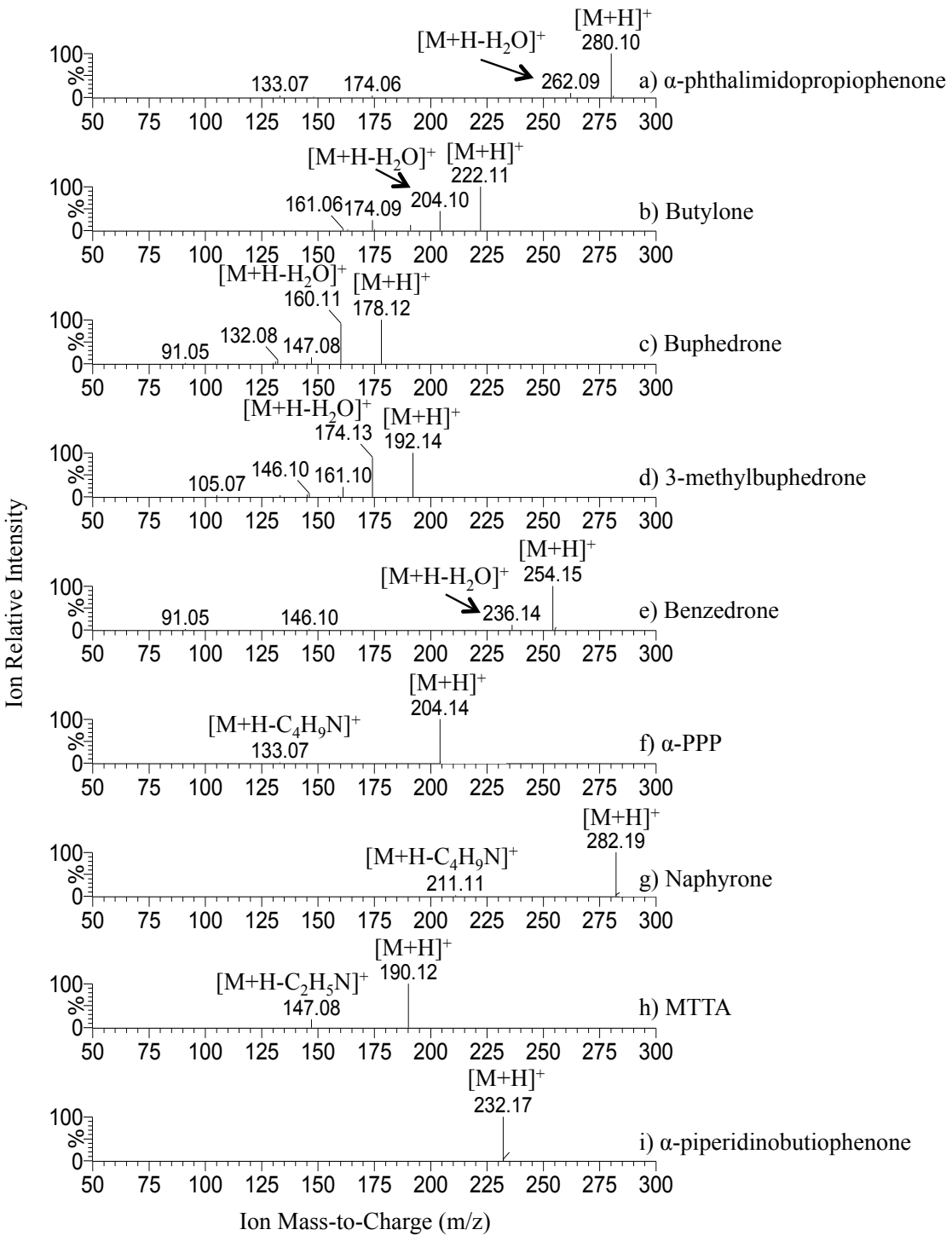

Figure 2.10. CID-MS spectra of the training set cathinones collected in positive mode at a collision potential of 10 V.

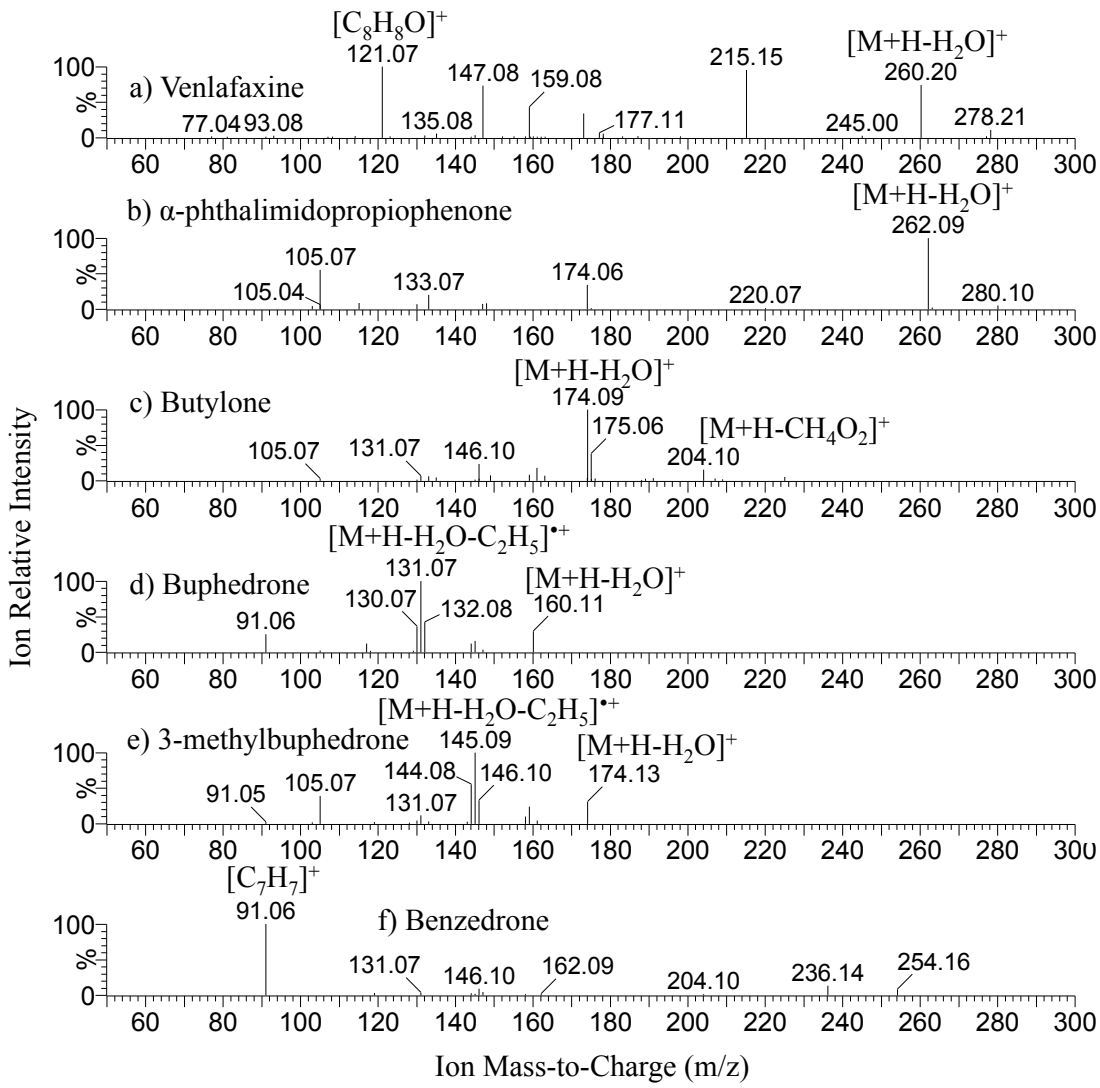

Figure 2.11. CID-MS spectra of one phenethylamine and five cathinones from the training set collected in positive mode at a collision potential of 20 V.

The remaining compounds in the training set compounds are the phenethylamines 3,4-MDPA, 2-methylamino-1-phenylbutane and 25E-NBOMe (Figure 2.9.e-g, respectively) and the cathinones α-PPP, naphyrone, MTTA and α-piperidinobutiophenone (Figure 2.10.f-i, respectively). These compounds have $[M+H]^+$ as the base peak but do not have the fragment corresponding to the loss of water as the

second most abundant ion. Like the 2C compounds, the phenethylamines 3,4-MDPA and 2-methylamino-1-phenylbutane also lose their amine group, although this peak is second in abundance to the molecular ion (Figure 2.9.e-f). The second most abundant ion for the remaining phenethylamine, 25E-NBOMe, at 10 V also results from the cleavage at the amine bond (Figure 2.9.g). However, the NBOMe series of phenethylamines have a second aromatic ring connected via the amine group and the most abundant fragment ion corresponds to a cleavage at the amine with the charge on this second aromatic rather than the one associated with the phenethylamine core structure. This is a driven by the location of protonation - the nitrogen of the amine group. Charge-directed fragmentation at the location of protonation is more kinetically favorable than a charge-remote fragmentation of the other aromatic ring. Since the resulting fragment ions, both charged aromatic rings, have the same resonance stability, it is the charge-directed fragmentation that dominates.

The 2nd most abundant ion for the cathinones α-PPP, naphyrone, and MTTA corresponds to the loss of their substituted amine group (Figure 2.10.f-h). The amine groups in α-PPP and naphyrone are pyrrolidines, or 5-membered rings that include the nitrogen, so there is no hydrogen on the amine group to facilitate the water loss observed in other cathinones. While there are other hydrogens present in the molecule, those on the nitrogen are more acidic (weaker held) than those bonded to carbons. Thus, it is not thermodynamically favorable for a hydrogen migration to occur from an alkyl chain to facilitate water loss.

Although classified as a cathinone, the amine group in MTTA is one alkyl chain length farther from the ketone than in the typical cathinone. As noted previously, the loss

of water is also facilitated by the proximity of the ketone to the amine, then this increased spacing is consistent with the amine loss for MTTA being the second most abundant ion at 10 V (Figure 2.10.h). Interestingly, α-piperidinobutiophenone did not produce any fragments greater than 1% relative abundance at 10 V (Figure 2.10.i) and the only ion present is the $[M+H]^+$ (no fragments observed). Leveraging all of these mass spectral features, an initial scheme for classification was built (Figure 2.12).

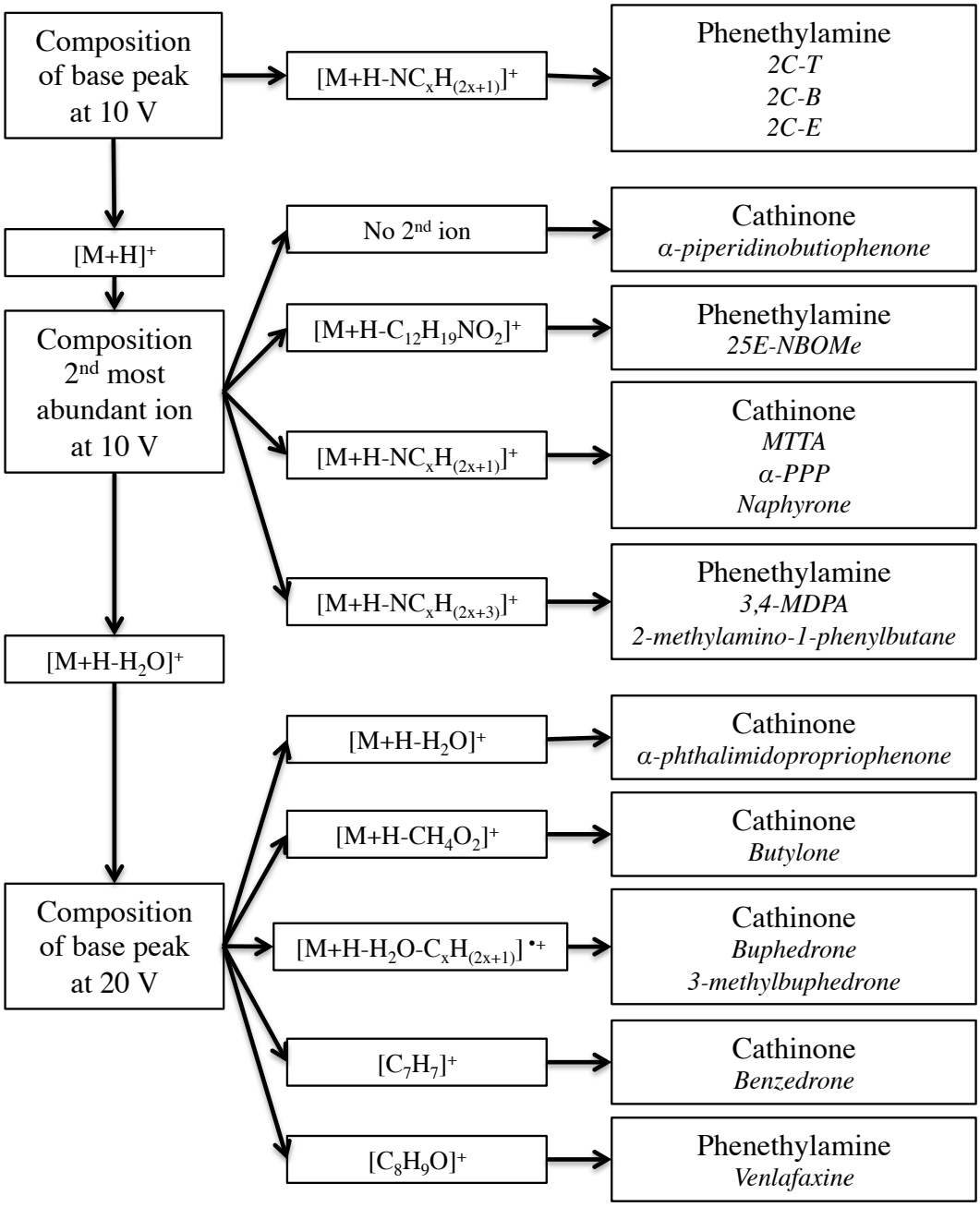

Figure 2.12. Scheme for cathinone and phenethylamine class identification using the most abundant ions present in the 10 and 20 V spectra.

2.3.3.2 Testing of the classification scheme

While the scheme in Figure 2.12 correctly assigns the cathinones and phenethylamines in the training set of compounds, this must be tested for use with an additional set of compounds. A test set containing six isomers of compounds was analyzed, including five cathinones and one phenethylamine, the structures of which can be seen in Figures 2.1.j.-n and 2.2.g, respectively. The mass spectra for each compound at collision potentials of 10 V and, when needed, 20 V (Figure 2.13) were used to classify each compound according the scheme. The results of the classification are outlined below and summarized in Figure 2.14.

Three compounds in the test set were correctly assigned. The base peak for the phenethylamine 2C-G at 10 V corresponds to the loss of the amine group (Figure 2.13.a). This is consistent with the 2C phenethylamines in the training set of compounds, so 2C-G was correctly classified 2C-G as a phenethylamine. The base peak at 10 V for both cathinones 3-ethylmethcathinone and ethylone (Figure 2.13.b and d, respectively) is the molecular ion and both have the fragment corresponding to the loss of water as the 2nd most abundant ion. At 20 V, the base peak for 3-ethylmethcathinone corresponds to the loss of water and an ethyl group as a radical (Figure 2.13.c). This classifies 3-ethylmethcathinone similarly to its isomer buphedrone and correctly assigns it as a cathinone. For ethylone, the base peak at 20 V corresponds to the combined loss of water and formaldehyde (Figure 2.13.e). This is similar to the fragmentation in butylone and correctly assigns ethylone as a cathinone.

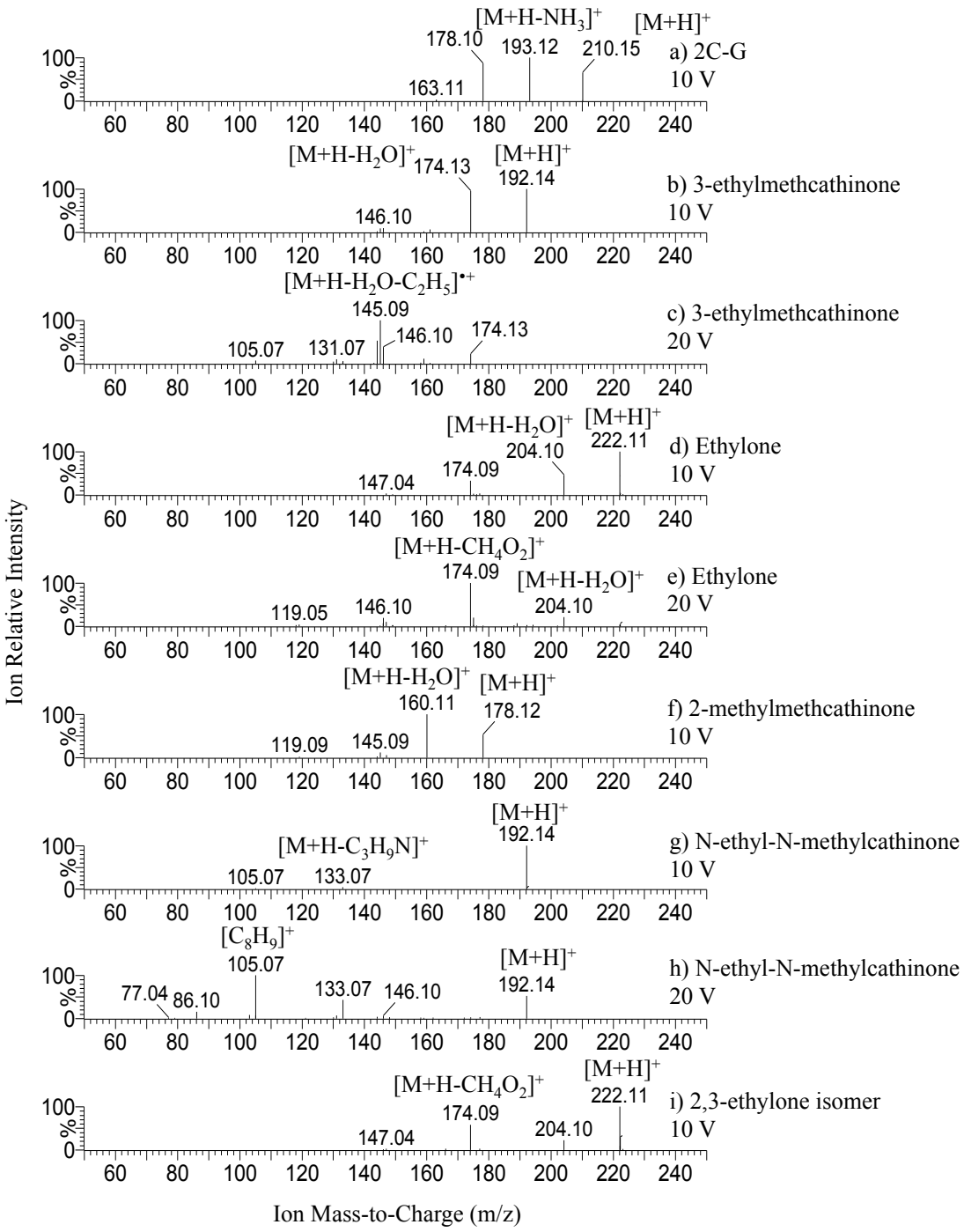

Figure 2.13. CID-MS spectra of one phenethylamine and five cathinones from the test set collected in positive mode at collision potentials of 10 and 20 V.

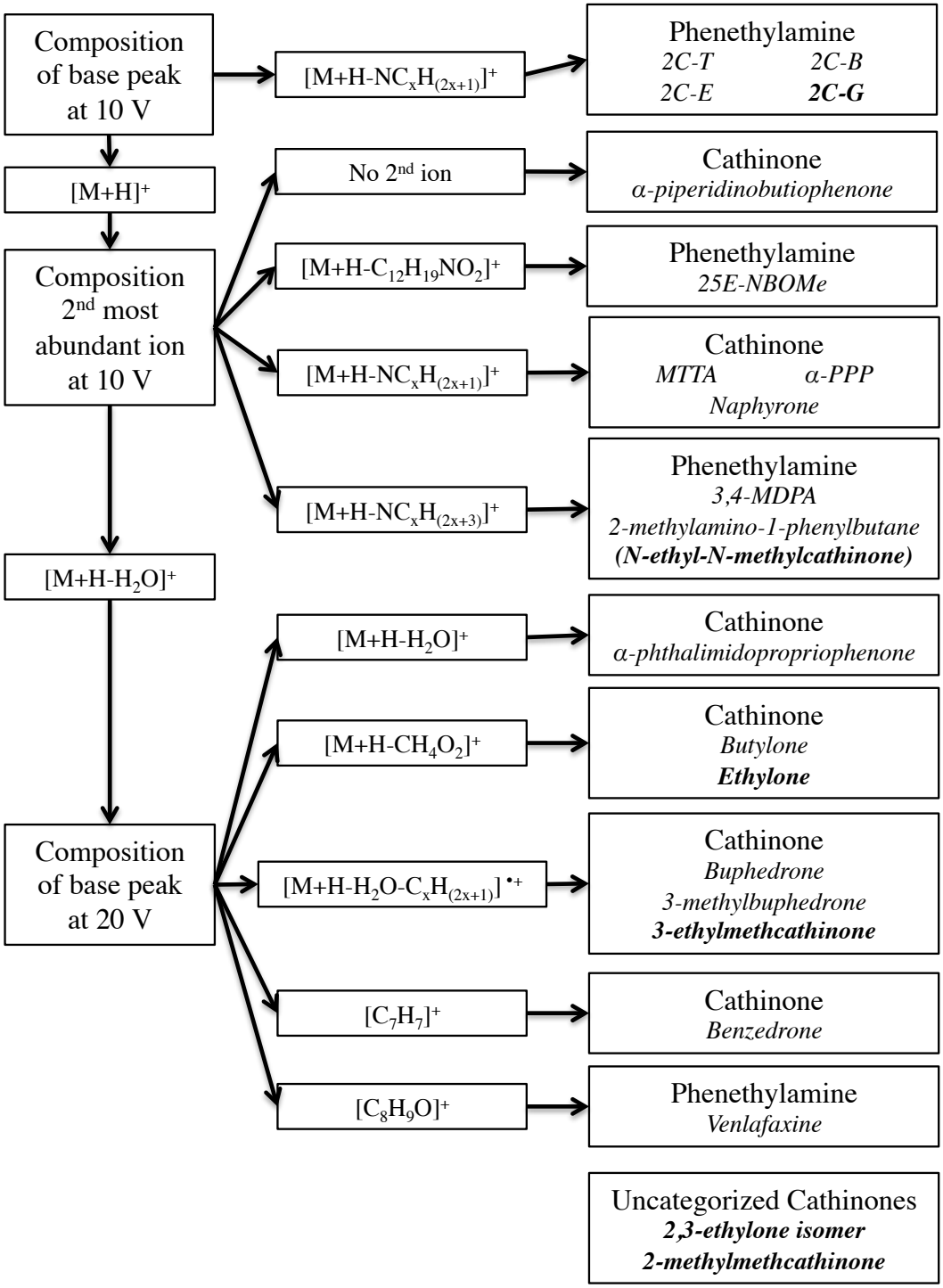

Figure 2.14. Scheme for cathinone and phenethylamine class identification from Figure 2.12 with the addition of the test set of isomers (in bold). Incorrect assignments are indicated by parentheses.

Following the same method for classification, the cathinone *N*-ethyl-*N*-methylcathinone is incorrectly categorized as a phenethylamine. Like other cathinones, $[M+H]^+$ is the base peak at 10 V for *N*-ethyl-*N*-methylcathinone (Figure 2.13.g). However, the second most abundant ion corresponds to the loss of the amine in the form of $NC_xH_{(2x+3)}$. This incorrectly categorizes *N*-ethyl-*N*-methylcathinone as a phenethylamine. To differentiate *N*-ethyl-*N*-methylcathinone from 2-methylamino-1-phenylbutane and 3,4-MDPA, the base peak at 20 V can be used. The base peaks for 2-methylamino-1-phenylbutane and 3,4-MDPA correspond to the amine loss (Figures B.1. and B.7. in the Appendix) while the base peak for *N*-ethyl-*N*-methylcathinone corresponds to an ethyl-substituted aromatic species, $[C_8H_9]^+$(Figure 2.13.h). The classification scheme will be revised to reflect this difference and correctly classify *N*-ethyl-*N*-methylcathinone as a cathinone.

In addition to the incorrectly classified cathinone, two cathinones, 2-methylmethcathinone and the 2,3-ethylone isomer, were categorized as neither a cathinone nor a phenethylamine using the scheme produced by the training set. Unlike other cathinones, the base peak at 10 V for 2-methylmethcathinone corresponds to the loss of water (Figure 2.13.f). While this fragment is commonly observed in cathinones, the loss of water was at a lower abundance than $[M+H]^+$ in other cathinones. An additional path through the flowchart can be added to classify 2-methylmethcathinone based on the fragment corresponding to the loss of water as a base peak. The other unclassified cathinone, the 2,3-ethylone isomer, is similar to its isomers butylone and ethylone in that the base peak for the 2,3-ethylone isomer at 10 V is $[M+H]^+$ (Figure 2.13.i). However, the next most abundant ion does not correspond to the loss of water but

rather corresponds to the combined loss of water and formaldehyde. While the combined loss of water and formaldehyde distinguishes butylone and ethylone from other cathinones as the base peak at 20 V, the classification scheme must be adjusted to add an option of this loss as the second most abundant ion at 10 V to correctly classify the 2,3-ethylone isomer as a cathinone.

The alterations described above were added to the classification scheme to properly identify all compounds in the test set as either phenethylamines or cathinones. The revised scheme is shown in Figure 2.15.

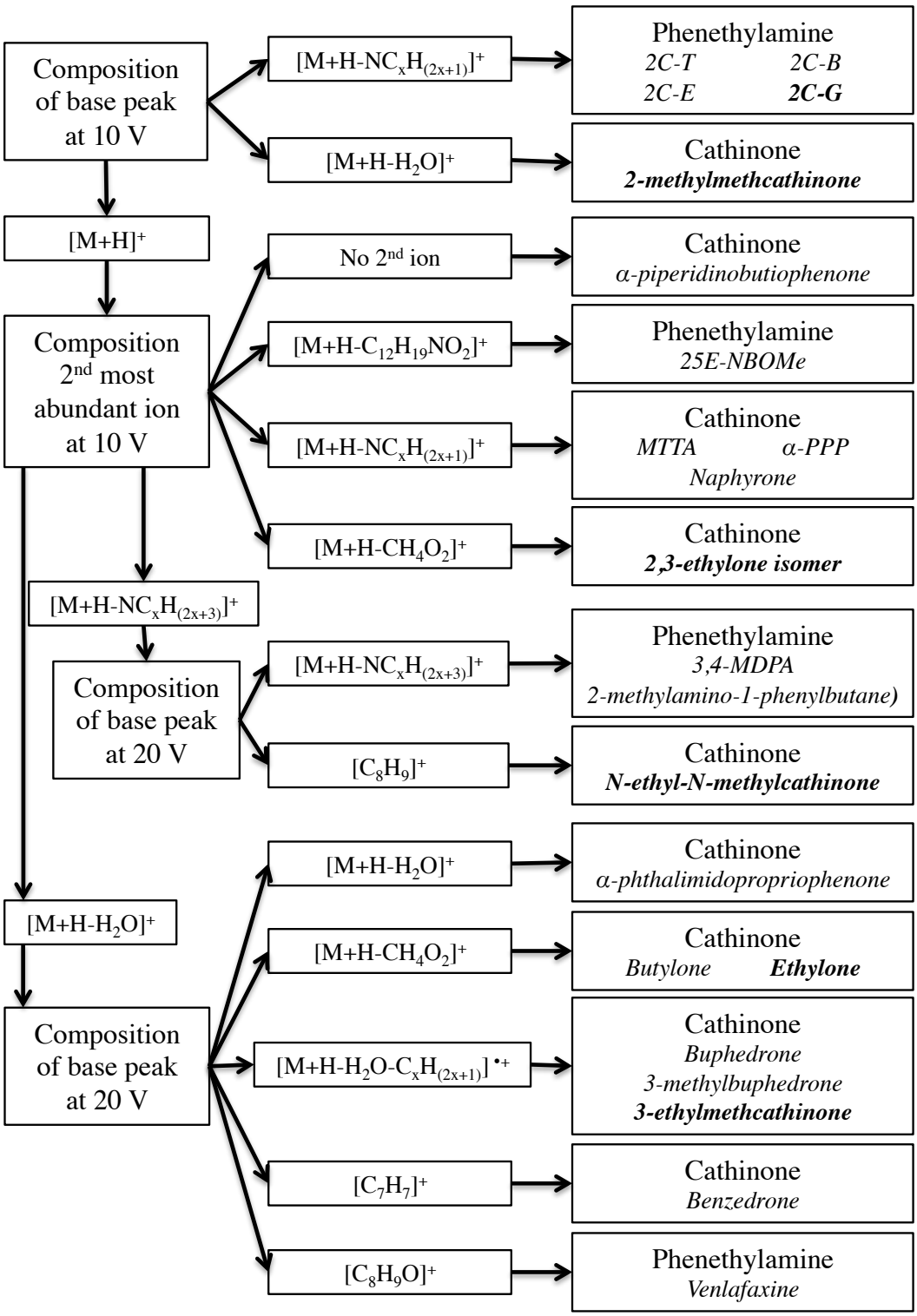

Figure 2.15. Revised scheme for cathinone and phenethylamine identification using the most abundant ions present in the 10 and 20 V spectra.

2.3.3.3 Literature comparison of the revised classification scheme

As an additional test for the revised scheme, spectra of cathinones and phenethylamines analyzed by CID-MS techniques and published in three different studies in the literature were assessed. These studies used a variety of cathinone and phenethylamine standards (Figure 2.16) analyzed by different instruments and under varying CID-MS conditions. The use of spectra from the literature gives an indication of how accurate this classification scheme is when used by other laboratories.

In the first of these studies, Welter *et al.* used CID-MS to identify the phenethylamines 6-APB and 6-MAPB, along with their associated 5-isomers, acetylated ions, and metabolites from urine samples (30). The CID-MS spectra of unacetylated 6-APB and 6-MAPB standards were presented. However, the exact collision potential used was not clear but is presumed to not have varied between samples. From the published spectra, the base peaks for 6-APB and 6-MAPB were identified to correspond to losses of C_2H_7N and CH_5N, respectively, from $[M+H]^+$. Using the revised scheme in Figure 2.15, these base peaks would correctly classify these compounds as phenethylamines. While the collision potential used was unclear, the correct assignment of these phenethylamines using the reported spectra is a positive indicator that this scheme can be used to correctly assign spectra obtained across multiple laboratories.

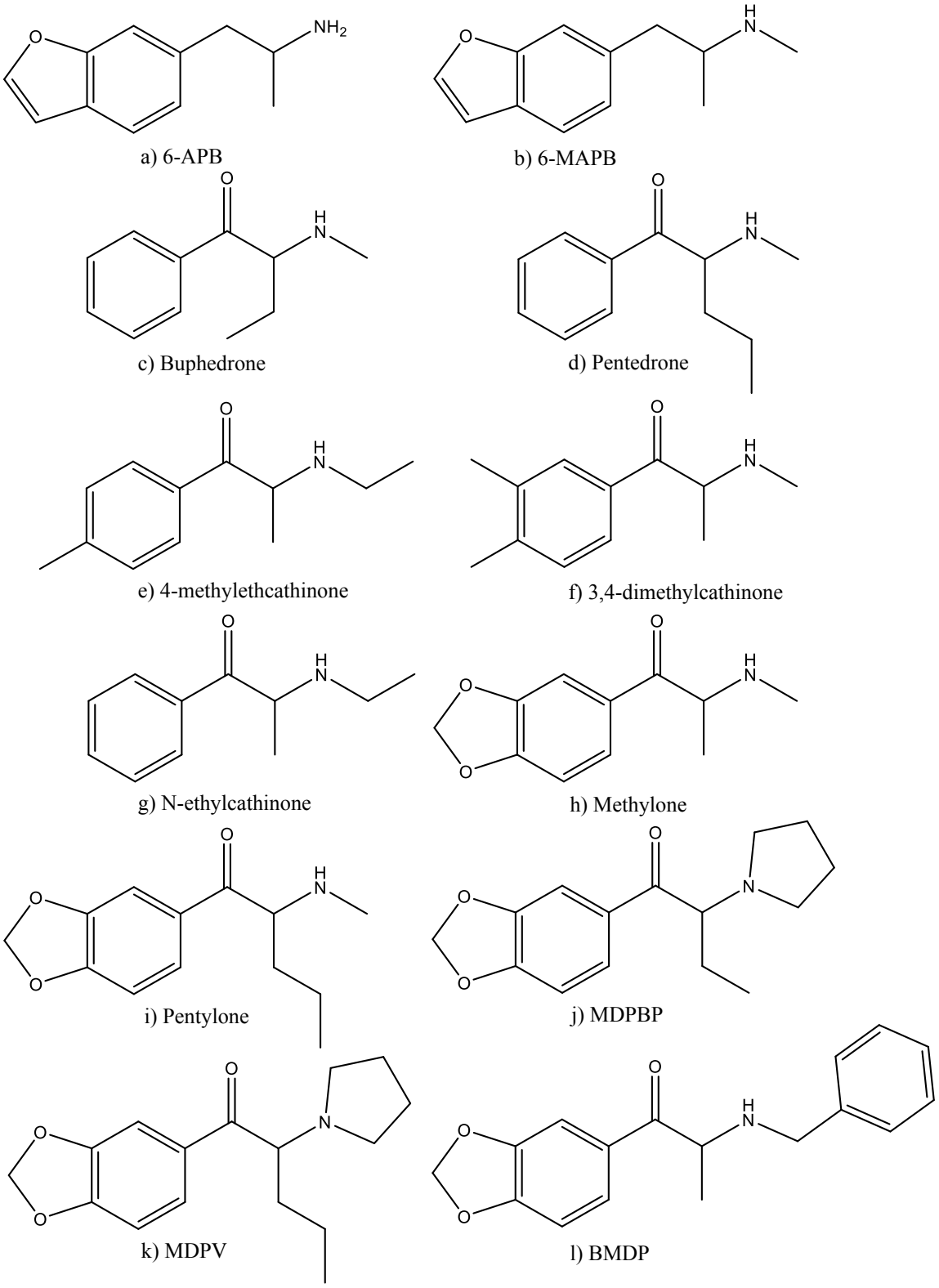

Figure 2.16. Structures of cathinone and phenethylamine structures composing the literature test set of compounds.

In the second study used to test the classification scheme, Snyder *et al.* used cathinone isomers as part of a larger set of organic compounds to compare traditional CID-MS with a multigenerational CID-MS method that would fragment the fragments produced in CID-MS (31). CID-MS was performed using resonant excitation in a linear ion trap with the collision potential used reported in "arbitrary units." As such, it is unclear how the voltage used to generate Snyder's data set compares to those used here. However, Snyder's data set does include buphedrone, which was also analyzed in this work. Visual comparison of the spectra, focusing on the composition of the fragments present and the relative abundances, suggests that Snyder's analysis using tradition CID-MS is most similar to the 10 V collision potential used in this work. One major difference, though, is that the fragment corresponding to the loss of water is the base peak in Snyder's buphedrone spectrum, while this fragment is the peak of second highest abundance in the 10 V buphedrone spectra generated in this work. However, using the loss of water as the base peak at 10 V does correctly assign buphedrone as a cathinone, even if it does not follow the same path through the flowchart as the buphedrone standard in the training set. The other cathinones reported in Snyder's studies (pentedrone, 4-methylethcathinone, 3,4-dimethylcathinone, and *N*-ethylcathinone) all had the same attribute of the base peak corresponding to the loss of water. Thus, all cathinones would result in the correct assignment as cathinones when using the revised classification scheme.

The final study, a work by Fornal in 2013 (25), is the most closely comparable with the data collected here. Fornal's work analyzed a series of 3,4-methylenedioxy substituted cathinones using CID-MS with 10, 20 and 40 V collision potentials. The

cathinone butylone is included in both Fornal's data set and the one reported here, providing a point of direct comparison between the two data sets. The butylone spectra in the literature exhibited $[M+H]^+$ as the base peak at 10 V with the loss of water as the second most abundant ion at this potential. At 20 V, the loss of 48 Da, attributed to methanediol (CH_4O_2) by Fornal, is the base peak at 20 V. This series of fragments correctly assigns butylone as a cathinone following the same progression through the classification scheme as the butylone standard analyzed in this work. This indicates that the data sets are comparable.

Four other cathinones in Fornal's work are correctly identified using the revised flow chart. The cathinones methylone, pentylone, MDPBP, and MDPV (Figure 16.h-k, respectively), all shared the same pathway through the flowchart as butylone and ethylone. The final cathinone, BMDP, remained uncategorized. This cathinone has the same core structure as methylone but with an aromatic substitution on the amine, similar to benzedrone (Figure 2.16.l). Unlike either methylone or benzedrone, the ion of second highest abundance at 10 V does not correspond to the loss of water but rather is the $[C_7H_7]^+$ ion. Analogous to the observation of this ion as the base peak for benzedrone at 20 V, this loss occurs by cleavage of the aromatic ring substituted on the amine group. However, given that this is more abundant than the loss of water at 10 V in BMDP, this cathinone remains uncategorized, even under the revised scheme. This indicates that, while the characterization scheme does successfully identify a number of literature-reported cathinones and phenethylamines, there remains room for improvement.

2.4 Conclusion

Designer drugs in the cathinone and phenethylamine classes have similar core structures and, with a variety of different substituents and substitution sites, can include a broad range of compounds. CID-MS at multiple collision potentials fragments these compounds, allowing structural features of the compounds to be identified. These features can be used to understand how the structure itself is arranged, including the location and composition of the substituents. Additionally, the proposed scheme can utilize the fragmentation as a method for distinguishing cathinones from phenethylamines. The compounds investigated here covered a range of potential substituents and structural arrangements. These built a foundational classification scheme that successfully assigned cathinones from the literature, even when the conditions of data acquisition were not identical. This facilitates incorporation of the scheme across multiple laboratories for the identification of unknowns. The scheme can also be continually expanded and refined as new standards become available for emerging cathinone and phenethylamine analogs. Ultimately, the scheme provides a quick reference for classifying suspected drugs as cathinones or phenethylamines and lays a foundation for the identification of new analogs.

CHAPTER THREE: Characterization and Differentiation of Cathinone Isomers

3.1 The isomer problem

The previous chapter described the distinction of cathinones from the structurally similar class of designer drugs, phenethylamines, based on characteristic mass spectral features at a range of collision potentials. In this chapter, the focus is turned to the specific identification of isomeric compounds. Isomers of a compound have the same chemical formulae but differing structural arrangements. For isomers within the same drug class, there are many similarities in the structures so the molecular ions and many of the fragments at low collision potentials will have the same *m/z* value. While this allows isomers to be identified as similar compounds, scheduling of emerging synthetic cathinones requires the identity of the cathinone to be confirmed. To address how CID-MS can be used specifically for isomer differentiation, three sets of cathinone isomers were investigated. The structures for each compound are shown in Figure 3.1.

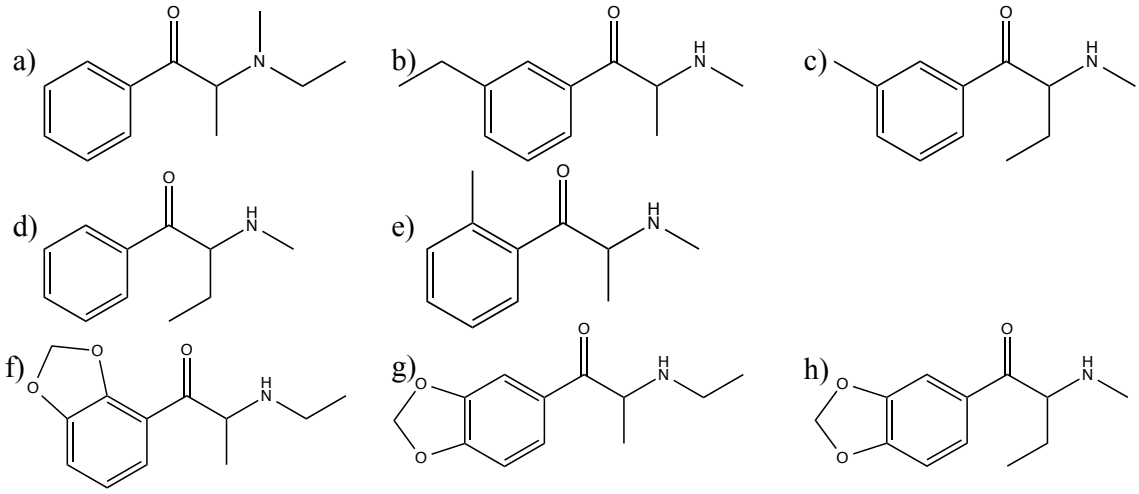

Figure 3.1. Structures for cathinone isomers investigated. Set 1 isomers (molecular formula $C_{12}H_{17}NO$) include a) *N*-ethyl-*N*-methylcathinone, b) 3-ethylmethcathinone, and c) 3-methylbuphedrone. Set 2 isomers (molecular formula $C_{11}H_{15}NO$) include d) buphedrone and e) 2-methylmethcathinone. Set 3 isomers (molecular formula $C_{12}H_{15}NO_3$) include f) 2,3-ethylone isomer, g) ethylone, and h) butylone.

The isomers in Set 1 and 2 have aliphatic substitutions, while those in Set 2 have one less carbon present in the alkyl chains than those in Set 1. Of the five aliphatic-substituted cathinones in Sets 1 and 2, only buphedrone is currently regulated as a Schedule I drug. Isomer Set 3 includes three cathinones with a methylenedioxy substitution on the aromatic ring: butylone, ethylone, and the 2,3-ethylone isomer. The location of the methylenedioxy substitution and length of the aliphatic chain at the alpha-carbon and amine position vary among the structures. Butylone and ethylone are currently Schedule I substances while the 2,3-ethylone isomer is unregulated. With some of the isomeric cathinones regulated and others not, it becomes increasingly important to distinguish isomers from each other.

3.2 Fragmentation of aliphatic-substituted cathinone isomers: Set 1

Chemical structures for three aliphatic-substituted isomers (*N*-ethyl-*N*-methylcathinone, 3-ethylmethcathinone, and 3-methylbuphedrone) and representative mass spectra at 10 V are shown in Figure 3.2. These isomers differ in the alkyl chain length at the 3-position on the aromatic ring, on the alpha carbon, and on the amine.

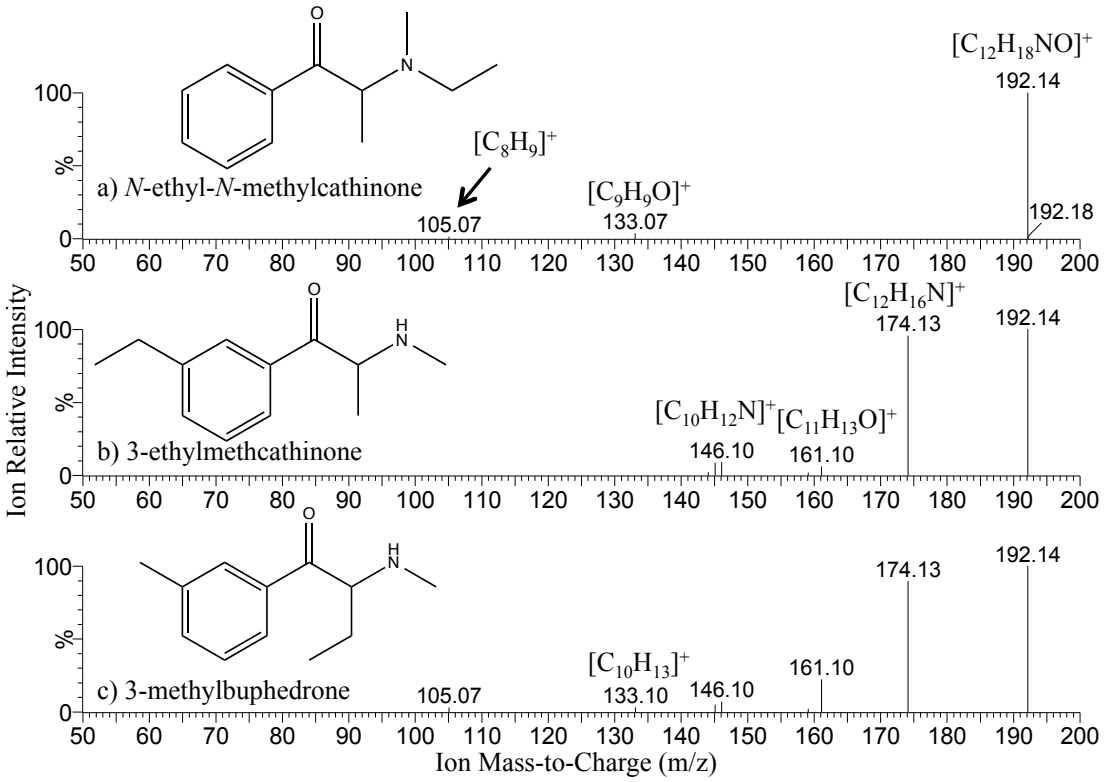

Figure 3.2. CID-MS spectra for a) *N*-ethyl-*N*-methylcathinone, b) 3-ethylmethcathinone, and c) 3-methylbuphedrone, collected in positive-ion mode at a collision potential of 10 V.

For all three isomers, $[M+H]^+$ ($[C_{12}H_{18}NO]^+$, *m/z* 192.14) is the base peak at 10 V. In the spectra for 3-ethylmethcathinone and 3-methylbuphedrone (Figure 3.H, b and c), the ion of second highest abundance is the fragment ion $[C_{12}H_{16}N]^+$ (*m/z* 174.13). This

corresponds to the loss of water from the molecular ion, a common loss for cathinones with a primary or secondary amine (7, 27). As *N*-ethyl-*N*-methylcathinone is a tertiary amine, loss of water from the molecular ion is not observed (Fig. 3.2.a). This distinguishes *N*-ethyl-*N*-methylcathinone from 3-ethylmethcathinone and 3-methylbuphedrone.

The loss of the amine group is also a common loss in cathinones and can also be used to distinguish *N*-ethyl-*N*-methylcathinone from the other two isomers (7, 27). In *N*-ethyl-*N*-methylcathinone, loss of the amine group results in a fragment ion at *m/z* 133.07 ($[C_9H_9O]^+$) whereas, for the other two isomers, loss of the amine group results in a fragment ion at *m/z* 161.10 ($[C_{11}H_{13}O]^+$). In addition, the abundance of this fragment ion differs between 3-ethylmethcathinone and 3-methylbuphedrone (6.0% compared to 22.2%, respectively), enabling distinction of these two isomers.

Further differentiation of the isomers 3-ethylmethcathinone and 3-methylbuphedrone is realized at higher collision potentials. The CID spectra for 3-ethylmethcathinone and 3-methylbuphedrone at 20 and 40 V are shown in Figure 3.3. These spectra are extremely similar, with only a few differences. Specifically, there are two fragments that are common to both isomers but have a greater than 10% difference in relative abundance between 3-ethylmethcathinone and 3-methylbuphedrone at higher energies: $[C_{11}H_{13}N]^{\bullet+}$ (*m/z* 159.10) and $[C_8H_9]^+$ (*m/z* 105.07).

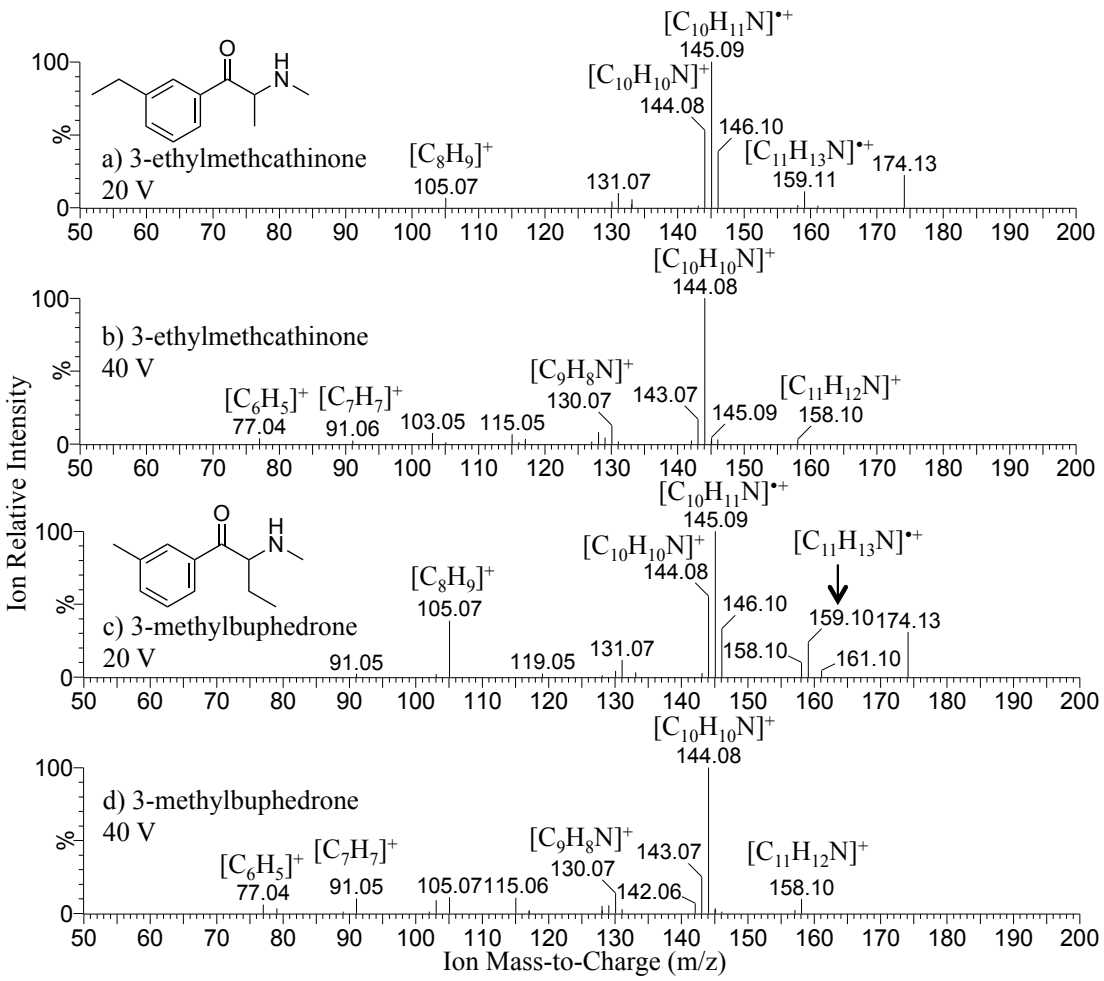

Figure 3.3. CID-MS spectra for 3-ethylmethcathinone at a) 20 V and b) 40 V and 3-methylbuphedrone at c) 20 V and d) 40 V. All spectra were collected in positive-ion mode.

As an alternative to viewing spectra side-by-side, breakdown curves can be used to more readily visualize differences in ion abundances over a range of collision potentials (32). Breakdown curves show how the relative abundance of a specific ion changes with an increase in collision potential and are useful for comparing such changes between multiple ions or compounds. For the differentiation of 3-ethylmethcathinone and

3-methylbuphedrone, breakdown curves for the fragment ions $[C_{11}H_{13}N]^{\bullet+}$ (*m/z* 159.10) and $[C_8H_9]^+$ (*m/z* 105.07) are shown in Figure 3.4.

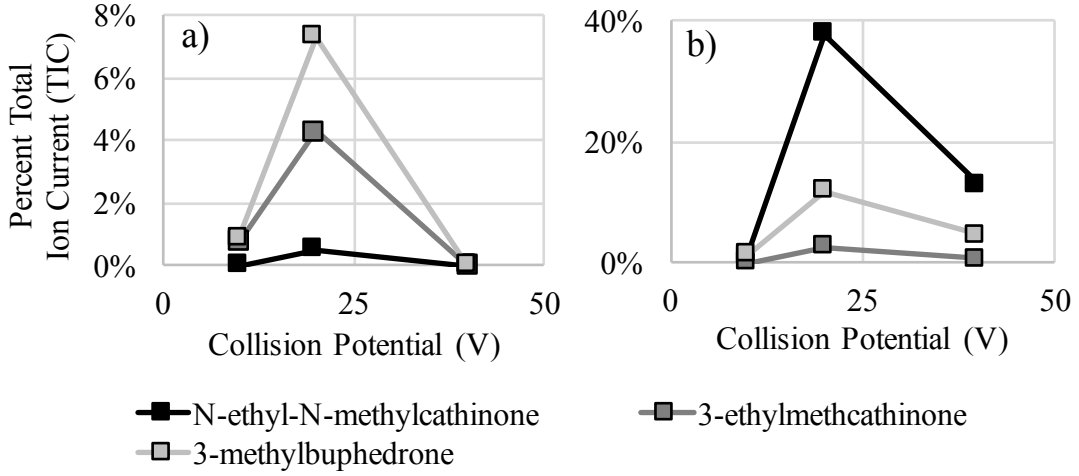

Figure 3.4. Breakdown curves showing the abundance, expressed as a percent of the total ion current, of the charged fragment for a) $[C_{11}H_{13}N]^{\bullet+}$ (*m/z* 159.10) and b) $[C_8H_9]^+$ (*m/z* 105.07) in *N*-ethyl-*N*-methylcathinone, 3-ethylmethcathinone and 3-methylbuphedrone.

The first of these fragments, $[C_{11}H_{13}N]^{\bullet+}$, is an odd-electron species. While not commonly generated from CID of even-electron precursors, these species can form in CID-MS during fragmentation of even-electron precursor ions providing there is delocalization of the unpaired electron (24). This fragment in particular corresponds to loss of water and a methyl radical and shows similarly low abundance in all three isomers at collision potentials of 10 V and 40 V (Fig. 3.4.a). However, at 20 V, differences in abundance are apparent for *N*-ethyl-*N*-methylcathinone (0.5% TIC), 3-methylbuphedrone (7.3% TIC) and 3-ethylmethcathinone (4.3% TIC). In *N*-ethyl-*N*-methylcathinone, the loss of water does not readily occur at low energy, so this further fragmentation is also

unlikely to occur, yielding the low relative abundance of the $[C_{11}H_{13}N]^{\bullet+}$ ion. Both 3-methylbuphedrone and 3-ethylmethcathinone have a secondary amine and two methyl substitutions from where the radical loss could occur, providing the basis for the higher relative abundance of this fragment ion. Although the position from which the methyl radical is lost is not clear from these data, it is likely that a combination of methyl losses from both substitution sites contributes to the ion abundances and the difference in relative abundance between the isomers reflects the presence of structural differences.

The second fragment ion of interest, $[C_8H_9]^+$ (*m /z* 105.07), is also present at similar abundance in all three isomers at a collision potential of 10 V with distinction between the isomers possible at higher collision potentials (Figure 3.4.b). At 20 V, $[C_8H_9]^+$ is the base peak for *N*-ethyl-*N*-methylcathinone and represents 37.8% of the total ions in the spectra, but only represents 11.9% and 2.5% of the total ion currents in the 20 V spectra for 3-methylbuphedrone and 3-ethylmethcathinone, respectively. At 40 V, the abundance of $[C_8H_9]^+$ decreases for all isomers but remains significantly greater in *N*-ethyl-*N*-methylcathinone (13.0% TIC) than in both 3-methylbuphedrone (4.7% TIC) and 3-ethylmethcathinone (0.6% TIC). Based on the molecular formula of this fragment, $[C_8H_9]^+$ corresponds to an ethyl-substituted aromatic ring. Given that this ion is present in all three structures and an ethyl substitution is only present on the aromatic ring in in 3-ethylmethcathinone, direct cleavage of the aromatic-ketone bond is not the primary mechanism by which this fragment ion forms. Further, the high abundance of $[C_8H_9]^+$ in *N*-ethyl-*N*-methylcathinone indicates that this mechanism does not require the initial loss of water in order to occur. In considering how this ion might be formed in *N*-ethyl-*N*-methylcathinone where it is most abundant at 20 V, the losses of both the amine group

and the ketone as a CO group would need to occur, along with a shift of the alpha-carbon side chain to the aromatic ring. However, following the same series of cleavages and rearrangements in 3-methylbuphedrone and 3-ethylmethcahtinone would yield ions of higher *m/*z, as their side chains and aromatic substitutions are longer than those in *N*-ethyl-*N*-methylcathinone. Thus, additional fragmentation would be required to achieve the $[C_8H_9]^+$ in 3-methylbuphedrone and 3-ethylmethcahtinone, explaining the lower abundance of this ion for these compounds. Overall, while these aliphatic isomers are distinguishable from each other at 10 V, the higher collision potentials give additional evidence regarding the structural differences of the isomers.

3.3 Fragmentation of aliphatic-substituted cathinone isomers: Set 2

Chemical structures for the other aliphatic-substituted isomers (buphedrone and 2-methylmethcathinone) and representative mass spectra at each collision potential are shown in Figures 3.5 and 3.6, respectively. There is one carbon less in the alkyl chains for these isomers than those in the first set. Given that isomers in both Set 1 and Set 2 have aliphatic substitutions, the Set 2 isomers are expected to fragment similarly to those in Set 1.

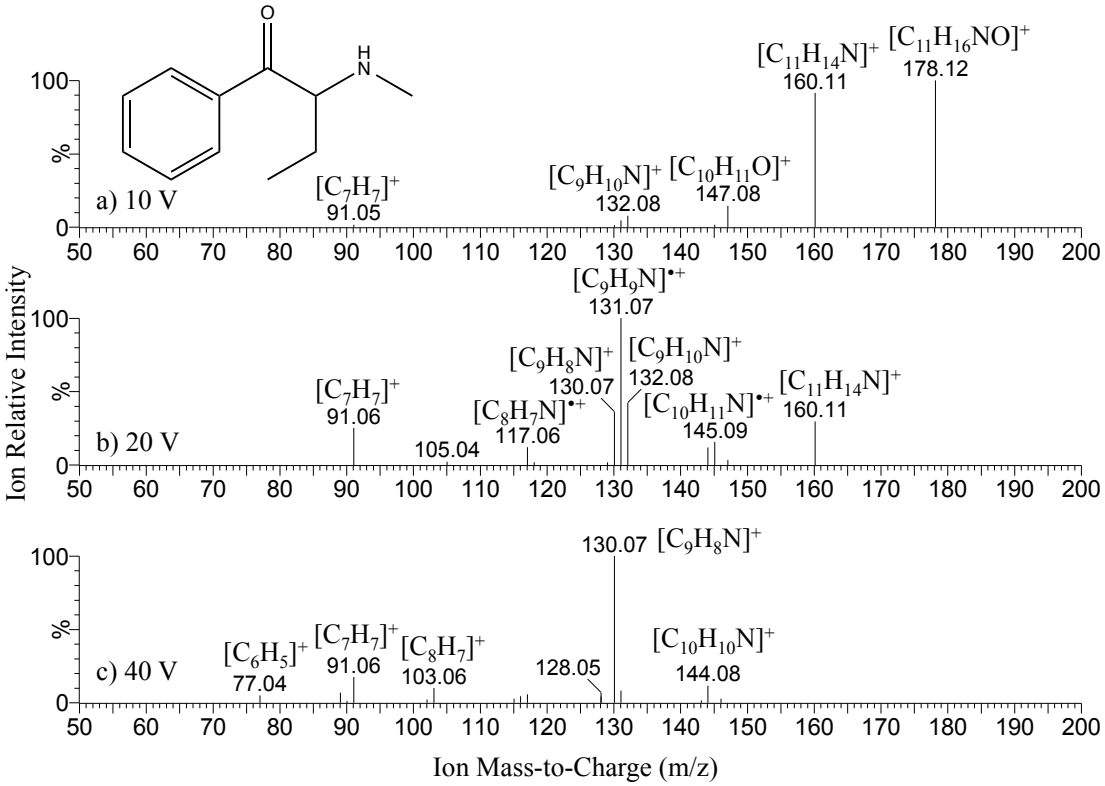

Figure 3.5. CID-MS spectra for buphedrone at collision potentials of a) 10 V, b) 20 V and c) 40 V. All spectra were collected in positive-ion mode.

The chemical structure of buphedrone, as well as representative mass spectra collected using a collision potentials of 10, 20, and 40 V, are shown in Figure 3.5. At 10 V, the base peak is $[M+H]^+$ ($[C_{11}H_{16}NO]$, *m/z* 178.12), while the next most abundant ion corresponds to the loss of water ($[C_{11}H_{14}NO]^+$, *m/z* 160.11). The fragment corresponding to the loss of methylamine ($[C_{10}H_{11}O]^+$, *m/z* 147.08) is also observed at 10 V. While the same fragment ions are also present in high abundance at 10 V in the CID spectrum for 2-methylmethcathinone (Figure 3.6.a), the loss of water is the base peak for this isomer.

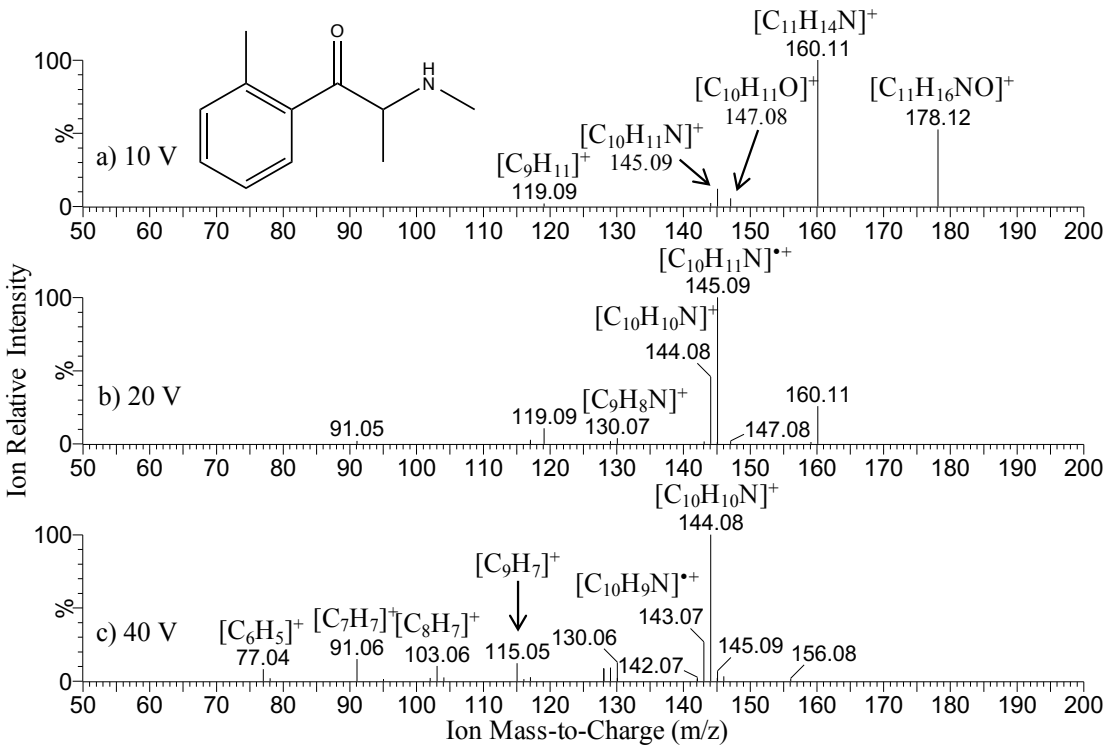

Figure 3.6. CID-MS spectra for 2-methylmethcathinone at a) 10 V, b) 20 V and c) 40 V. All spectra were collected in positive-ion mode.

With increasing collision energy, additional differences between these isomers are observed. One distinctive difference is in the base peaks at 20 and 40 V. For buphedrone, the base peaks at 20 and 40 V correspond to the loss of water and an ethyl group as either a radical species ($[C_9H_9N]^{\bullet+}$, *m/z* 131.07) or an even-electron species ($[C_9H_8N]^+$, *m/z* 130.07), respectively (Figure 3.5, b and c). This loss likely results from a cleavage of the ethyl side chain at the alpha position alongside the loss of water. Similar losses of water and the alpha-position side chain compose the base peaks at 20 and 40 V in 2-methylmethcathinone, although the cleavage of the alpha position side chain in this isomer involves the loss of a methyl group as either a radical ($[C_{10}H_{11}N]^{\bullet+}$, *m/z* 145.09) or

an even-electron species ($[C_{10}H_{10}N]^+$, *m/z* 144.08) (Figure 3.6, b and c, respectively). To more clearly compare these fragments, breakdown curves for these fragments are shown in Figure 3.R.

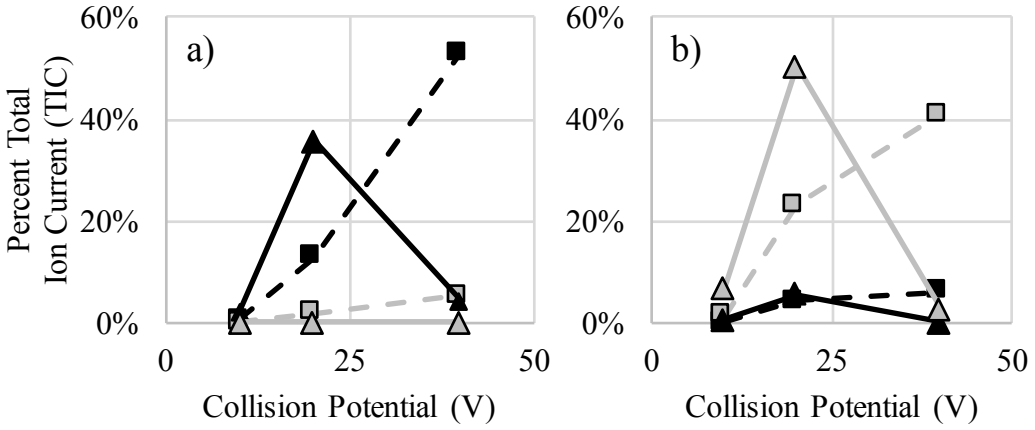

Figure 3.7. Breakdown curves showing the abundance, expressed as a percent of the total ion current, of fragments corresponding to loss of water and either a) an ethyl group or b) a methyl group as even electron (square, dashed line) and radical (diamond, solid line) fragments for buphedrone (black) and 2-methylmethcathinone (grey).

The fragments shown in the breakdown curves in Figure 3.7 each represent less than 7% of the total ion current in their respective spectra at the 10 V collision potential. At 20 V, the loss of water with either an ethyl radical or a methyl radical are the base peaks for buphedrone and 2-methylmethcathinone, respectively. While both of these peaks are the most abundant peaks in their respective spectra, the base peak for buphedrone (Figure 3.7a, black diamond, 35.6% TIC) at 20 V accounts for a lower percentage of all ions present in its spectrum than the base peak for 2-

methylmethcathinone (Figure 3.7b, grey diamond, 50.4% TIC), represented by the lower percent of total ion current for buphedrone. At 20 V, the even-electron fragments have lower abundances than their odd-electron counterparts - 12.9% TIC for the loss of water and ethane in buphedrone and 23.0%% TIC for the loss of water and methane in 2-methylmethcathinone. At 40 V, the ratio between the odd and even electron fragments changes with the abundances of the even electron fragments exceeding those of the odd-electron fragments that dominated at 20 V. The even-electron fragments are the base peaks at 40 V, with the loss of water the ethyl group representing 52.9% of the total ion current for buphedrone at 40 V and the loss of water and a methyl group representing 41.1% of the total ion current for 3-methylmethcathinone.

Given that buphedrone has an ethyl substitution at the alpha carbon and 3-methylmethcathinone has a methyl group at the same location, it could be hypothesized that these odd- and even-electron fragments are the result of a cleavage of the side chain after the loss of water. However, the alpha carbon side chains in 3-methylbuphedrone and 3-ethylmethcathinone are also ethyl and methyl groups, respectively, but the dominant series of odd- and even-electron fragments corresponds to the loss of water and an ethyl group for both compounds (Figure 3.3, *m/z* 145.09 $[C_{10}H_{11}N]^{*+}$ and 144.08 $[C_{10}H_{10}N]^{+}$). This indicates that the alpha side chain is not the only location at which the alkyl loss could occur and this loss could also occur from an aromatic site. Given that radical alkyl groups have increasing stability with increased size and substitution, the loss of an ethyl group will be more energetically favorable than the loss of a methyl group. Thus, this series of odd- and even-electron losses is not a specific indicator of the composition of

the alpha side chain, but the most abundant series gives evidence of the longest alkyl chain present at either the alpha carbon or aromatic ring.

3.4 Fragmentation of methylenedioxy-substituted cathinone isomers: Set 3

Chemical structures for the three methylenedioxy-substituted cathinones (2,3-ethylone isomer, ethylone, and butylone), as well as representative mass spectra collected using a collision potential of 10 V are shown in Figure 3.8. For all three isomers, the base peak is $[M+H]^+$ ($[C_{12}H_{16}NO_3]$, *m/z* 222.11) while the next two ions of highest abundance correspond to the loss of water ($[C_{12}H_{14}NO_2]^+$, *m/z* 204.10) and the loss of 48 Da from $[M+H]^+$ ($[C_{11}H_{12}NO]^+$, *m/z* 174.09). The loss of 48 Da corresponds to a loss of CH_4O_2 and has been previously attributed to the loss of the methylenedioxy ring as methanediol. However, the loss of methanediol is unlikely owing to its low stability and this neutral loss is more likely to be successive losses of formaldehyde (CH_2O) and water (H_2O). Since the identity and mechanism of this loss is unclear, it is referred to simply as a loss of 48 Da.

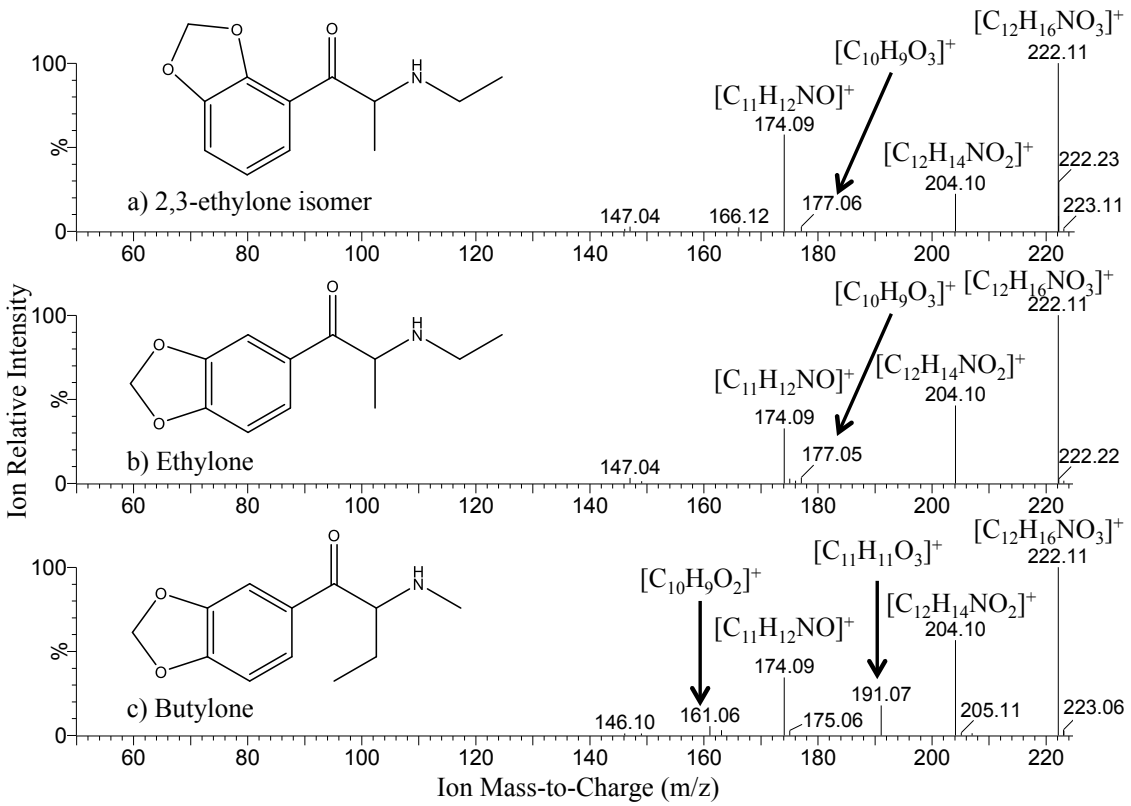

Figure 3.8. CID-MS spectra for a) 2,3-ethylone isomer, b) ethylone, and c) butylone collected in positive-ion mode at a collision energy of 10 V.

The loss of 48 Da indicates a methylenedioxy substitution on the aromatic ring (25) and, as all three isomers contain methylenedioxy-substitutions on the ring, the presence of this loss does not allow distinction. However, the difference in the alkyl group substitution on the amine can be used to distinguish the isomers: butylone contains a methyl group on the amine whereas, the ethylone isomers contain an ethyl group. Thus, loss of the amine from the butylone $[M+H]^+$ results in a fragment ion at higher *m/z* (*m/z* 191.07, 17.7% relative abundance) than the corresponding amine loss from the ethylone isomers (*m/z* 177.05, 2.5% and 3.3% relative abundance for 2,3-ethylone isomer and ethylone, respectively).

While the fragments at 10 V mainly represent common cathinone fragmentation pathways, the fragment at *m/z* 161.06 in butylone, corresponding to $[C_{10}H_9O_2]^+$, is not accounted for in these pathways. The neutral loss associated with this charged fragment is C_2H_7NO. Given the structure of butylone (Figure 3.8.c), there is no single cleavage that would result in this loss, so it is likely due to a series of multiple fragmentation steps and rearrangements. One potential series of losses involves the initial loss of methylamine (charged fragment observed at *m/z* 191.07, $[C_{11}H_{11}O_3]^+$) with a subsequent loss of formaldehyde from a cleavage in the methylenedioxy ring. Similar observations are observed at 10 V in the two ethylone isomers, with the loss of ethylamine (*m/z* 177.05, $[C_{10}H_9O_3]^+$) and formaldehyde (*m/z* 147.04, $[C_9H_7O_2]^+$).

As the collision potential increases, so does the corresponding internal energy of the ion after collision. With increased internal energy available to overcome the activation energy of fragmentation pathways, a wider array of fragments can occur and additional differences between the isomers observed. Spectra at the three collision potentials for butylone, ethylone, and the 2,3-ethylone isomer can be seen in Figures 3.9, 3.10, and 3.11, respectively. Since the ethylone isomers differ only in the location of the methylenedioxy ring substitution, fragmentation that involves the loss of more than one oxygen atom, requiring cleavage of the methylenedioxy ring, provides a source of known differences between these two isomers. Thus, breakdown curves were generated for several fragment ions that correspond to neutral losses previously reported in the literature as well as those that require the loss of one or more oxygen atoms. The fragments plotted in Figure 3.12. include both the loss of water and the loss of 48 Da (Figure 3.12.a and b, respectively), as well as the three fragment ions $[C_{10}H_8NO_2]^+$ (m/z

174.05), $[C_{10}H_{12}N]^+$ (*m/z* 146.10) and $[C_9H_9N]^{\bullet+}$ (*m/z* 131.07) (Figure 3.12.c-e, respectively).

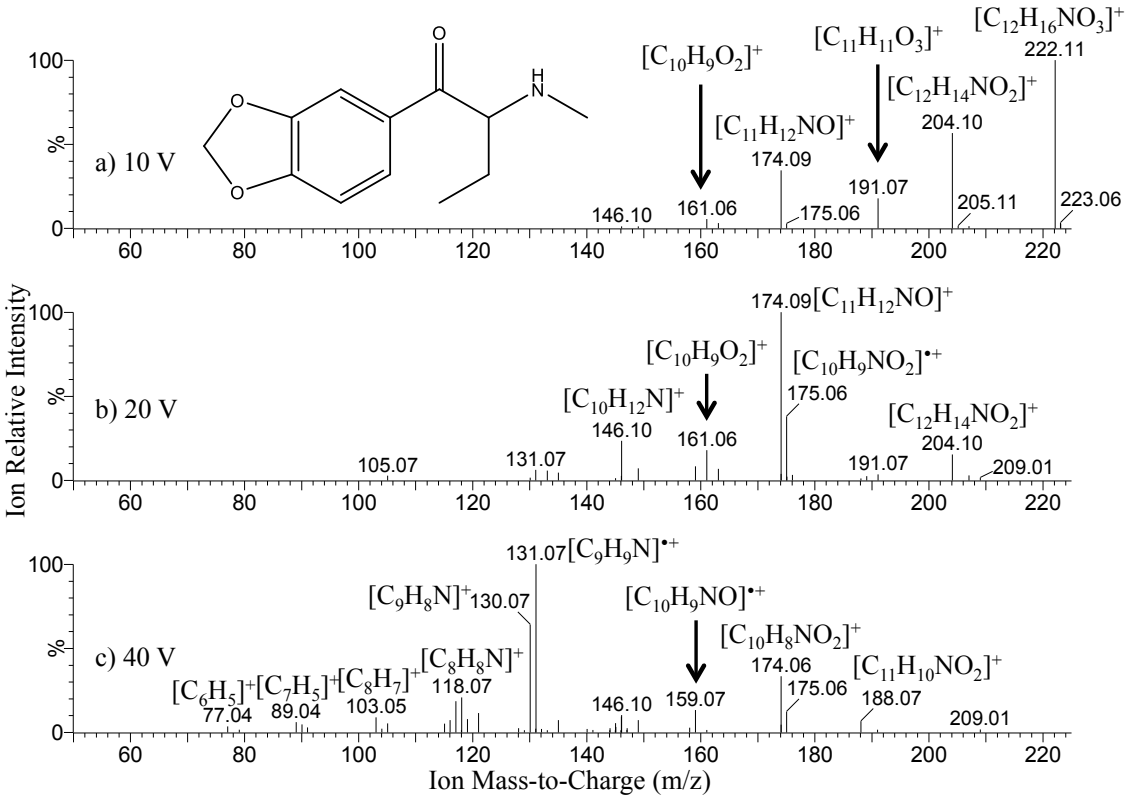

Figure 3.9. CID-MS spectra for butylone at a) 10 V, b) 20 V and c) 40 V. All spectra were collected in positive-ion mode.

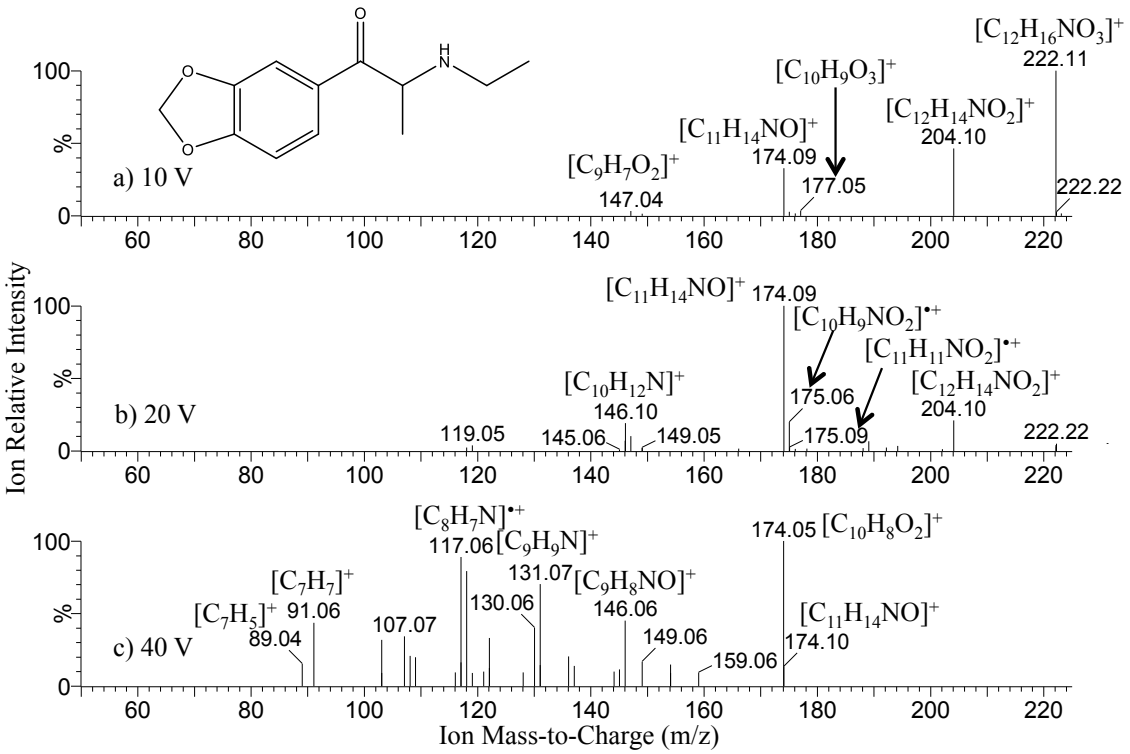

Figure 3.10. CID-MS spectra for ethylone at a) 10 V, b) 20 V and c) 40 V. All spectra were collected in positive-ion mode.

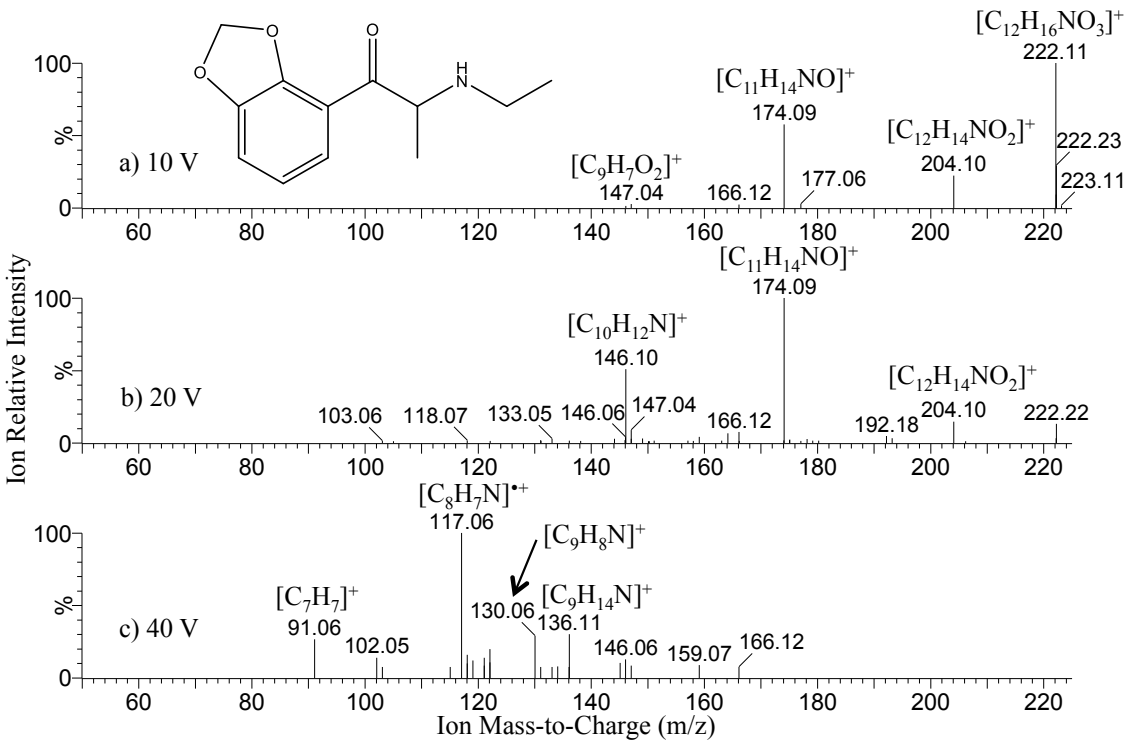

Figure 3.11. CID-MS spectra for the 2,3-ethylone isomer at a) 10 V, b) 20 V and c) 40 V. All spectra were collected in positive-ion mode.

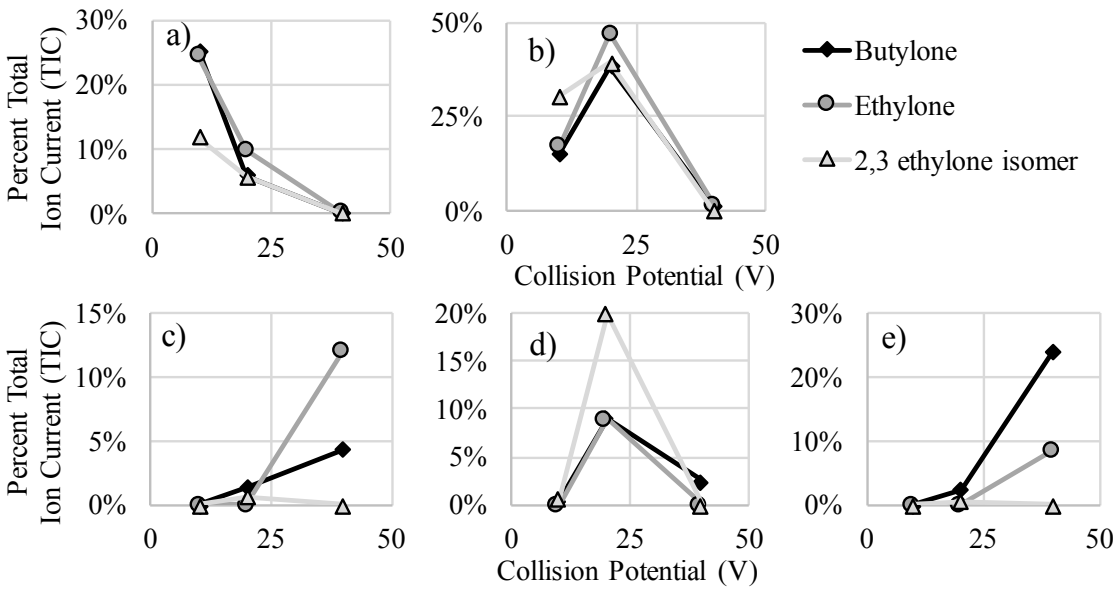

Figure 3.12. Breakdown curves showing the abundance, expressed as a percent of the total ion current, at each collision energy for the charged fragments a) $[C_{12}H_{14}NO_2]^+$ (*m/z* 204.10) which corresponds to the loss of water, b) $[C_{11}H_{12}NO]^+$ (*m/z* 174.09) which corresponds to the loss of 48 Da, c) $[C_{10}H_8NO_2]^+$ (m/z 174.05), d) $[C_{10}H_{12}N]^+$ (*m/z* 146.10), and e) $[C_9H_9N]^{\bullet+}$ (*m/z* 131.07).

While presence of fragments corresponding to both the loss of water ($[C_{12}H_{14}NO_2]^+$, *m/z* 204.10, Fig. 3.12.a) and loss of 48 Da ($[C_{11}H_{12}NO]^+$, *m/z* 174.09, Fig. 3.12.b) are common for methylenedioxy-substituted cathinones, the breakdown curves clearly represent the differences in abundance of these ions in ethylone and the 2,3-ethylone isomer. These losses are present at similar abundances at higher collision potentials, but differences are observed at 10 V. At 10 V, the abundance of $[C_{12}H_{14}NO_2]^+$ is 12.5% higher in ethylone than in the 2,3-ethylone isomer (Fig. 3.12.a) while the abundance of $[C_{11}H_{12}NO]^+$ is 13.4% higher in the 2,3-ethylone isomer (Fig. 3.12.b).

Differences between the two ethylone isomers are also observed in other losses. Most notably, the base peak for ethylone at 40 V, $[C_{10}H_8NO_2]^+$ (*m/z* 174.05), is not present in the 2,3-ethylone isomer but is present in butylone (Fig. 3.12.c). This fragment corresponds to the neutral loss of water and ethane. Since a similar neutral loss has been observed in other cathinones that do not have a methylenedioxy group, this loss does not directly require cleavage of the methylenedioxy group. However, if one of the oxygen atoms of the methylenedioxy group is the site of protonation, the change in position on the aromatic ring could lead to different charge-remote fragmentation pathways occurring for each isomer. The differences of the fragmentation pathway explains why $[C_{10}H_8NO_2]^+$ is present at 40 V in both of the 3,4-substituted isomers but does not occur in the 2,3-isomer.

The fragment ions at *m/z* 146.10 ($[C_{10}H_{12}N]^+$) and *m/z* 131.07 ($[C_9H_9N]^{\bullet+}$) are both the result of fragmentation pathways that require the loss of methanediol from the ring. The first of these fragments, $[C_{10}H_{12}N]^+$, is present in all three isomers at all three collision potentials (Fig. 3.12.d). However, at 20 V, the abundance of this fragment in the 2,3-subsituted isomer is twice as high as in the 3,4-substituted isomers, indicating it is more likely to occur with a 2,3-substitution. The $[C_9H_9N]^{\bullet+}$ fragment ion is an odd-electron species corresponding to the loss of $C_3H_7O_3$. $[C_9H_9N]^{\bullet+}$ is present at low abundance (<3% TIC) for all three isomers at 10 and 20 V, but at higher abundance for butylone and ethylone at 40 V (24.2% and 8.5% TIC, respectively) (Fig. 3.12.e). It is not present in the 2,3-ethylone isomer at 40 V, indicating it is more likely to occur with the 3,4-methylenedioxy substitution.

For both $[C_{10}H_{12}N]^+$ and $[C_9H_9N]^{\bullet+}$, Thus, differences in the abundance of these three ions reflect the ring position of the methylenedioxy group, and the 2,3-ethylone isomer is distinguished from butylone and ethylone based on the higher abundance of $[C_{10}H_{12}N]^+$ at 20 V and the absence of $[C_{10}H_8NO_2]^+$ and $[C_9H_9N]^{\bullet+}$ at 40 V.

3.5 Conclusion

Cathinone isomers are distinguished using CID-MS at multiple collision potentials. When the same fragments are present across multiple isomers and energies, breakdown curves provide clear visualization of fragment abundances. While the fragments present at low collision potential (10 V) are useful for characterizing these compounds as cathinones and distinguishing isomers with differing amine substitutions, more extensive fragmentation at higher energies (20 V and 40 V) is required to distinguish isomers with the same amine groups.

In the case of methylenedioxy-substituted isomers, the fragments that firmly distinguish between the 3,4- and 2,3-substitutions in ethylone involve cleavage of the methylenedioxy ring and the loss of species that include multiple oxygen atoms with fragmentation mechanisms that are driven by the site of protonation. Specifically, differentiation can be achieved using the higher abundance of $[C_{10}H_{12}N]^+$ in the 2,3-isomer at 20 V and the absence of $[C_{10}H_8NO_2]^+$ and $[C_9H_9N]^{\bullet+}$ in this isomer at 40 V. For the aliphatic-substituted isomers with the same amine-group substitutions (3-ethylmethcathinone and 3-methylbuphedrone; buphedrone and 2-methylmethcathinone), the discriminating losses involved loss of water and the longest alkyl substitution as either a radical or neutral species. All of these losses highlight structural differences

between cathinone isomers and allow clear differentiation of them for compound identification. Since isomer identification is not easily achieved using the current standard method of analysis, this work addresses how the fragmentation of isomers under multiple collision potentials in CID-MS can be leveraged to achieve isomer differentiation.

CHAPTER 4: Conclusions and Future Work

4.1 Conclusion

The overarching goal in this research was to provide forensic scientists a simple process for identification of emerging synthetic cathinone analogs, including isomers. To accomplish this, the specific aims of this research were twofold. First, this work outlined a workflow for identification and distinction of emerging cathinone analogs from the structurally similar class of designer drugs, phenethylamines. High-resolution mass data and controlled fragmentation obtained using collision-induced dissociation mass spectrometry (CID-MS) with multiple collision potentials was used to investigate a variety of cathinone and phenethylamine standards. Ultimately, a characterization scheme was developed based on characteristic mass spectral features of these compounds. The characterization scheme provides step-by-step instruction to facilitate the assignment of unknown compounds as cathinones or phenethylamines, even when no standards are available for comparison. This scheme does accurately assign cathinones based off spectra obtained from multiple laboratories and be further expanded and refined as additional standards are analyzed.

The second specific aim of this work was to address isomer distinction. Through the investigation of three sets of cathinone isomers, differences in the mass spectral features that reflect the differing structural arrangements were identified. In general, isomers within each set had many fragment ions in common with each other. Breakdown curves facilitated comparison of the relative abundances of these common ions across the three collision potentials. The differences that emerged could be correlated to the

structural differences between the isomers and allowed isomer distinction. Overall, the characterization scheme and isomer fragmentation analysis presented here highlight how CID-MS can streamline the process of class assignment and isomer identification, minimizing the resources required for the analysis of new cathinone analogs.

4.2 Future work

There are several directions for further analysis of cathinones and phenethylamines using CID-MS. First, the fragmentation of these designer drugs could be further probed. In this work, the molecular formulae of fragments are identified, but the exact structure of each fragment and the mechanism through which the fragmentation occurs remain unclear. Further studies using deuterium-labelled compounds would indicate the specific locations from which hydrogens are being lost during each fragmentation pathway. This would give added clarity as to which bonds are breaking and what internal rearrangements are most likely to occur. The deeper understanding of fragmentation mechanisms could then be further applied in the structure elucidation of cathinones when no standards are available.

Another direction for the future would be in expanding and refining the classification scheme. The analysis of additional cathinone and phenethylamine standards would increase the accuracy of the classification scheme by taking into account an even broader range of structural arrangements. The scheme could also be expanded to other designer drug classes, such as synthetic cannabinoids, that are also plagued by the rapid introduction of new analogs.

As forensic laboratories look to adopt this method of analysis, the reproducibility of cathinone fragmentation by instruments across multiple laboratories must be thoroughly assessed. As seen in the literature, there is currently not a standard operating procedure for CID-MS analysis and the collision potentials used have been reported in various formats. While similarities between data sets can be observed, the inconsistency in procedure makes direct comparison of results obtained across multiple labs difficult. Thus, additional work that standardizes data acquisition and compares the results between labs is vital for the widespread adoption of CID-MS by the forensic community. Overall, there are many available avenues of further investigation that can continue to show CID-MS as a powerful tool for the forensic analysis of designer drugs.

APPENDICES

APPENDIX A

CID-MS Spectra of Cathinones

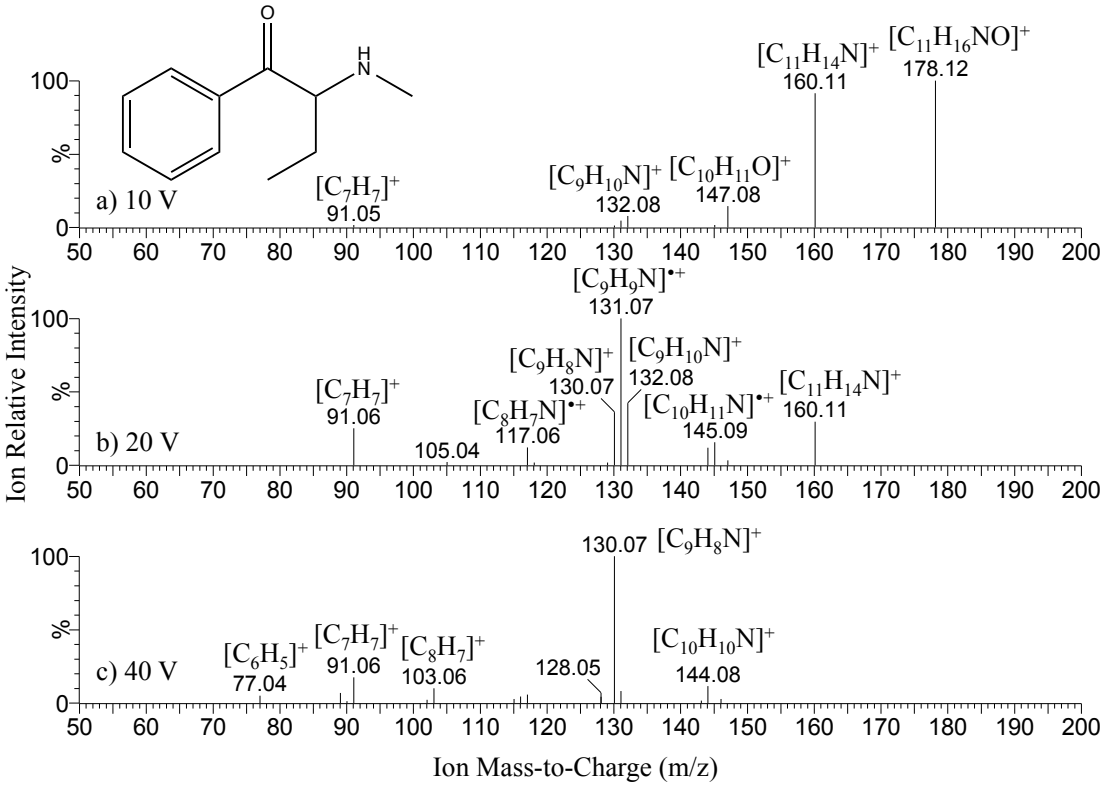

Figure A.1. CID-MS spectra for the cathinone buphedrone at collision potentials of a) 10 V, b) 20 V, and c) 40 V. All spectra collected in positive-ion mode.

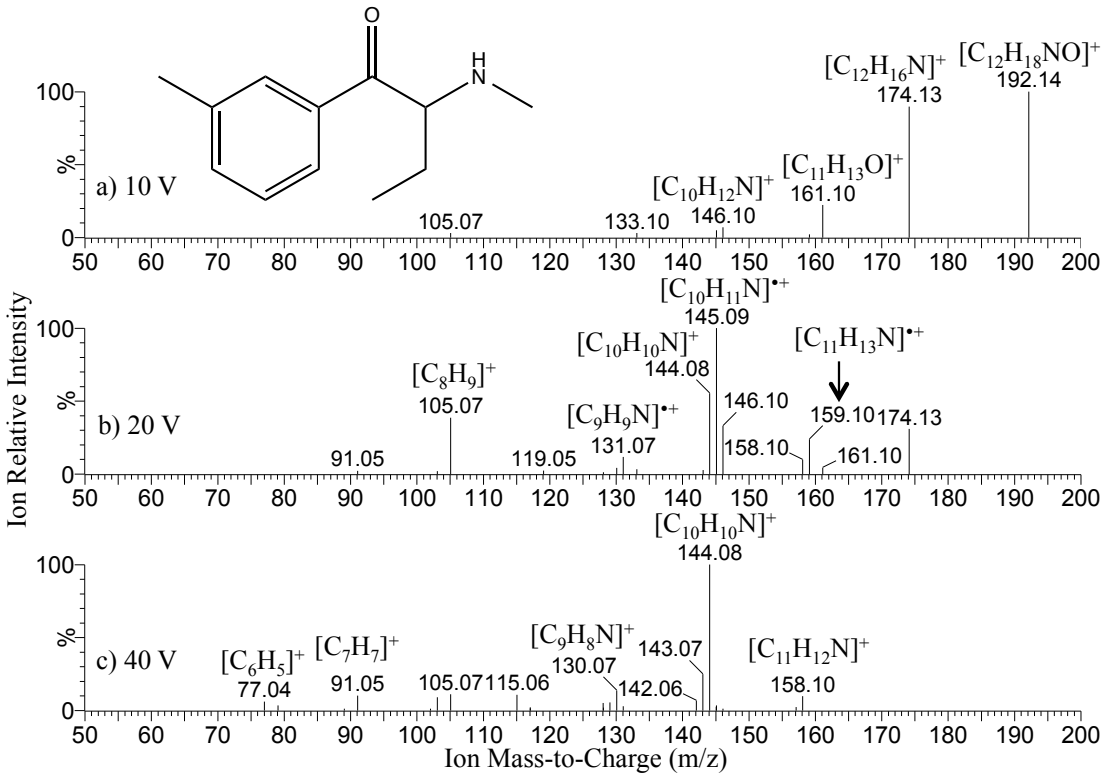

Figure A.2. CID-MS spectra for the cathinone 3-methylbuphedrone at collision potentials of a) 10 V, b) 20 V, and c) 40 V. All spectra collected in positive-ion mode.

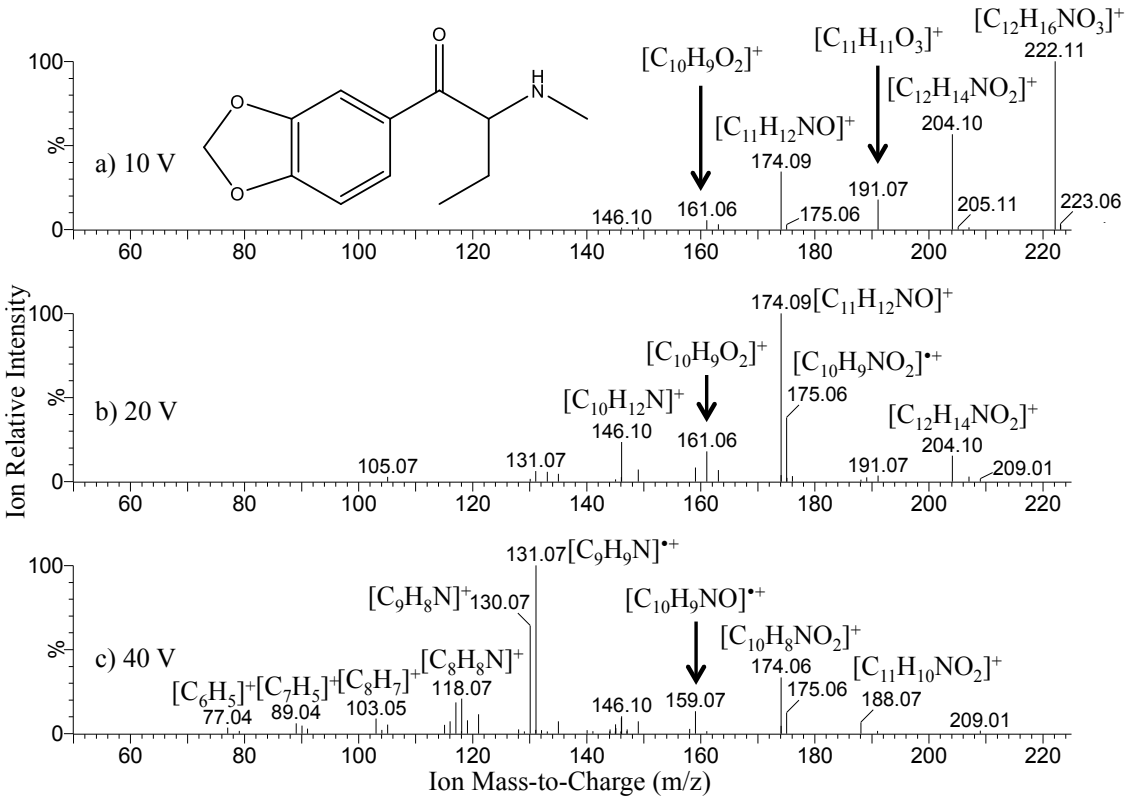

Figure A.3. CID-MS spectra for the cathinone butylone at collision potentials of a) 10 V, b) 20 V, and c) 40 V. All spectra collected in positive-ion mode.

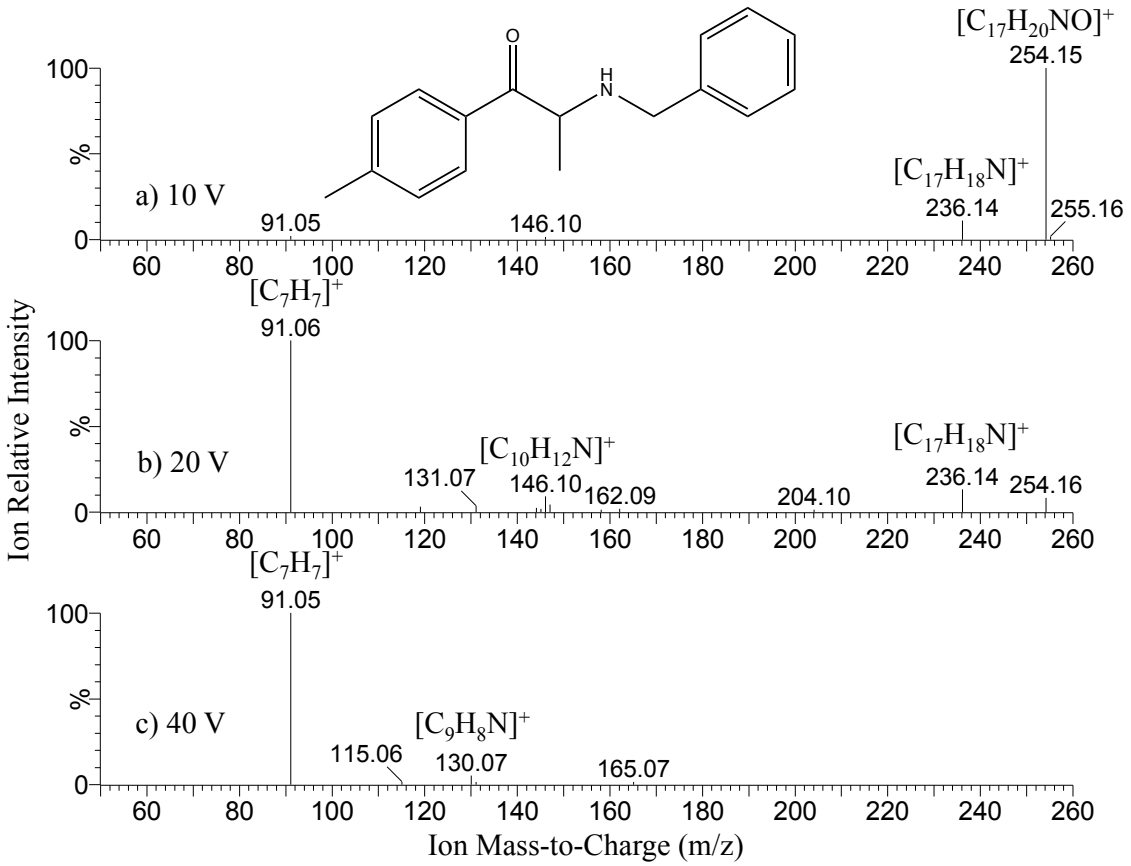

Figure A.4. CID-MS spectra for the cathinone benzedrone at collision potentials of a) 10 V, b) 20 V, and c) 40 V. All spectra collected in positive-ion mode.

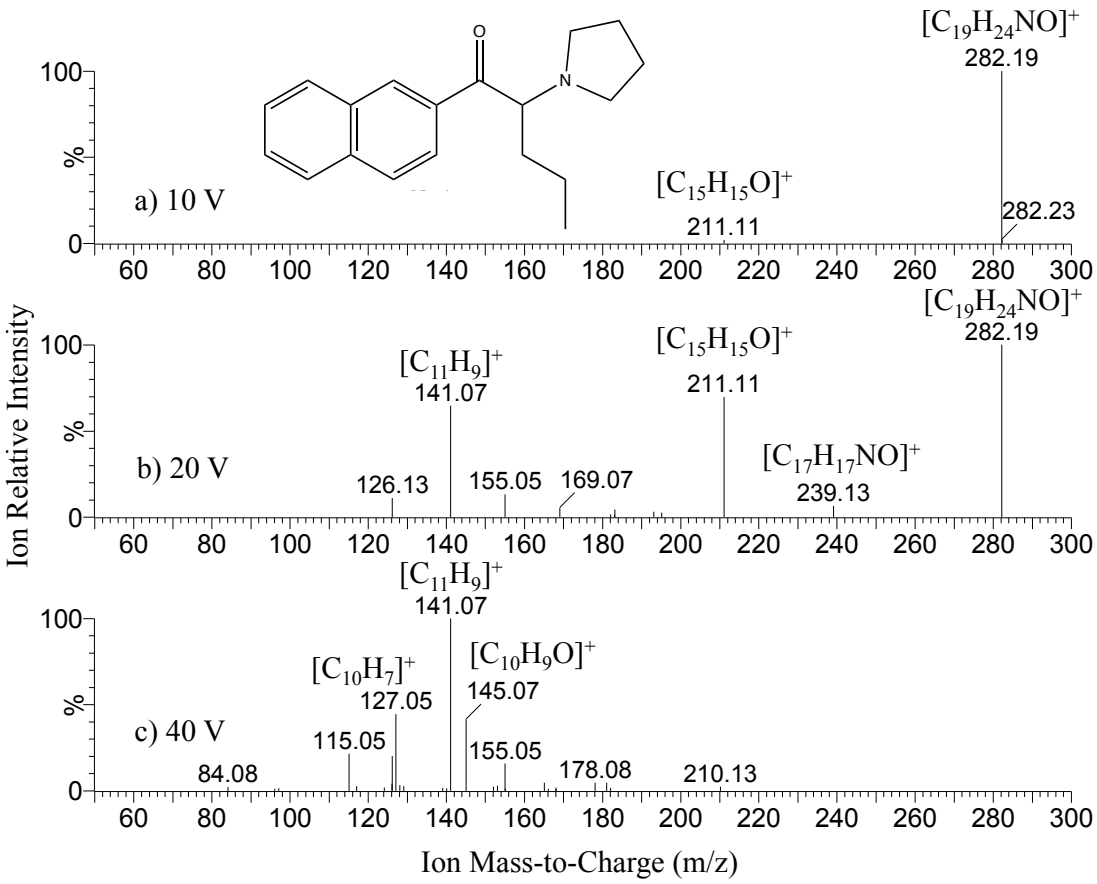

Figure A.5. CID-MS spectra for the cathinone naphyrone at collision potentials of a) 10 V, b) 20 V, and c) 40 V. All spectra collected in positive-ion mode.

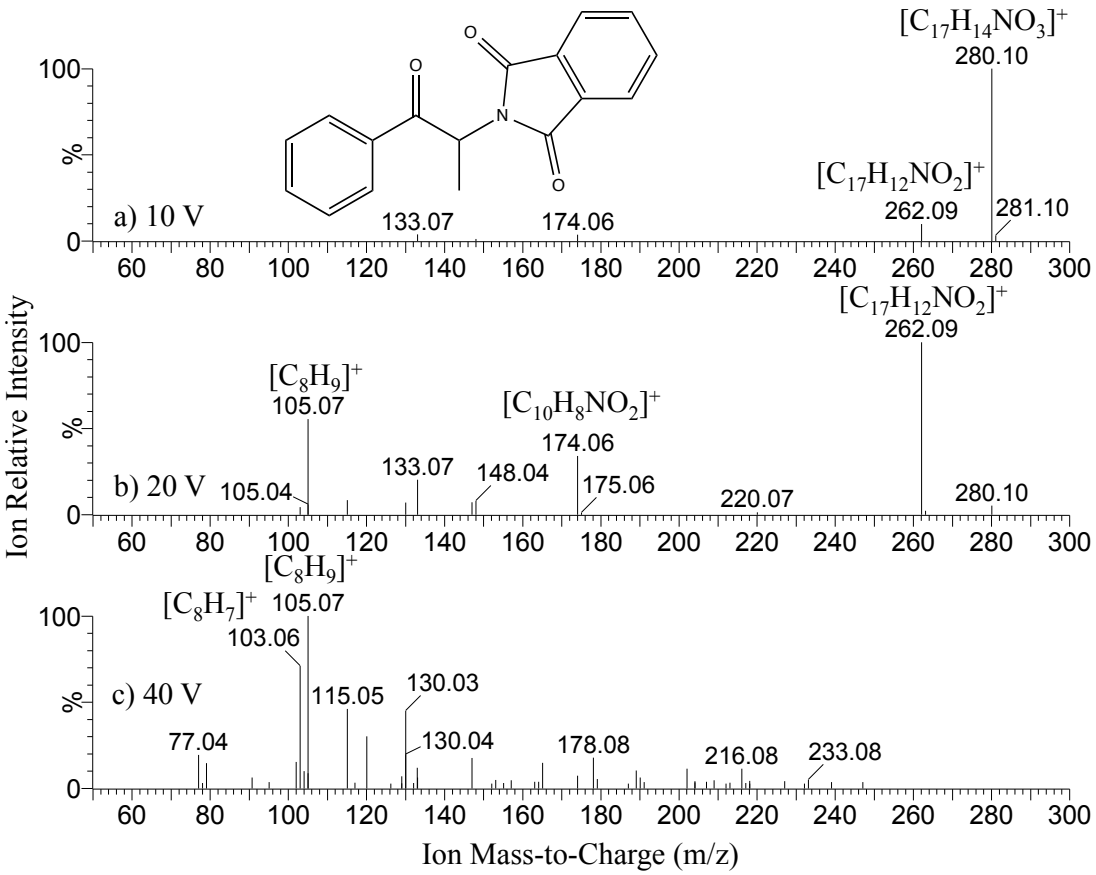

Figure A.6. CID-MS spectra for the cathinone α-phthalimidopropiophenone at collision potentials of a) 10 V, b) 20 V, and c) 40 V. All spectra collected in positive-ion mode.

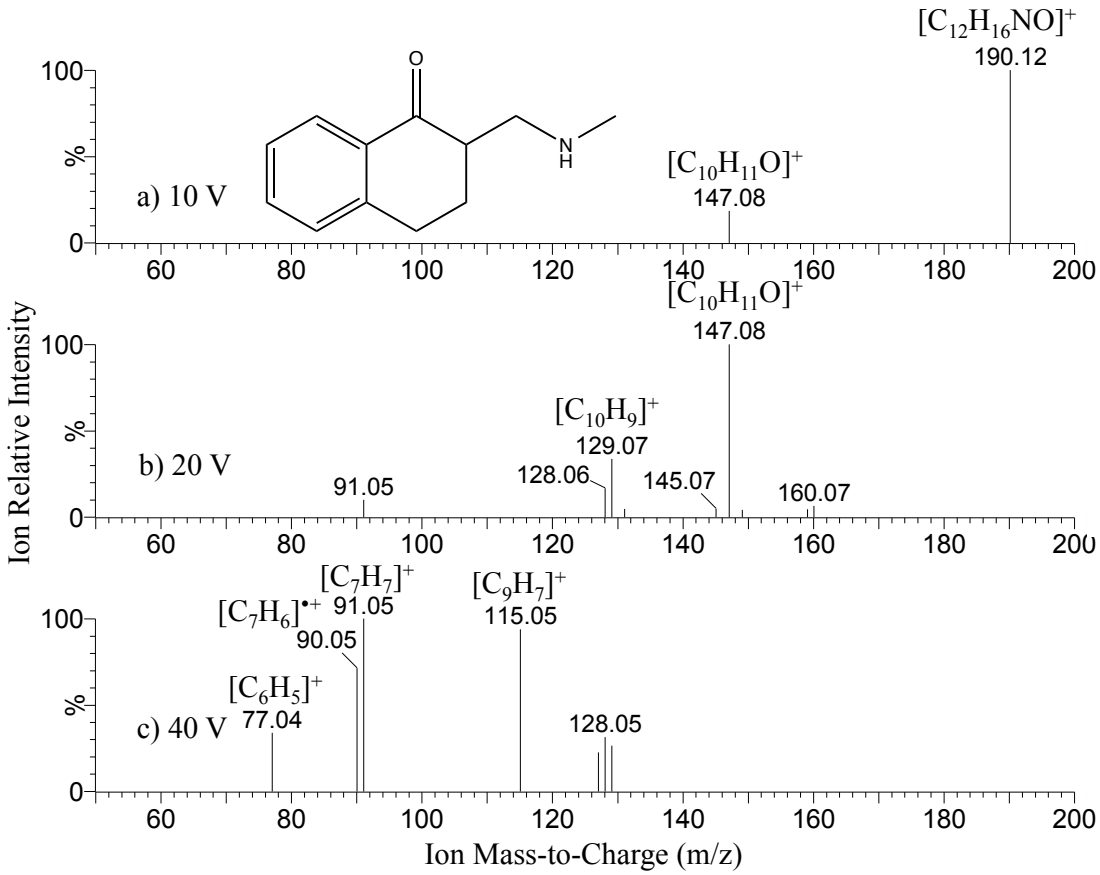

Figure A.7. CID-MS spectra for the cathinone MTTA at collision potentials of a) 10 V, b) 20 V, and c) 40 V. All spectra collected in positive-ion mode.

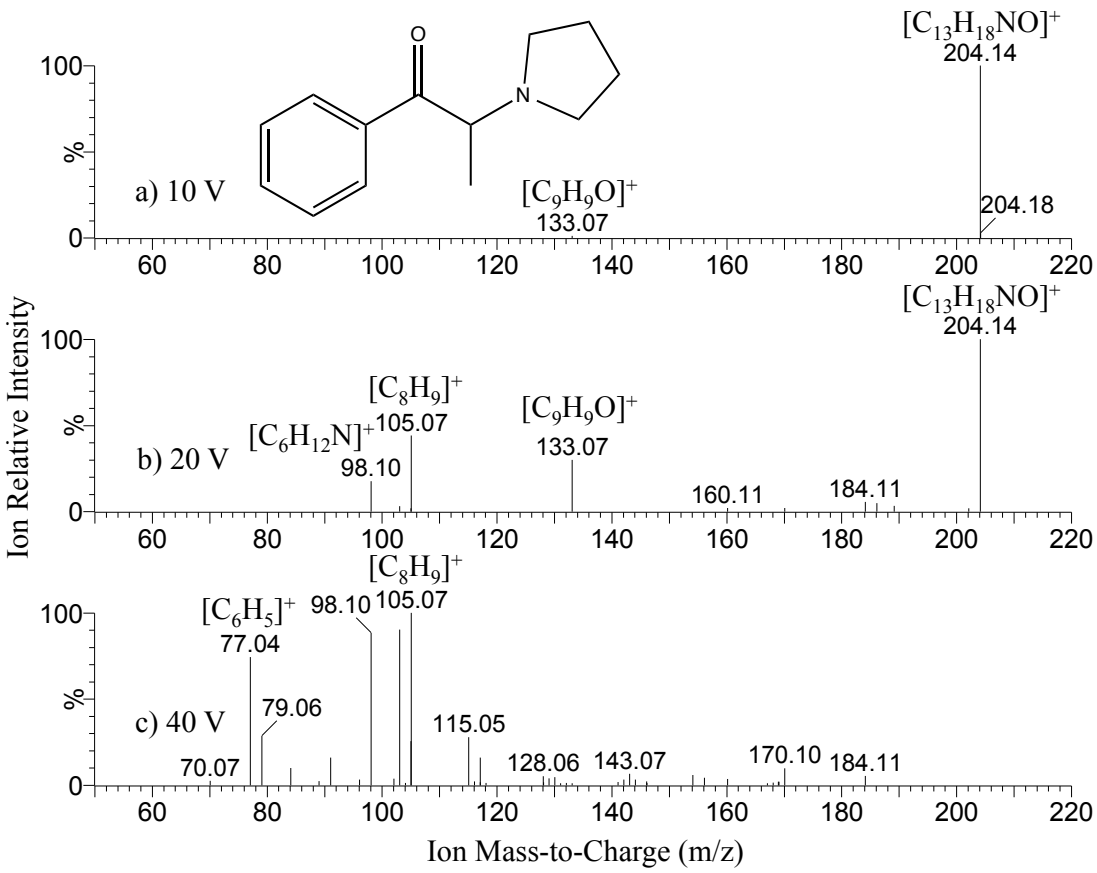

Figure A.8. CID-MS spectra for the cathinone α-pyrrolidinopropiophenone (α-PPP) at collision potentials of a) 10 V, b) 20 V, and c) 40 V. All spectra collected in positive-ion mode.

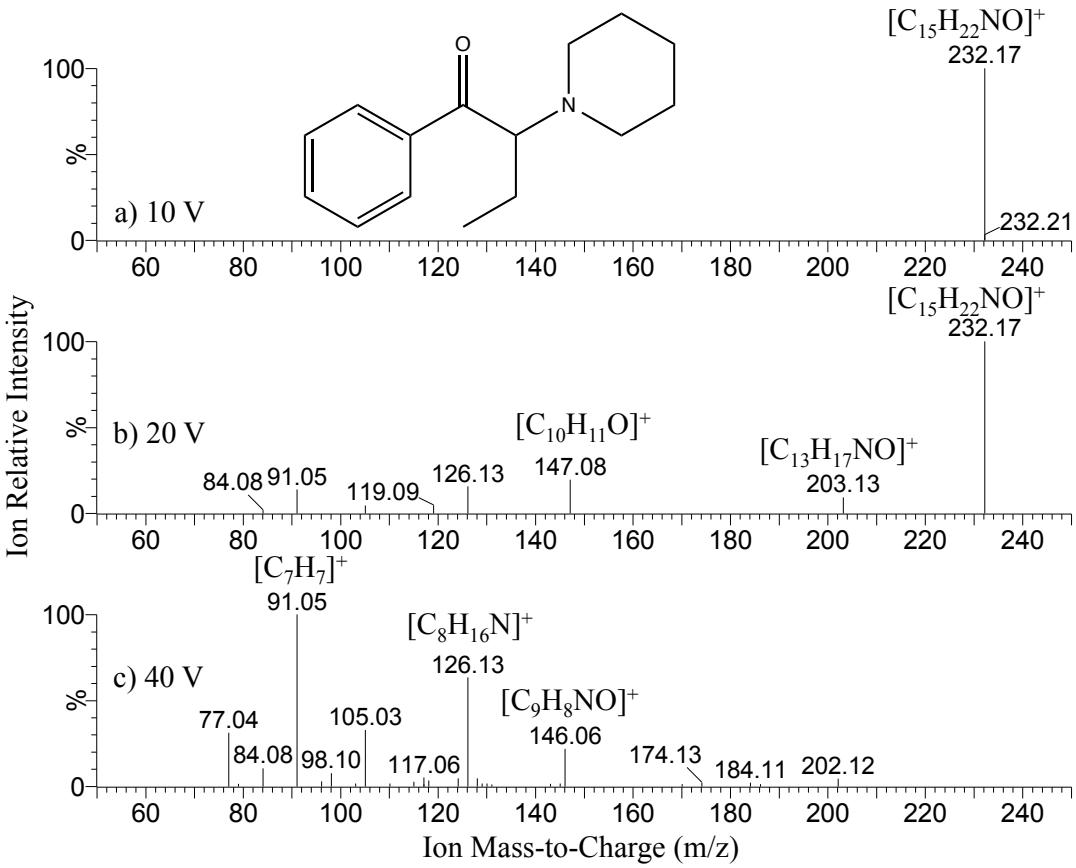

Figure A.9. CID-MS spectra for the cathinone α-piperidinobutiophenone at collision potentials of a) 10 V, b) 20 V, and c) 40 V. All spectra collected in positive-ion mode.

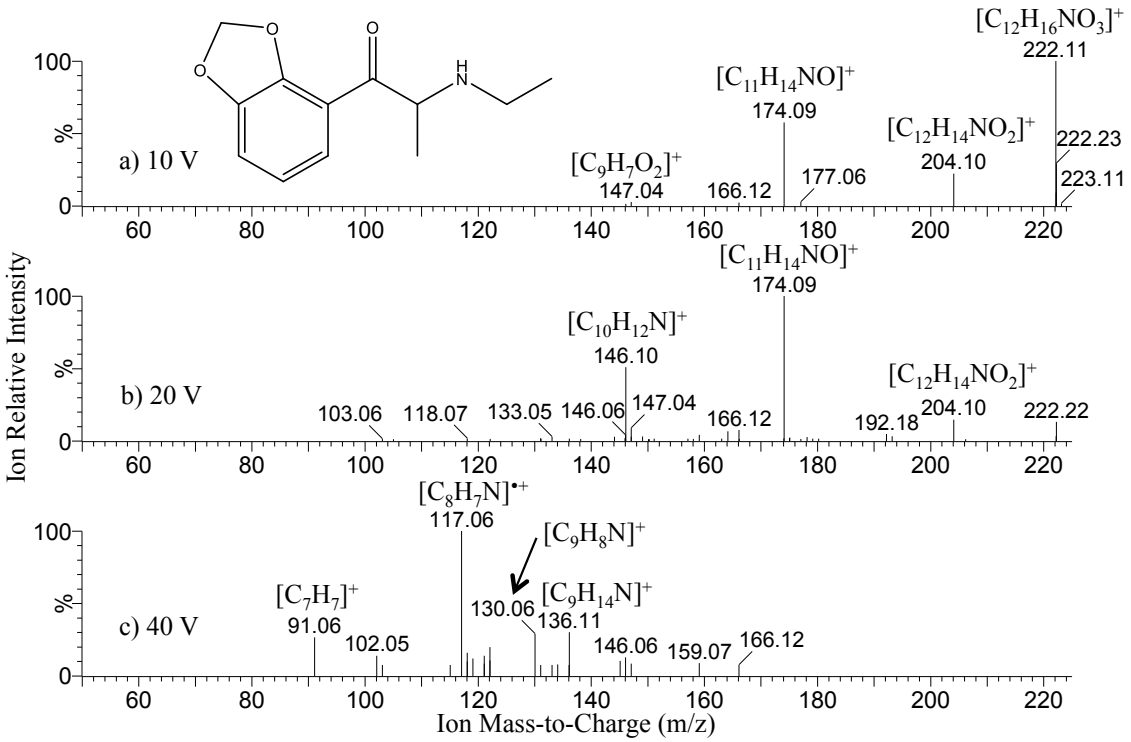

Figure A.10. CID-MS spectra for the cathinone 2,3-ethylone isomer at collision potentials of a) 10 V, b) 20 V, and c) 40 V. All spectra collected in positive-ion mode.

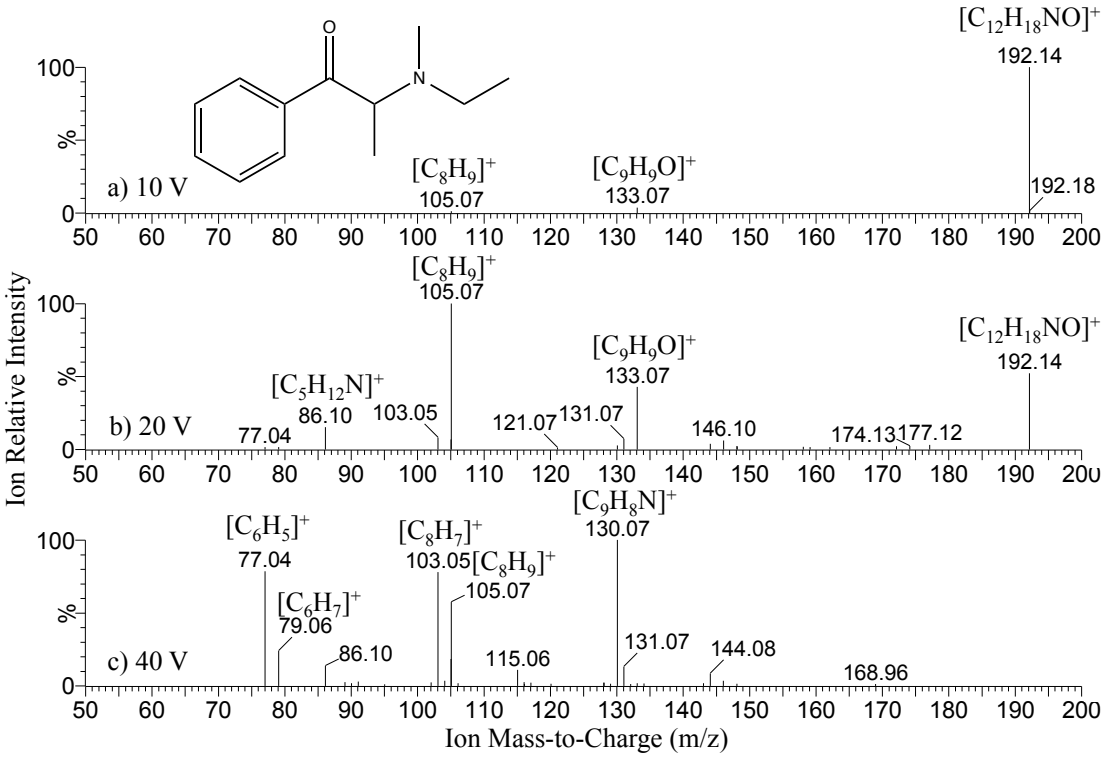

Figure A.11. CID-MS spectra for the cathinone *N*-ethyl-*N*-methylcathinone at collision potentials of a) 10 V, b) 20 V, and c) 40 V. All spectra collected in positive-ion mode.

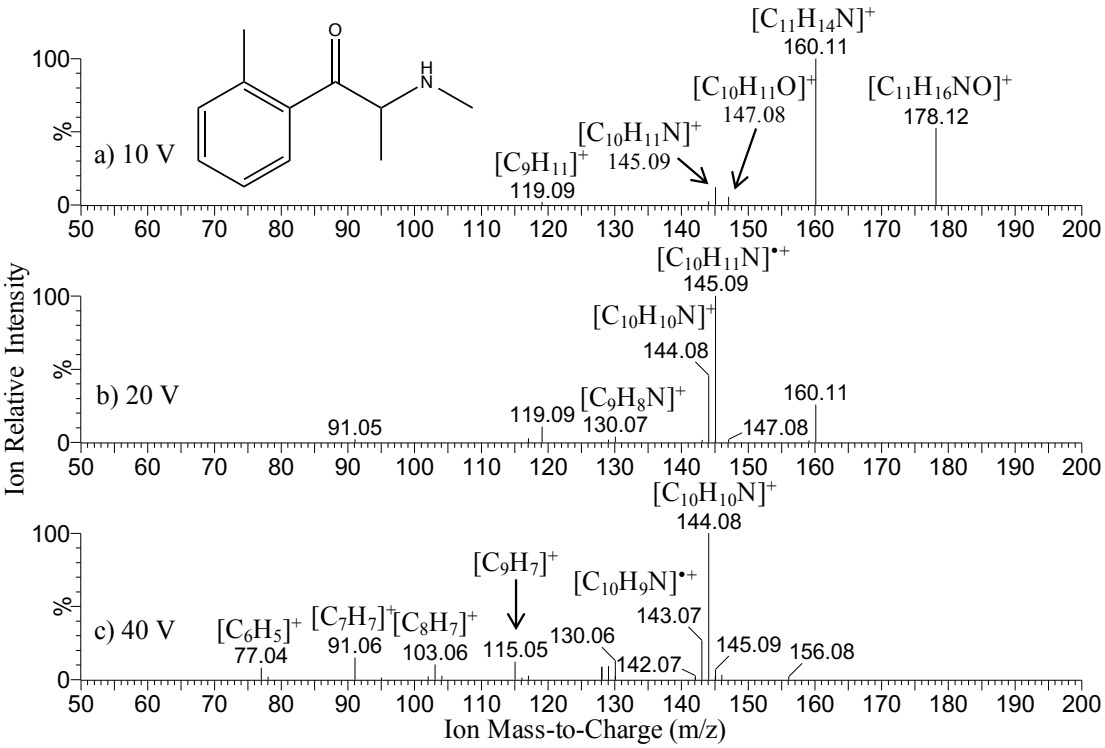

Figure A.12. CID-MS spectra for the cathinone 2-methylmethcathinone at collision potentials of a) 10 V, b) 20 V, and c) 40 V. All spectra collected in positive-ion mode.

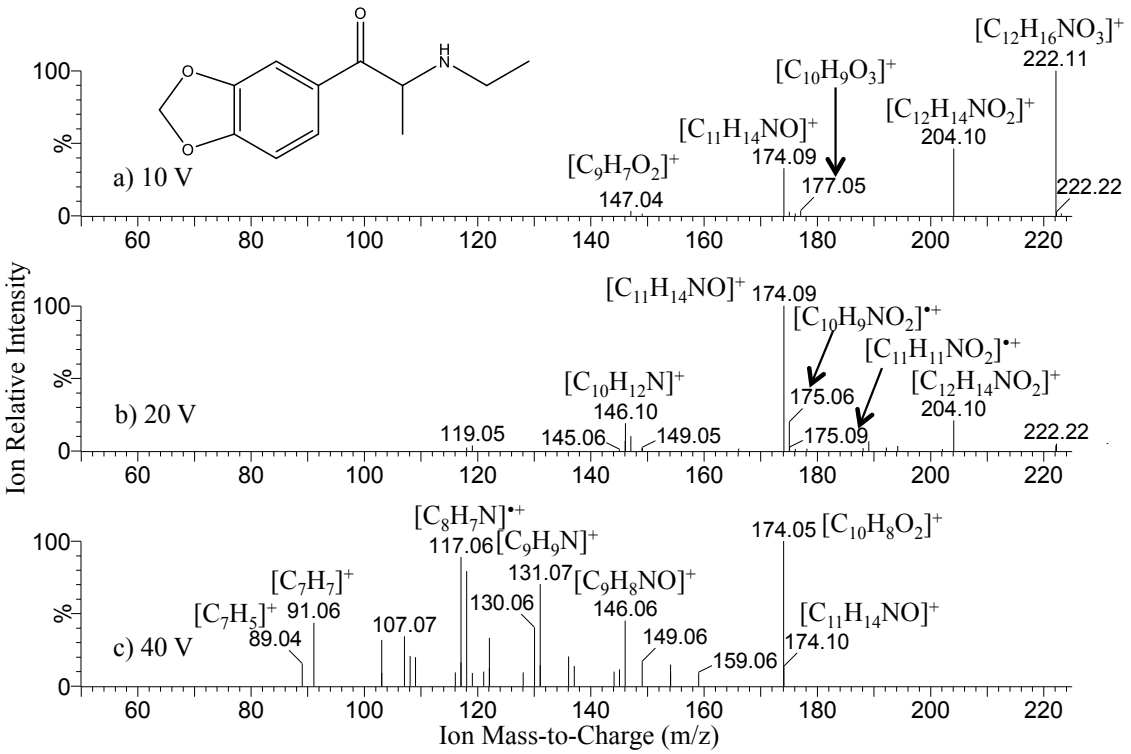

Figure A.13. CID-MS spectra for the cathinone ethylone at collision potentials of a) 10 V, b) 20 V, and c) 40 V. All spectra collected in positive-ion mode.

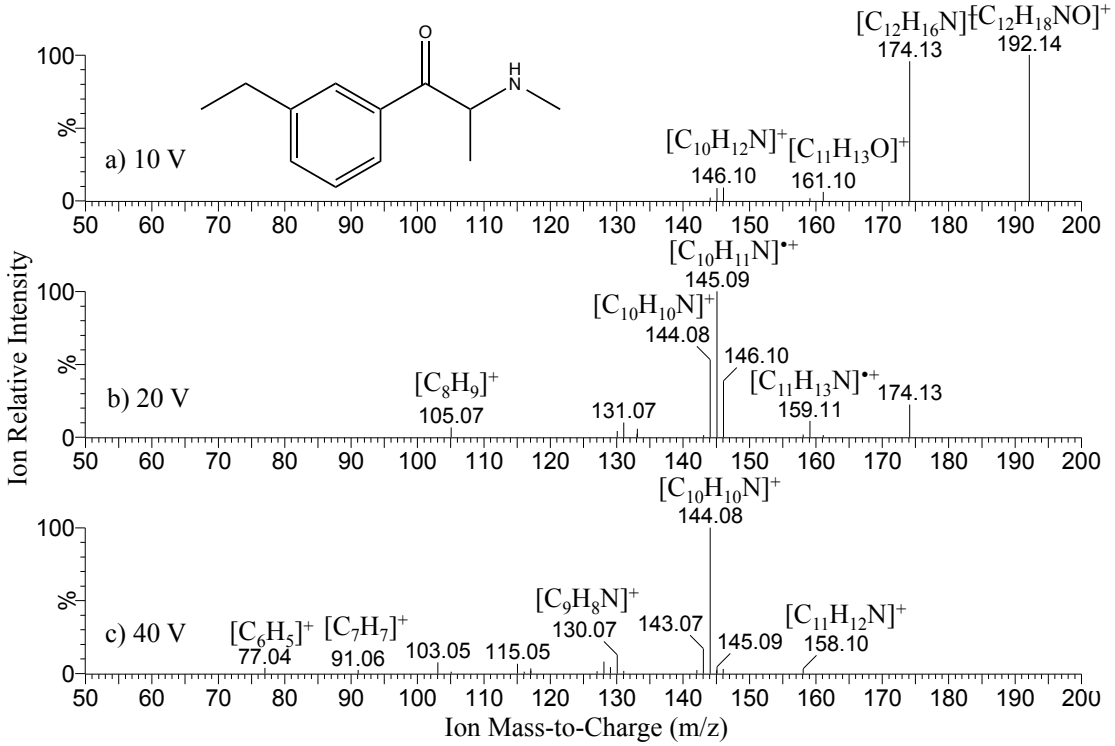

Figure A.14. CID-MS spectra for the cathinone 3-ethylmethcathinone at collision potentials of a) 10 V, b) 20 V, and c) 40 V. All spectra collected in positive-ion mode.

APPENDIX B

CID-MS Spectra of Phenethylamines

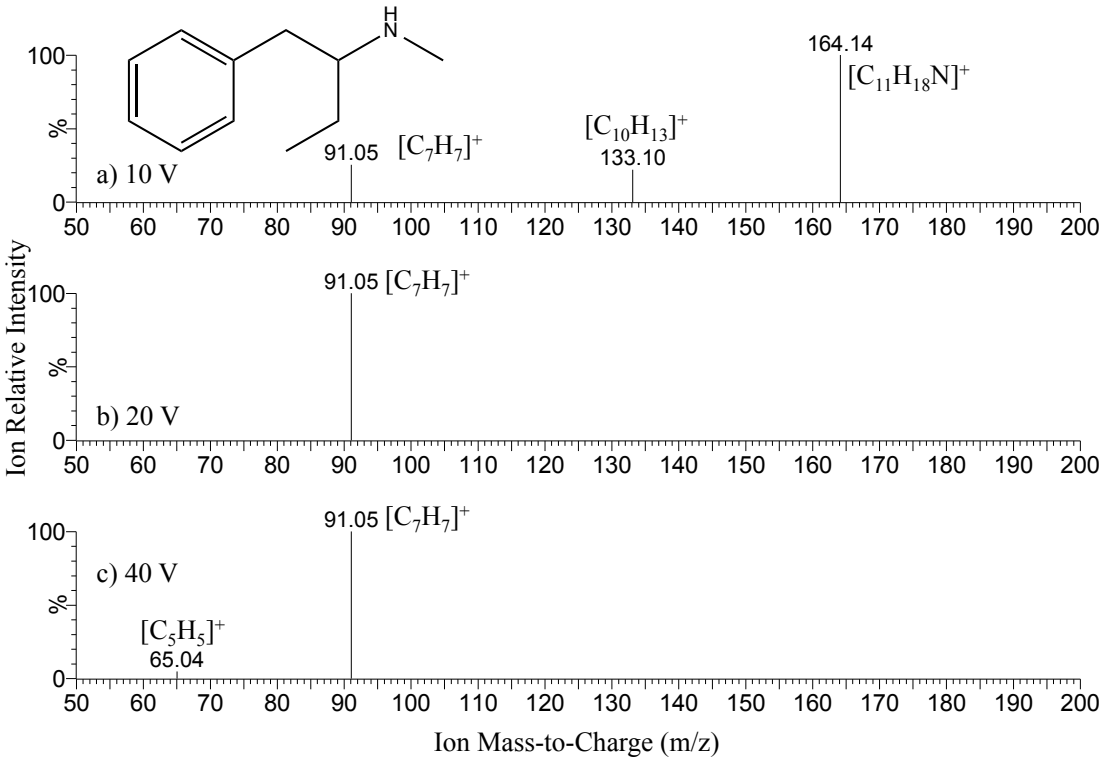

Figure B.1. CID-MS spectra for the phenethylamine 2-methylamino-1-phenylbutane at collision potentials of a) 10 V, b) 20 V, and c) 40 V. All spectra collected in positive-ion mode.

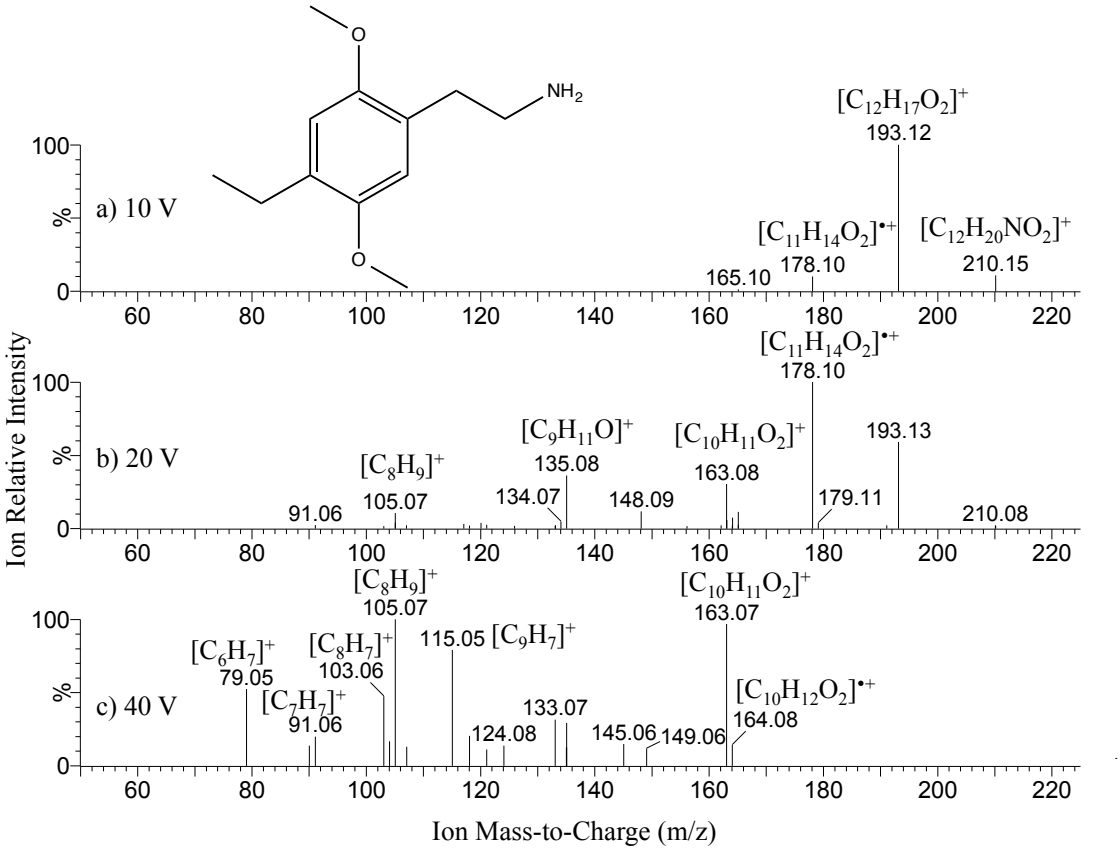

Figure B.2. CID-MS spectra for the phenethylamine 2C-E at collision potentials of a) 10 V, b) 20 V, and c) 40 V. All spectra collected in positive-ion mode.

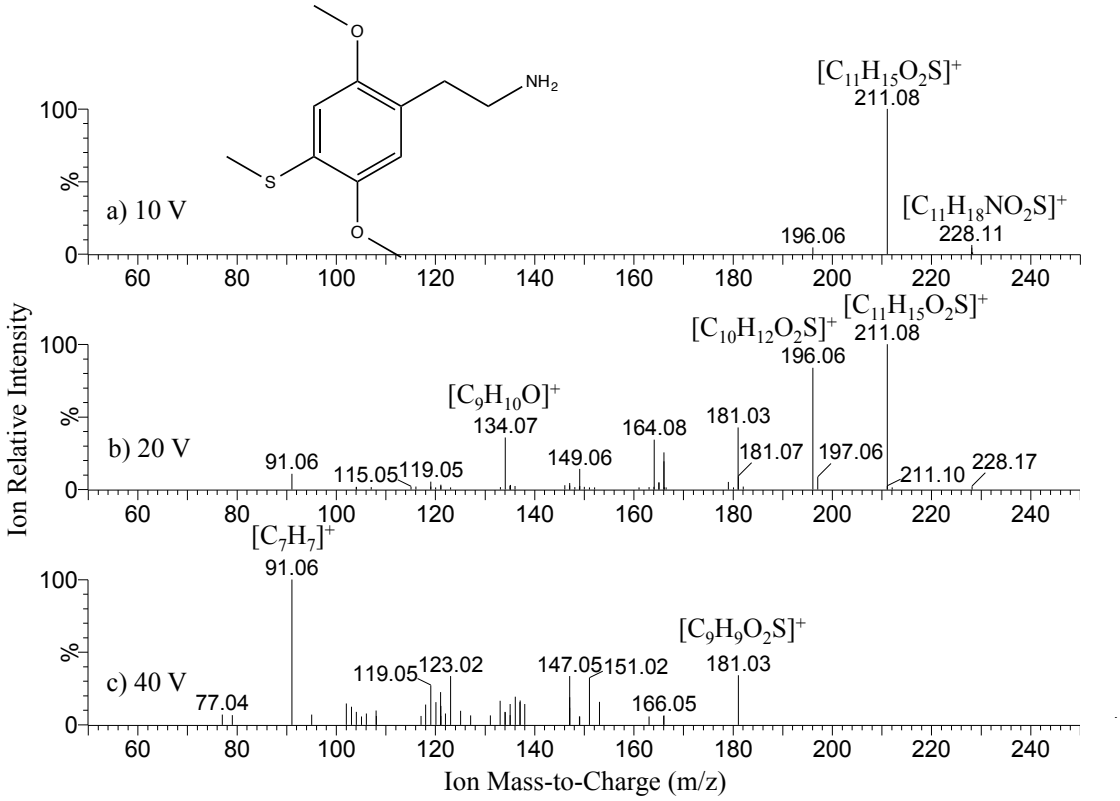

Figure B.3. CID-MS spectra for the phenethylamine 2C-T at collision potentials of a) 10 V, b) 20 V, and c) 40 V. All spectra collected in positive-ion mode.

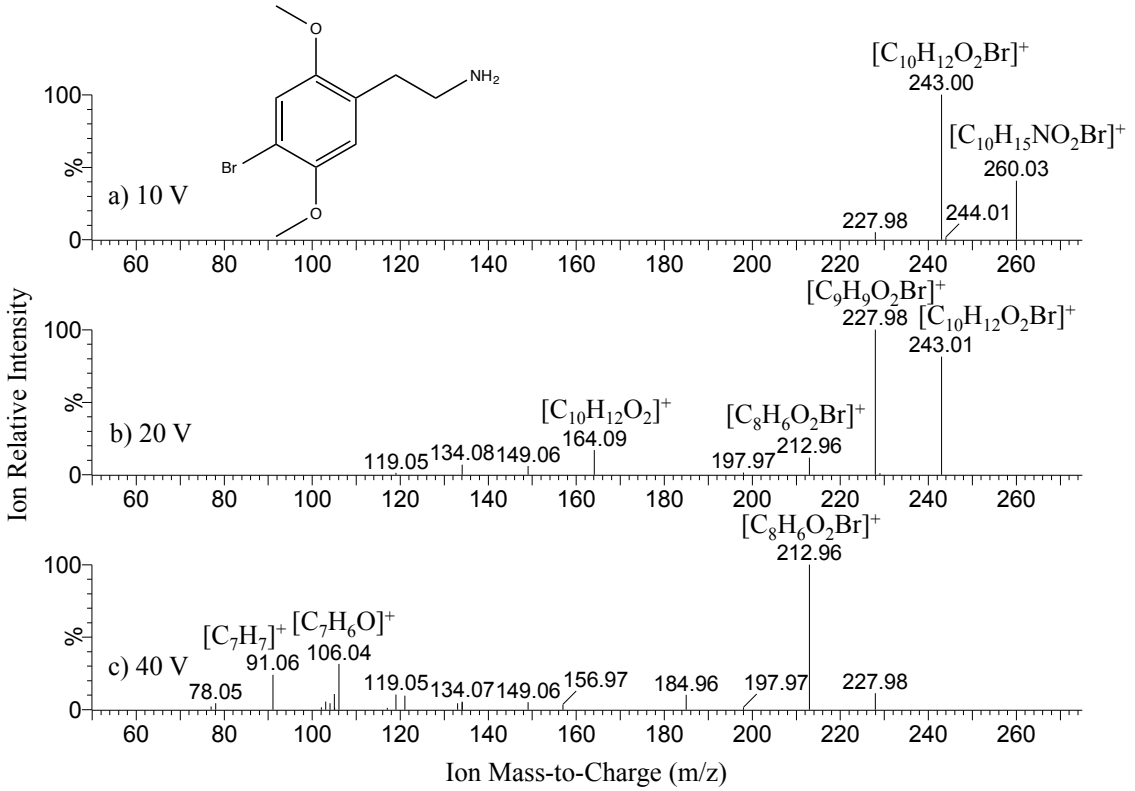

Figure B.4. CID-MS spectra for the phenethylamine 2C-B at collision potentials of a) 10 V, b) 20 V, and c) 40 V. All spectra collected in positive-ion mode.

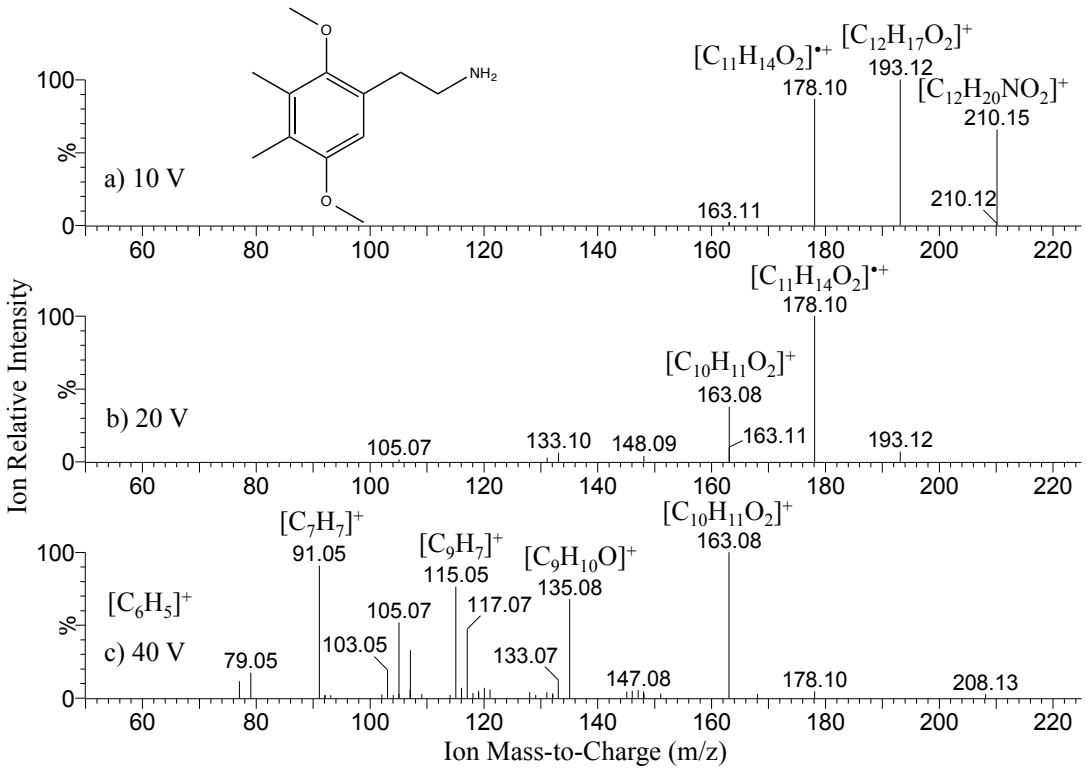

Figure B.5. CID-MS spectra for the phenethylamine 2C-G at collision potentials of a) 10 V, b) 20 V, and c) 40 V. All spectra collected in positive-ion mode.

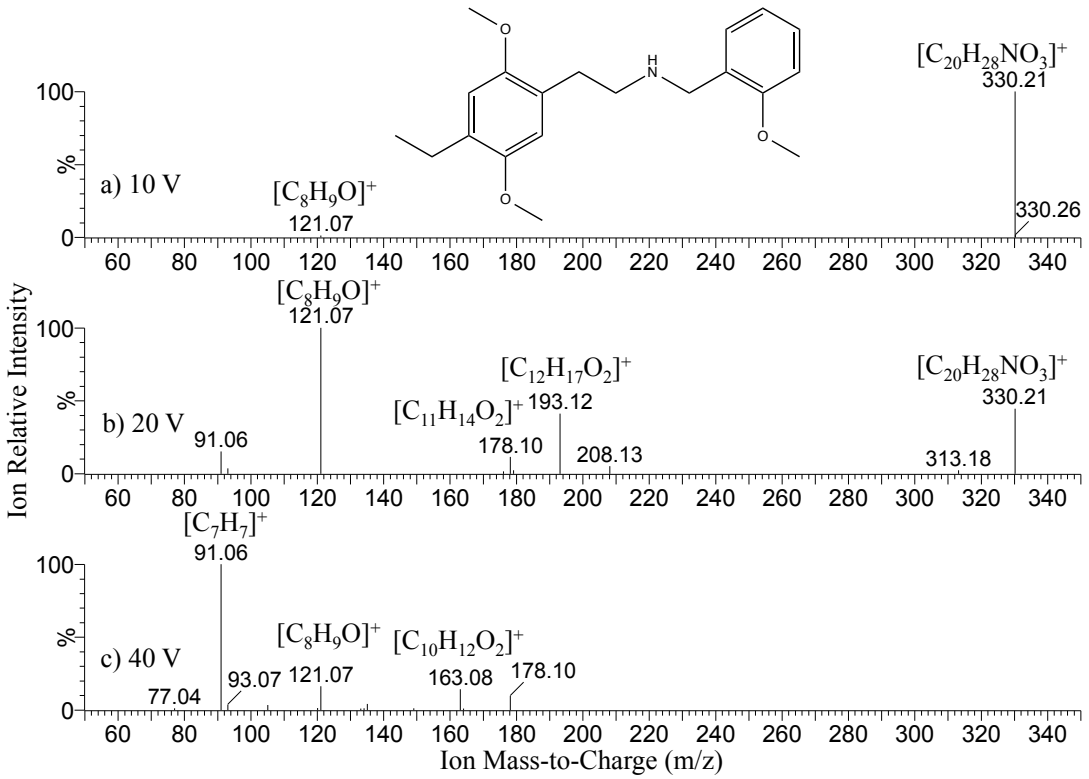

Figure B.6. CID-MS spectra for the phenethylamine 25E-NBOMe at collision potentials of a) 10 V, b) 20 V, and c) 40 V. All spectra collected in positive-ion mode.

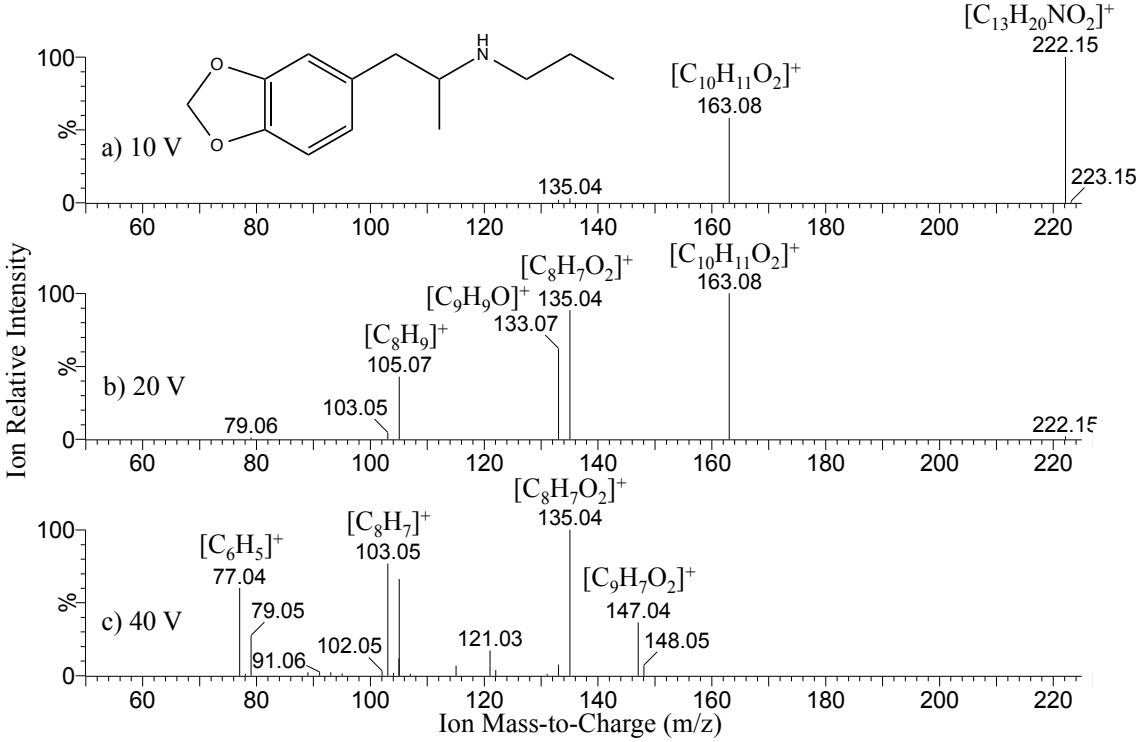

Figure B.7. CID-MS spectra for the phenethylamine 3,4-MDPA at collision potentials of a) 10 V, b) 20 V, and c) 40 V. All spectra collected in positive-ion mode.

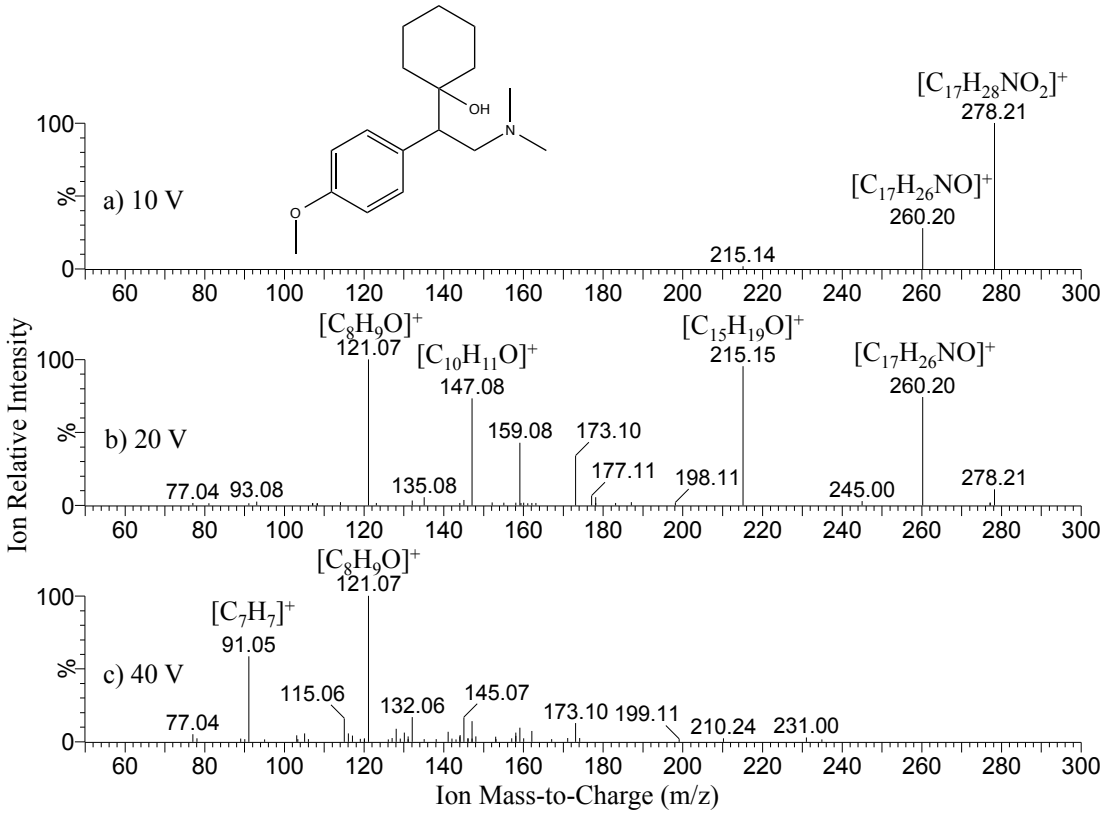

Figure B.8. CID-MS spectra for the phenethylamine venlafaxine at collision potentials of a) 10 V, b) 20 V, and c) 40 V. All spectra collected in positive-ion mode.

REFERENCES

REFERENCES

1. Drug Enforcement Administration. Statistics and Facts. DEA.gov; 2015. Available from: http://www.dea.gov/resource-center/statistics.shtml#seizures. Last accessed 9/16/16.

2. Federal Bureau of Investigation. Crime in the U.S. 2014. Available from: https://ucr.fbi.gov/crime-in-the-u.s/2014/crime-in-the-u.s.-2014/persons-arrested/main. Last accessed 9/16/16.

3. National Center for Health Statistics. Health, United States, 2015: With Special Feature on Racial and Ethnic Health Disparities. Hyattsville, MD. 2016.

4. Henderson GL. Designer drugs: past history and future prospects. J Forensic Sci. 1988;33(2):569-75.

5. Kelly JP. Cathinone derivatives: a review of their chemistry, pharmacology, and toxicology. Drug Test Anal. 2011;3(7-8):439-53.

6. Drug Enforcement Administration. Drugs of Abuse, 2015 Edition: A DEA Resource Guide. 2015.

7. Fornal E. Study of collision-induced dissociation of electrospray generated protonated cathinones. Drug Test Anal. 2014;6(7-8):705-15.

8. Zawilska JB, Wojcieszak J. Designer cathinones – An emerging class of novel recreational drugs. Forensic Sci Int. 2013;231(1-3):42-53.

9. Kau, Gregory. Flashback to the Federal Analog Act of 1986: Mixing Rules and Standards in the Cauldron. 156 U. Pa. L. Rev. 2008:156:1077-115.

10. Food and Drug Administration. Controlled Substances Act, Title 21 – Food and Drugs, Chapter 13 – Drug Abuse Prevention and Control, Subchapter 1 – Control and Enforcement. Available from: http://www.fda.gov/regulatoryinformation/legislation/ucm148726.htm. Last accessed: 11/28/16.

11. Caulkins JP, Coulson C. To schedule or not to schedule: how well do we decide? J Global Drug Policy Pract. 2010:5(4):1-20.

12. King, L. Legal Classification of Novel Psychoactive Substances: An International Comparison. As printed in Novel Psychoactive Substances: Classification, Pharmacology, and Toxicology. Eds. Dargan PI, Wood DM. Amsterdam: Elsevier/Academic Press. 2013:3-27.

13. Drug Enforcement Administration. List of Controlled Substances, Alphabetical Order. Last updated 10/27/16.

14. National Conference of State Legislatures. Available from: http://www.ncsl.org/research/civil-and-criminal-justice/synthetic-drug-threats.aspx. Last accessed: 11/28/16.

15. Toole KE, Fu S, Shimmon RG, Kraymen N. Color Tests for the Preliminary Identification of Methcathinone and Analogues of Methcathinone. Microgram Journal. 2012:9(1): 27-32.

16. SWGDRUG. Scientific Working Group for the Analysis of Seized Drugs (SWGDRUG) Recommendations. Version 7-1. June 9, 2016.

17. Watson JT, Sparkman OD. Introduction to Mass Spectrometry: Instrumentation, Applications, and Strategies for Data Interpretation, Fourth Edition. 2007, John Wiley & Sons, Ltd.

18. Yamashita M, Fenn JB. Electrospray ion source. Another variation on the free-jet theme. *J Phys Chem*, 1984;88(20):4451–59.

19. Wells JM, McLuckey SA. Collision-Induced Dissociation (CID) of Peptides and Proteins. Methods Enzymol. 2005;402:148-85.

20. Sheldon MT, Mistrik R., Croley TR. Determination of ion structures in structurally related compounds using precursor ion fingerprinting. J Am Soc Mass Spectrom. 2009;20(3):370-6.

21. Yang Z, Nakabayashi R, Okazaki Y, Mori T, Takamatsu S, Kitanaka S, Kikuchi J. Saito K. Toward better annotation in plant metabolomics: isolation and structure elucidation of 36 specialized metabolites from *Oryza sativa* (rice) by using MS/MS and NMR analyses. Metabolomics. 2014;10(4):543-555.

22. Vismeh R, Lu F, Chundawat SPS, Humpula JF, Azarpira A, Balan V, Dale BE, Ralph J, Jones AD. Profiling of diferulates (plant cell wall cross-linkers) using ultrahigh-performance liquid chromatography-tandem mass spectrometry. Analyst. 2013;138(21):6683-92.

23. Concheiro M, Anizan S, Ellefsen K, Huestis MA. Simultaneous quantification of 28 synthetic cathinones and metabolites in urine by liquid chromatography high-resolution mass spectrometry. Anal Bioanal Chem. 2013 Nov;405(29):9437-48.

24. Fornal E. Formation of odd-electron product ions in collision-induced fragmentation of electrospray-generated protonated cathinone derivatives: aryl α-primary amino ketones. Rapid Commun Mass Spectrom. 2013;27(16):1858-66.

25. Fornal E. Identification of substituted cathinones: 3,4-methylenedioxy derivatives by high performance liquid chromatography-quadrupole time of flight mass spectrometry. J Pharm Biomed Anal. 2013;81-82:13-9.

26. Power JD, McDermott SD, Talbot B, O'Brien JE, Kavanagh P. The analysis of amphetamine-like cathinone derivatives using positive electrospray ionization with in-source collision-induced dissociation. Rapid Commun Mass Spectrom. 2012;26(22):2601-11.

27. Zuba D. Identification of cathinones and other active components of 'legal highs' by mass spectrometric methods. Trends Anal Chem. 2012;32:15–30.

28. Borth S, Hansel W, Rosner P, Junge T. Regioisomeric differentiation of 2,3- and 3,4- methylenedioxy ring-substituted phenylalkylamines by gas chromatography tandem mass spectrometry. J Mass Spectrom. 2000;35(6):705-10.

29. De Hoffmann E, Stroobant V. Mass Spectrometry: Principles and Applications, Third Edition. 2007, John Wiley & Sons, Ltd.

30. Welter J, Brandt SD, Kavanagh P, Meyer MR, Maurer HH. Metabolic fate, mass spectral fragmentation, detectability, and differentiation in urine of the benzofuran designer drugs 6-APB and 6-MAPB in comparison to their 5-isomers using GC-MS and LC-(HR)-MS^n techniques. Anal Bioanal Chem. 2015;407(12):3457-70.

31. Snyder DT, Fedick PW, Cooks RG. Multigenerational Collision-Induced Dissociation for Characterization of Organic Compounds. Anal Chem. 2016;88(19):9572-9581.

32. Weinmann W, Wiedmann A, Eppinger B, Renz M, Svoboda M. Screening for drugs in serum by electrospray ionization/collision-induced dissociation and library searching. J Am Soc Mass Spectrom. 1999;10(10):1028-37.